



## Applications of Metal-Organic Frameworks in Heterogeneous Supramolecular Catalysis

Journal:	<i>Chemical Society Reviews</i>
Manuscript ID:	CS-REV-02-2014-000094.R1
Article Type:	Review Article
Date Submitted by the Author:	07-May-2014
Complete List of Authors:	Liu, Jiewei; Sun Yat-Sen University, Chen, Lianfen; Sun Yat-Sen University, Cui, Hao; Sun Yat-Sen University, Zhang, Jianyong; Sun Yat-Sen University, School of Chemistry and Chemical Engineering Zhang, Li; Sun Yat-sen University, School of chemistry and chemical engineering Su, Cheng-Yong; Sun Yat-Sen University, School of Chemistry and Chemical Engineering

## ARTICLE

# Applications of Metal-Organic Frameworks in Heterogeneous Supramolecular Catalysis

Cite this: DOI: 10.1039/x0xx00000x

Jiewei Liu, Lianfen Chen, Hao Cui, Jianyong Zhang, Li Zhang\* and Cheng-Yong Su\*

Received 00th January 2012,  
Accepted 00th January 2012

DOI: 10.1039/x0xx00000x

www.rsc.org/

This review summarizes the use of metal-organic frameworks (MOFs) as a versatile supramolecular platform to develop heterogeneous catalysts for a variety of organic reactions, especially in liquid-phase reactions. Following a background introduction about catalytic relevance to various metal-organic materials, crystal engineering of MOFs, characterization and evaluation methods of MOF catalysis, we categorize catalytic MOFs based on the types of active sites, including coordinatively unsaturated metal sites (CUMs), metalloligands, functional organic sites (FOS), as well as metal nanoparticles (MNPs) embedded in the cavities. Throughout the review, we emphasize the incidental or deliberate formation of active sites, the stability, heterogeneity and shape/size selectivity for MOF catalysis. Finally, we briefly introduce their relevance to photo- and biomimetic catalysis, and compare MOFs with other typical porous solids such as zeolites and mesoporous silica with regard to their different attributes, and provide our view on future trends and developments of MOF-based catalysis.

## 1. Introduction

### 1.1 Assembly of MOMs with Catalytic Relevance

Supramolecular catalysis inherent in natural enzymatic systems has been pursued for decades with the goals to develop “artificial enzyme catalysts” for synthetic chemistry or to understand fundamental mechanisms with regard to enzyme active sites.<sup>1</sup> Supramolecular coordination chemistry provides a promising platform for such supramolecular catalytic purposes, for example, to mimic pocket nature or host-guest interactions of enzymes by assembly of various size and shape predefined nanoreactors or molecular flasks.<sup>2</sup> Recently, rapid progress in supramolecular catalysis was achieved for porous coordination solids which can offer well-defined coordination nanospace and functional groups/sites appropriate for catalysis.<sup>3</sup> These persistent catalytic interests take the advantages that the coordination assembly feature in good bond direction, moderate bond energy, self-correcting kinetic reversibility and plentiful metal geometries, thus driving the metal- or ligand-directed self-assembly to produce a variety of metal-organic materials (MOMs)<sup>4</sup> with varied relevance to catalysis.

As exemplified in Fig. 1, four prototypes of MOMs with distinct structural identities and attributes are often pursued for multifarious catalytic purposes: (I) mon- or multinuclear metal complexes possessing specific functionality in a supramolecular sense; (II) discrete coordination rings, cages, tubes or capsules attributable to metal-organic polygons/polyhedra (MOPs) or metal-organic containers/cages (MOCs); (III) infinite metal-organic frameworks (MOFs) or coordination polymers (CPs) which often possess periodically repeating units in crystalline solid-state, including amorphous CPs which also subject to a wide range of catalytic studies,<sup>d,e</sup> and (IV) metal-organic gels

(MOGs) which are jelly-like materials containing cross-linking coordination network.<sup>5</sup> In point of catalysis, type-I MOMs may represent the simple but most popular structural models investigated in transition metal catalysis, in special cases the supramolecular catalysis can be achieved.<sup>6</sup> The type-II MOMs are pertinent to supramolecular catalysis because they are able to provide specific substrates recognition and coordination space for stereochemical confinement.<sup>2</sup> Both these two types of coordination compounds could be studied in homogeneous conditions. On the contrary, MOFs and MOGs are applicable in heterogeneous catalysis.<sup>3,5</sup> In contrast to MOGs and amorphous CPs, MOFs are typically crystalline porous solids resembling zeolites, able to use a minimum amount of metal ions and organic ligands to build maximum surface areas with predictable, controllable, tailorable and post-modifiable pores and cavities. Such intrinsic structure attributes make MOFs emerge as the new interface between heterogeneous catalysis and supramolecular chemistry to behave as promising candidates for heterogeneous supramolecular catalysis.

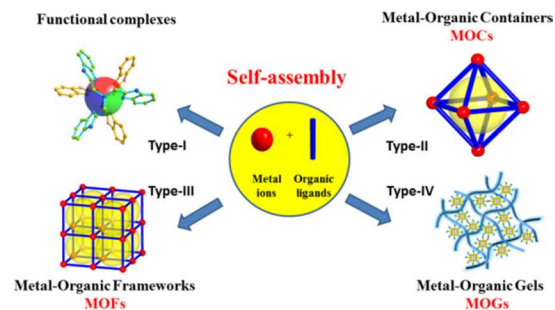


**Fig. 1** Schematic illustration of representative structural models driven by metal-ligand coordination assembly.

Since MOFs possess uniform, continuous and permeable channels, they can provide active sites on the pore surface and transport reactants/products to or from inner reactive vessels (such as cage-like cavities inside the MOFs). In a supramolecular sense, the uniqueness of MOF structures lies in the coordination-driven self-assembly, the tunable pore sizes, exceptionally high pore volume and surface area, and versatile inner cavity (one- to three-dimensional pores capable of incorporating interior cages and windows), which endow the catalytic microenvironment with a variety of tunable properties, such as charge, polarity, chirality, redox potential, photoactivity, hydrophobicity/hydrophilicity, aromatic/lipophilic character, and stereochemistry. The porosity of MOFs spans from ultramicroporous to mesoporous materials, well bridging the gap between the small pore size of zeolites and large pore size of mesoporous silicate materials. This makes supramolecular catalysis easily taking place in an appropriate coordination space under nanoscale confinement, allowing multicomponent reactions as well as a wide range of substrates from small molecules to large polyaromatics and carbohydrates. Meanwhile, using MOFs as heterogeneous supramolecular catalysts could take advantages of the following principal characters: (1) enhanced catalyst reactivity and stability due to the spatial separation of multiple catalytic sites in the framework, which also can contribute to cooperative catalysis character of enzymes; (2) permeable channels and coordination nanospace which bestow recognition effects and allow the facile access of substrates to the catalytically active sites located within the cavities, endowing the catalytic reactions with shape-, size-, chemo-, or enantio-selectivity; (3) framework flexibility and dynamics<sup>7</sup> in the solid-state, which may bring new applications to heterogeneous catalysis by enforcing physical, chemical and environmental stimuli responses, and utilize the guest-host responses to accomplish transition-state recognition and regulation reminiscent of allosteric nature of enzymes; and (4) easy tunability and modification of the polar-nonpolar and hydrophobic-hydrophilic properties of the porous solids, which is essential for many bimolecular reactions, and helpful to practical synthetic chemistry. Moreover, the ability to separate and reuse a heterogeneous catalyst would be highly attractive in large-scale reactions, where separation and waste disposal can be costly. The last but important feature of MOFs for supramolecular catalysis is that, assembly process of MOFs combines merits of various metal ions or clusters and designable and tailorable organic ligands, which offers innumerable structural topologies and diversified porosities. Therefore, in contrast to the analogous zeolites (178 structures to date), the assembly approach endows MOFs with unlimited structural models from “designable” crystal engineering.

## 1.2 Crystal Engineering of MOFs for Catalysis

As a new class of crystalline porous materials, MOFs have attracted tremendous interests, and witnessed by an enormous amount of MOF structures which have been designed and synthesized for various energy and environment relevant applications, such as gas sorption/storage, separation, chirality, conductivity, non-linear optics, luminescence, sensors, magnetism, drug delivery, as well as catalysis. The scientific achievements in this burgeoning field have been summarized in MOF Themed Issues such as *Microporous and Mesoporous Materials* (2004, **73**, 1-108), *Chem. Soc. Rev.* (2009, **38**, 1213-1504), *Top. Curr. Chem.* (2010, **293**, 1-262), *Chem. Rev.* (2012, **112**, 673-1268) and *RSC Catalysis Series* (2013, No. 12). Even

though, investigations on catalytic applications of MOFs are relatively lagging behind other topics, which might be due to, in general, the relatively low chemical, hydrolytic and thermal stability (usually stable under 350–400 °C) of MOFs. Nevertheless, the situation improved dramatically since 2009. Fig. 2 shows the development of MOF fields on the basis of articles appeared in the last twenty years. It is clear that MOF catalysis underwent a rapid development in recent five years.

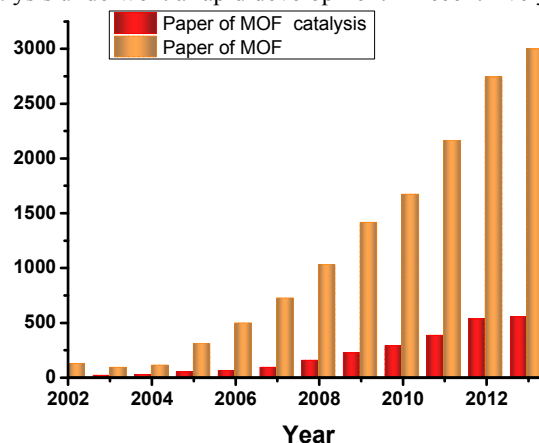


**Fig. 2** Development of MOF fields in comparison to the MOF catalysis in the last ten years (SciFinder until Jan. 15, 2014).

The progress in MOF catalysis may thank to the gradual maturation of crystal engineering.<sup>8</sup> Engineering of crystalline MOF solid materials demands proper design and synthetic strategies to organize basic building blocks (BBs) strictly in a periodic way of specific network topology. This is implicit in two interrelated steps: (a) choosing or creating BBs with desired structure and property, and (b) connecting or arranging BBs through predefined interactions or crystal growth. Undoubtedly, advances in synthetic strategy and design methodology have motivated in-depth study in functionality of crystalline solids, shifting research interests from original structural engineering of MOFs to the functional engineering of MOFs targeting in collective or specific property like catalysis.

Crystal engineering of MOFs for catalytic purpose relies not only on the permanent porosity, but also on other framework attributes like reversible structural transformation, framework integrity upon post-modification, as well as the ability to retain crystallinity and regularity after catalytic reactions. In this context, an attributive classification of MOFs, referring to Kitagawa's categories of porous CPs,<sup>9</sup> may be helpful to understand the structure-catalysis relationship of MOFs. As depicted in Fig. 3, the 1<sup>st</sup> generation MOFs only has nonpermanent porosity because of inseparable host-guest dependence, which has often been observed in MOFs containing charged frameworks with pores filled by counter anions. On the contrary, the 2<sup>nd</sup> generation MOFs possesses stable and robust porosity against guest removal, typical of neutral and zeolite-like MOFs. Whereas 3<sup>rd</sup> generation MOFs display framework flexibility and dynamics, being able to response to guest exchange or external stimuli. The 4<sup>th</sup> generation MOFs is correlated to the recently developed postsynthetic modifications (PSM) for MOFs,<sup>10</sup> and may be broadly defined as post-processing MOFs which can maintain underlying topology and structural integrity towards various post-modifications. In principal, MOF catalysis is applicable from 2<sup>nd</sup> to 4<sup>th</sup> generations; however, only until 3<sup>rd</sup> and 4<sup>th</sup> generation MOFs were fully understood and extensively

explored, MOF catalysis was springing up in this field. Understanding of the solid-state flexibility and dynamics of MOFs may alter the intuitive notion that crystalline solids are structurally stiff and static like common inorganic solids. This prepared the ground for MOF catalysis because the structural transformation and transition-state are essential in catalytic reactions, which may be easily imaged to occur in solution but not in the solid-state. Emergency of the 4<sup>th</sup> generation is helpful to lead MOF catalysis to a new stag, probably because various post-syntheses and post-functionalization methods open the door for a wider range of catalytic reactions and strategies. Functional engineering of catalytic MOFs in this manner implies that pre-design of MOF structure at the very start may not be necessary since active sites in the MOF can be post-designed.

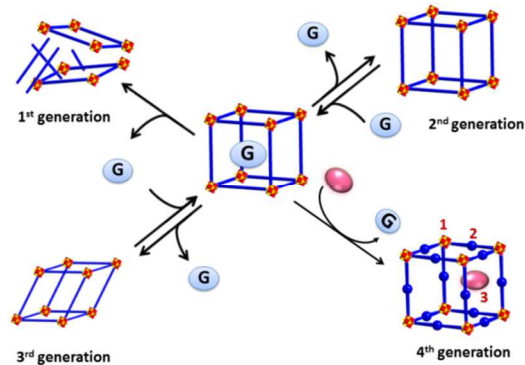


**Fig. 3** Classification of MOFs: 1<sup>st</sup> generation MOFs collapse on guest removal, 2<sup>nd</sup> generation MOFs have permanent porosity against guest removal, 3<sup>rd</sup> generation MOFs show flexible and dynamic properties, and 4<sup>th</sup> generation MOFs can sustain post-processing (modifiable positions: (1) metal/cluster sites, (2) organic linkers, and (3) vacant space).

In light of the synthesis for MOFs, three conceptually different approaches have been used to gain catalytically active sites: (a) using catalytic metal salts to construct the frameworks, (2) incorporating existing homogeneous catalysts, either organocatalysts or transition metal catalysts, into the organic linkers, and (3) loading of MOFs with active species (Fig. 4). Concerning the first strategy, however, it should be noticed that a large portion of MOF structures are not effective as adsorbents or catalysts, because the metal nodes are unavailable for bonding with substrates due to coordination saturation. In this regard, open metal sites can become available after removing weakly bonded solvent molecules through mild heating or vacuum treatment. Considering the second method, the existing homogeneous catalysts can be either directly incorporated to the organic linkers or through PSM. The PSM techniques include complexation of active metal sites via the uncoordinated functional groups (e.g. bipyridine, binol and catechol) of the organic linkers, and grafting organocatalysts such as pyrrolidine onto the coordinatively unsaturated metal sites on the nodes (Fig. 4b). The third approach that derives from the large pore volume available in MOFs consists of the incorporation of guest species in the internal void space that will act as a catalytic sites. The guest molecules can be indeed catalytically active or be converted to active species such as metal nanoparticles (Fig. 4c).

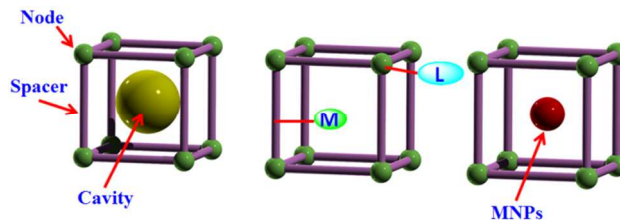


**Fig. 4** Schematic illustration of the potential catalytic sites (left), the post-synthetic modification methods (middle), and metal nanoparticles (MNPs) embedded in the cavities (right) of MOFs.

### 1.3 Characterization and Evaluation Methods of MOFs as Heterogeneous Catalysts

To obtain stable and porous multifunctional materials suitable for catalysis is one of the goals of MOFs design and synthesis. When evaluating the potential of a given MOF structure as heterogeneous catalyst, a main point is to confirm its stability and porosity under reaction conditions. All the factors involved in the reaction system, such as external drive conditions (magnetic stirring, electric stirring, microwave heating, etc.), solvent, temperature, time, pH, environment (inert gas and vacuum conditions) and so on, may affect the stability of the catalyst, despite the fact that some catalysts whose structures have changed or collapsed after catalytic reactions can regain the original model through certain methods. Analytical methods that are useful and applicable in MOF catalysis are simply listed but not limited below.

- 1) Thermogravimetric analysis (TGA) is frequently used to determine the thermal stability of MOF catalysts before catalysis. It is helpful to choose a suitable model reaction.
- 2) Powder X-ray diffraction (XRD) patterns reflect the crystallinity of the MOF catalyst. By comparing the PXRD patterns of the MOF catalyst after catalysis with those of the fresh sample, we can determine whether the integrity of the MOF catalyst is maintained.
- 3) Automatic gas absorption analyzer can test the absorption capability of the catalyst for a certain gas or vapor. Based on the adsorption and desorption isotherms, the surface area and pore size distribution can be evaluated. However, once the cavities or the windows of the pore of MOF catalyst were blocked by substrates or products, the surface area might be largely reduced.
- 4) Scanning electron microscope (SEM) and transmission electron microscope (TEM) are able to picture the morphology and sizes of the MOF catalyst before and after catalysis. In some cases, even the crystallinity and porosity of the MOF catalyst could be identified.
- 5) X-ray photoelectron spectroscopy (XPS) is a useful surface quantitative spectroscopic technique that measures the elemental composition, chemical state and electronic state of the atoms in the MOF catalyst before and after catalysis.
- 6) Energy-dispersive X-ray (EDX) spectroscopy is another analytical technique used for the elemental analysis or chemical characterization of the MOF catalyst. It also can provide evidence whether the substrate or product had been adsorbed in the MOF through the appearance of new elements after catalysis.
- 7) Inductively coupled plasma optical emission spectrometry (ICP-OES), atomic absorption spectroscopy (AAS) and X-ray fluorescent spectroscopy (XFS) are used for the detection and quantitative determination of trace metal

- elements in MOF catalyst, as well as for testing whether metal species have been leached from the solid catalyst to the solution during the reaction.
- 8) The UV-Visible diffuse reflectance spectrum can tell the information of the coordination environment of the metal before and after catalysis.
  - 9) Infrared spectroscopy (IR) can afford information about the adsorbed substrate or product in the MOF catalyst after catalytic reactions.
  - 10) Nuclear magnetic resonance (NMR) is the most frequently used technique to characterize reactant, product, byproduct, as well as intermediate. It also can help measure selective adsorption of the catalyst towards substrates if possible.
  - 11) Gas/liquid chromatography–mass spectrometry (GC/LC-MS) are the powerful methods to monitor the catalytic reaction and identify the product. For asymmetric reaction, chiral column may be needed to separate the enantiomers.
  - 12) Hot filtration test functions as a control experiment to compare catalytic activity before and after filtering the hot active catalyst solution to determine if any homogeneous species is involved.

#### 1.4 Scope of This Review

Excellent review articles dealing with catalytic applications of MOFs are already available.<sup>11–27</sup> The very early review in this area was presented in 2009 by Farrusseng, who gathered the early examples of MOF catalysis that was focused on the intrinsic activity of MOFs, e.g. the Lewis acidity or redox of the metal nodes, and the potential Lewis basicity of the functional groups such as amide and amino groups in the organic linkers.<sup>11</sup> In the first *Chemical Society Reviews* MOF Themed Issue (2009), Hupp for the first time presented the review discussing the functions of different parts of MOFs (e.g. metal nodes, organic linkers and cavities), exemplified by a selected fraction of published works.<sup>12a</sup> A more detailed review talking about the three major parts acting as the active sites was shown in 2010 by Corma, and one of distinguished features of this review lies in their strong attention to the catalytic reactions (e.g. hydrogenation, oxidation, CO oxidation, cyanosilylation, hydrodesulfurization and photocatalysis) that the metal nodes can take part in.<sup>13</sup> Besides these three reviews, García<sup>14a–c</sup>, Ahn<sup>15</sup> and De Vos<sup>16</sup> reported their understanding about intrinsic catalysis exhibited by CUMs, Lin,<sup>17</sup> Kim<sup>18</sup> and Kaskel<sup>19</sup> demonstrated applications of homochiral MOFs in asymmetric catalysis, Hupp<sup>2b</sup> discussed catalysis at the organic ligands in detail, Fischer<sup>20</sup>, García<sup>14d</sup>, Gascon<sup>21a</sup> and Juan-Alcañiz<sup>21b</sup> presented MOFs as hosts for the encapsulation of active species. More recently, Zhou<sup>22a</sup> and Wu<sup>22b</sup> reviewed the applications of MOFs as biomimetic catalysts, Lin<sup>17</sup> and García<sup>14e</sup> introduced the advances in photocatalysis by MOFs, and Llabrés i Xamena<sup>21c</sup> and Gascon<sup>21d</sup> summarizes the strengths and weaknesses of MOFs as heterogeneous catalysts.

The main body of this review describes catalytic applications of MOFs that are subdivided into four classes according to the catalytic sites: coordinatively unsaturated metal sites (CUMs),<sup>23–53</sup> metalloligands,<sup>54–61</sup> functional organic sites (FOS),<sup>62–81</sup> as well as metal nanoparticles (MNPs) embedded in the framework cavities (MNPs@MOFs).<sup>82–95</sup> Each classification has been further organized in light of metals, metalloligands or organic groups by collecting relevant catalytic reactions. We hope this will help readers to grasp a general but in-depth overview of MOF catalysis. Due to limited space, we only concisely introduce fast-moving advances in photo- and biomimetic catalysis with MOFs as heterogeneous

catalysts in this review,<sup>14e,17c,22</sup> because excellent reviews on these state-of-art topics just appeared, which are highly recommended to readers due to their close pertinence to supramolecular catalysis. Concerning the catalytic MOFs with CUMs, they are introduced to the reader by sorting these MOFs according to the metals that provide the CUMs. We have discussed syntheses, structures (especially the channels and surfaces), and catalytic applications of MOFs built on with a range of metal ions (e.g. Cr<sup>3+</sup>, Fe<sup>3+</sup>, Al<sup>3+</sup>, Sc<sup>3+</sup>, V<sup>4+</sup>, Mn<sup>2+</sup>, Co<sup>2+</sup>, Cu<sup>2+/1+</sup>, Zn<sup>2+</sup>, Ag<sup>+</sup>, Mg<sup>2+</sup>, Zr<sup>4+</sup>, Pd<sup>2+</sup>, Ce<sup>4+</sup> and Bi<sup>3+</sup>). As for the MOFs showing versatile catalytic reactions or investigated under varied conditions, such as MIL-101(Cr), we try to collect their catalytic applications, and put them together for better comparison. Considering the MOFs constructed with metalloligands, two typical kinds of metalloligands, namely metalloporphyrin and metallosalen, are selected and discussed. As for catalytic MOFs incorporated/immobilized with FOS, they are presented in line with the functional groups, such as pyridyl, amide, amino, sulfoxy, pyrrolidine, carbene, urea and bipyridyl. In addition, PSM MOFs through complexation of some FOS (e.g. amino, bionol, bipyridyl and catechol) with catalytically active metal complexes have also been presented. In the section of MNPs@MOFs, syntheses and catalytic applications of Cu@MOF, Ru@MOF, Au@MOF, Pd@MOF and Pt@MOF have been discussed. Different approaches of loading MOFs with metal complex precursors are compared. As for the same metal nanoparticles embedded, different choices of MOF hosts are displayed. Emphasis is placed on the micro structural characterization of the MNPs@MOFs with a particular focus on the sizes of embedded nanoparticles using TEM methods. It should be noted here that, various other hybrid MOFs materials, including those incorporated with catalytically active polyoxometalates (POMs) and simple metal complexes in molecular level inside the MOF pores,<sup>22c–g</sup> have also been vigorously studied. The host-guest adaptability and catalytic synergist/selectivity are inherent in these hybrid MOFs systems for supramolecular catalysis, however, could not fit into the scope of this review.

Our review herein is also organized and written on the basis of our interests in the development of MOF catalysts from different research groups. By putting together the same group's works, the readers might have a better view of the rapid development in the past ten years, especially since 2009, when researchers on other fields such as organic methodology started to show their interests to explore catalytic applications of MOFs. From then on, the chosen reactions for tests are leading to the formation of more valuable products. We tried our best to cover as wide and updated works as possible in this review; however, it is no doubt that some wonderful works have been missed, since we are intended to sort out the relevant research lines but not to give a comprehensive literature collection.

In this review, all of the data with regard to heterogeneity and size-/shape-selective catalysis along with the porous structures (dimensionality and pore size) have been gathered and demonstrated to the reader. As in any use of MOFs in catalysis, the key points to be addressed are their activity, stability and selectivity under the reaction conditions. The stability of the material can be addressed by checking whether the frameworks retain after catalytic reactions, as well as performing analysis of the solutions with the removal of the solid catalysts. Porous MOFs can behave as size-/shape-selective catalysts due to the potential that the substrates might enter the channels and then undergo reactions in the cavities. Tests about the selective catalysis have been introduced

wherever possible to demonstrate such supramolecular feature of MOF catalysis under heterogeneous conditions. One last but not least feature of this review, we make the figures informative to indicate the MOFs' syntheses, structures and catalytic applications, which help readers to have a straightforward but all-around view of MOF supramolecular catalysis.

## 2. MOFs with Coordinatively Unsaturated Metal Site (CUMs)

The introduction or incorporation of coordinatively unsaturated metal sites (CUMs) into porous MOFs is very beneficial since CUMs can strongly interact with organic molecules in catalysis. For example, it has been found that CUMs can offer a promising tool to induce regioselectivity and shape-/size-selectivity towards guest molecules or reaction intermediates in catalytic reactions because of the regular arrangements and well-understood surrounding environments of the metal centers in the MOF pore channels. It is the CUMs on the pore surface, rather than those on the crystal surface, endow the MOF catalysts with supramolecular sense by involving porous microenvironments of specific host-guest and stereochemical features in the catalytic reactions. These characteristics make the MOFs advantageous compared to the catalytic properties of other porous materials such as inorganic zeolites and mesoporous materials. A broad range of metal ions (e.g.  $\text{Cr}^{3+}$ ,  $\text{Fe}^{3+}$ ,  $\text{Al}^{3+}$ ,  $\text{Sc}^{3+}$ ,  $\text{V}^{4+}$ ,  $\text{Mn}^{2+}$ ,  $\text{Co}^{2+}$ ,  $\text{Cu}^{2+/1+}$ ,  $\text{Zn}^{2+}$ ,  $\text{Ag}^+$ ,  $\text{Mg}^{2+}$ ,  $\text{Zr}^{4+}$ ,  $\text{Pd}^{2+}$ ,  $\text{Ce}^{4+}$  and  $\text{Bi}^{3+}$ ) can be members of CUMs.<sup>23-53</sup> A selection of MOFs containing CUMs is listed in Table 1. For example, a series of MILs (MIL for materials of institute Lavoisier), such as MIL-101(Cr)<sup>23-26</sup>, MIL-100(Fe)<sup>27-28</sup>, MIL-53(Al)<sup>29</sup>, MIL-100(Sc)<sup>30</sup> and MIL-47(V)<sup>31</sup>, have been shown to catalyze a wide variety of organic reactions, concentrating on the Lewis acid catalyzed reactions or oxidation reactions. Among the plentiful transition metal ions that are able to build up MOFs,  $\text{Mn}^{2+}$ ,  $\text{Co}^{2+}$ ,  $\text{Cu}^{2+/1+}$ ,  $\text{Zn}^{2+}$ , and  $\text{Ag}^+$  represent the most commonly used ions with the frameworks exhibiting excellent catalytic performances in a variety of valuable reactions, including Mukaiyama-aldol reaction, cycloaddition of  $\text{CO}_2$  and styrene epoxide, cyclopropanation of olefins, Friedländer reaction, the Pechmann condensation, Biginelli reaction, Henry reaction, 1,3-dipolar cycloaddition of azides and alkynes, three-component coupling of amines, aldehydes and alkynes, as well as three-component coupling of azides, alkynes and amines.<sup>31-48</sup> Moreover, a series of homochiral MOFs containing CUMs have been successfully synthesized and employed in asymmetric catalysis. For example, homochiral MOFs of  $\text{Zn}_3(\text{chirbtb-1})_2$  and  $\text{Zn}_3(\text{chirbtb-2})_2$  was found to catalyze Mukaiyama aldol reaction with good yields and modest *ee* values,<sup>46</sup> Ag-tpha-based materials can catalyze the 1,3-dipolar cycloaddition of methyl-2(benzylideneamino)-acetate and *N*-methylmaleimide, yielding cycloadduct with remarkable *ee* values (up to 90% *ee*),<sup>48</sup> and Ce-mdip1 and Ce-mdip2 can catalyze the cyanosilylation reactions of aromatic aldehydes and cyanotrimethylsilane to achieve high conversion (> 95%) in 24 h and excellent *ee* (up to 98% *ee*).<sup>52</sup>

### 2.1 MILs with High Valent Metal Ions (Cr, Fe, Al, Sc, V)

**MIL-101(Cr).** In 2005, Férey et al. reported the synthesis of the famous chromium terephthalate, MIL-101(Cr) with the formula of  $\text{Cr}_3\text{X}(\text{H}_2\text{O})_2\text{O}(\text{bdc})_3$  ( $\text{X} = \text{F}, \text{OH}$ ;  $\text{bdc} = 1,4$ -benzenedicarboxylate), whose framework was made of trimeric chromium(III) octahedral clusters interconnected by 1,4-benzenedicarboxylate anions containing removable terminal

water molecules.<sup>23a</sup> MIL-101(Cr) has two kinds of quasispherical cages with free internal diameters of ca. 29 and 34 Å, accessible through microporous windows of ca. 12 and 16 Å. It has huge BET and Langmuir surface areas ( $4100 \pm 200 \text{ m}^2 \text{ g}^{-1}$ ;  $5900 \pm 300 \text{ m}^2 \text{ g}^{-1}$ ). After removal of terminal water molecules, MIL-101(Cr) possesses potentially catalytic CUMs, and therefore can be applied in various reactions. Indeed, CUMs of MIL-101 were found to be active in cyanosilylation of aldehydes, oxidation of hydrocarbons and sulfides, and cycloaddition of  $\text{CO}_2$  to the organic epoxides (Fig. 5).

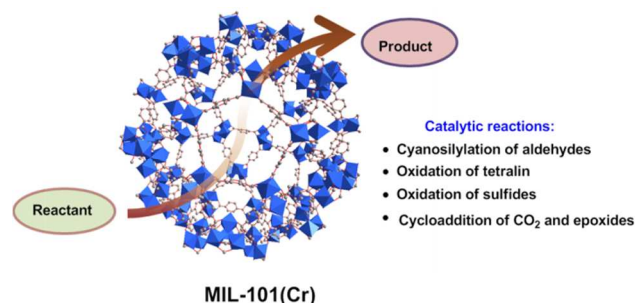


**Fig. 5** Ball-and-stick view of MIL-101(Cr) and illustration of its catalytic applications. The Cr atoms are shown in blue polyhedral.

To evaluate the catalytic activity of MIL-101(Cr), Kaskel et al. used the cyanosilylation of aldehydes as a test reaction.<sup>23b</sup> MIL-101(Cr) displayed an excellent activity towards the addition of trimethylsilylcyanide (TMSCN) to benzaldehyde. The framework of MIL-101(Cr) was intact after usage as a catalyst, verified by the powder X-ray diffraction (XRD) patterns of the catalyst after cyanosilylation. To prove the heterogeneity of the reaction, the catalyst was filtered off after 15 min of reaction, and stirring of the filtrate was continued at the same reaction temperature. Neither additional benzaldehyde was consumed nor was product formed after filtration. Recycling test showed that the conversion of the product didn't reduce remarkably in the second and third run.

Ahn et al. employed MIL-101(Cr) in selective oxidation of tetralin to 1-tetralone using *tert*-butylhydroperoxide (TBHP) or acylperoxy radicals generated in situ from trimethylacetaldehyde and  $\text{O}_2$  as oxidants.<sup>23c</sup> They found that both systems can afford 1-tetralone in high yields and selectivity. The authors checked the heterogeneity of MIL-101(Cr) catalyst. The hot filtration experiment showed that the reaction in the filtrate proceeded with much slower conversion of tetralin than in the presence of catalyst. ICP-MS also suggested that only a trace amount of chromium leached to the solution (0.12 ppm). Furthermore, MIL-101(Cr) catalyst can be recycled and reused for 5 times with the identical catalytic activity and selectivity. Powder XRD patterns of the fresh catalyst and that after the fifth cycle confirmed the structural integrity of MIL-101 during the reaction. The UV-visible diffuse reflectance spectrum of the solid catalyst after reuse was also indistinguishable from that of the fresh dry catalyst, suggesting that no change in the coordination environment of the Cr(III) centre took place during the catalytic reaction. Alternatively, Chang and Kim et al. reported that MIL-101(Cr) was catalytically active in the oxidation reactions of aryl sulfides to selectively produce the corresponding sulfoxides in the presence of hydrogen peroxide.<sup>24</sup>

The potential of MIL-101(Cr) as a heterogeneous catalyst for the oxidation of alkenes, such as cyclohexene (CyH),  $\alpha$ -pinene

and limonene, has been explored by Kholdeeva et al. using TBHP as oxidant. They found that the main oxidation products were the corresponding  $\alpha,\beta$ -unsaturated ketones.<sup>25</sup> The MIL-101(Cr) catalyst didn't lose its activity and selectivity after at least five catalytic cycles of CyH oxidation with TBHP. The powder XRD study confirmed the preservation of the MIL-101(Cr) structure after catalytic reactions. The hot catalyst filtration test revealed no further substrate conversion in the filtrate after removal of the catalyst. A trace amount of chromium (<1 ppm) was determined in the filtrate by ICP-AES.

The application of MIL-101(Cr) in solvent-free coupling of CO<sub>2</sub> and epoxides to produce cyclic carbonates was reported by Zalomaeva et al.<sup>26</sup> They found that MIL-101(Cr) can promote the reaction at both high-pressure (100 atm CO<sub>2</sub>) and low-pressure (8 atm CO<sub>2</sub>) conditions in the temperature range of 25–120 °C. After optimization, it was found that the presence of tetrabutylammonium bromide (TBABr) as co-catalyst could largely accelerate the cycloaddition reaction. Heterogeneous nature of catalysis was proved by hot catalyst filtration test, and no further substrate conversion in the filtrate occurred after catalyst removal at the reaction temperature. However, the catalytic activity tends to decrease after several reuses. Partial regeneration of the catalyst is possible through treatment with hot DMF before use in the next catalytic run.

**MIL-100(Fe).** Serre et al. reported the synthesis and structure determination of MIL-100(Fe) with the formula of Fe<sub>3</sub>F(H<sub>2</sub>O)<sub>2</sub>O(btc)<sub>2</sub> (1,3,5-btc = benzene tricarboxylic or trimesic acid), which possess two types of mesoporous cages of free apertures of ca. 25 and 29 Å, accessible through microporous windows of ca. 5.5 and 8.6 Å.<sup>27</sup> The permanent porosity of this porous solid was measured by N<sub>2</sub> adsorption experiments performed in liquid nitrogen, revealing an adsorption isotherm characteristic of microporosity. The thermal stability of MIL-100(Fe) has been determined by X-ray thermogravimetry to be up to 270 °C. The catalytic activities of MIL-100(Fe) were studied by the same group for the first time. They examined its catalysis in Friedel-Crafts benzylation of benzene by benzyl chloride (Fig. 6), and found that MIL-100(Fe) could afford diphenylmethane with high activity and selectivity (nearly 100%) after a short induction period (5 min).

In Garcia's group, MIL-100(Fe) has been extensively used for catalytic reactions such as benzylic oxidation using *tert*-butylhydroperoxide (TBHP), ring-opening of styrene oxide with alcohols, Claisen Schmidt condensation reaction, aerobic oxidation of thiophenol to diphenyldisulfide, and the isomerization of  $\alpha$ -pinene oxide.<sup>28</sup> In all kinds of the reactions examined, MIL-100(Fe) could be recycled with no significant loss of catalytic efficiency and crystallinity in subsequent runs.



**Fig. 6** Ball-and-stick view of MIL-100(Fe) and illustration of its catalytic applications. The Fe atoms are shown in pink polyhedral.

**MIL-53(Al).** The well-known and vigorously investigated Al-containing porous framework, MIL-53(Al) (Al<sub>2</sub>(bdc)<sub>3</sub>), was also developed by Férey's group.<sup>29a</sup> The crystal structure of MIL-53(Al) is constructed from corner sharing octahedral Al<sup>3+</sup> ions linked by bdc ligands. MIL-53(Al) has the pore dimension of 8.5 Å with good thermal stability and BET surface area of 1140 m<sup>2</sup>g<sup>-1</sup> in its dehydrated and large pore form.

Garcia et al. applied MIL-53(Al) as heterogeneous catalyst for hydrazine-mediated hydrogenation (Fig. 7).<sup>29b</sup> Both of terminal and internal olefins can be reduced in this catalytic system, giving rise to the corresponding alkanes with high conversion and selectivity (99-100%). The reusability of MIL-53(Al) was investigated, showing a gradual decrease in the styrene percentage conversion upon reuse. The powder XRD patterns of the reused MIL-53(Al) sample in four consecutive hydrogenation reactions of styrene to ethylbenzene matched with those of the fresh catalyst, suggesting that the crystallinity of MIL-53(Al) was preserved during the course of the reactions.

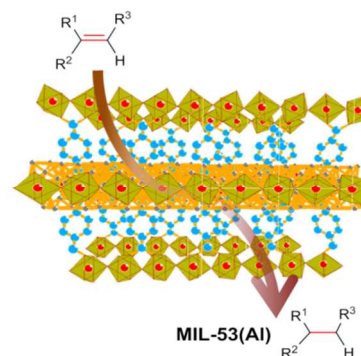


**Fig. 7** Ball-and-stick view of MIL-53(Al) and illustration of its catalytic application in reduction of carbon-carbon multiple bonds. AlO<sub>4</sub>(OH)<sub>2</sub> is shown in yellow polyhedra.

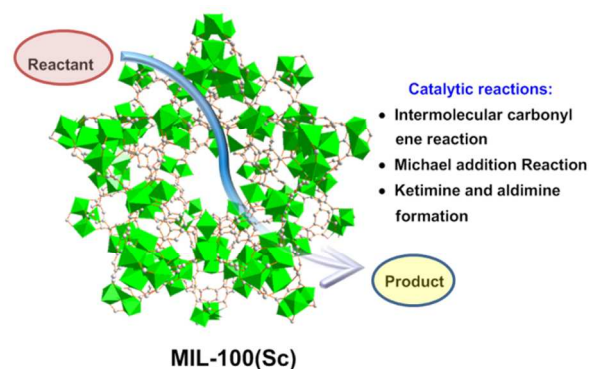


**Fig. 8** Ball-and-stick view of MIL-100(Sc) and illustration of its catalytic applications. The Sc atoms are shown in bright green polyhedral.

**MIL-100(Sc).** Wright et al. have reported the synthesis of a range of porous scandium carboxylate MOFs with structures analogous to those of MIL-88, MIL-100 and MIL-101 containing different trivalent metals (such as Cr and Fe). The large pore scandium trimesate MIL-100(Sc)

( $\text{Sc}_3(\text{OH})(\text{H}_2\text{O})_2\text{O}(\text{btc})_2$ ) was prepared using the 1,3,5-benzenetricarboxylic acid at 293 K in DMF.<sup>30a</sup> MIL-100(Sc) contains two types of supercages of free apertures of ca. 25 and 30 Å, accessible through microporous windows of ca. 5 and 9 Å. The scandium in  $\text{Sc}_3\text{O}(\text{BTC})_2(\text{OH})(\text{H}_2\text{O})_2$  trimers of MIL-100(Sc) can lose coordinated water to leave five-fold coordinated scandium cations, acting as the strong Lewis acid catalytic sites. Clarke and Wright et al. then applied MIL-100(Sc) in a series of C–C bond forming reactions,<sup>30b</sup> including (i) the intermolecular carbonyl ene reaction of nucleophilic alkenes and electron-poor aldehydes, (ii) a Friedel–Crafts type Michael addition between electron-rich heterocycles and electron-deficient alkenes, and (iii) ketimine and aldimine formation (Fig. 8). In each of these reactions, MIL-100(Sc) was both catalytically active and selective. Filtration experiments and recycle tests confirmed that the catalytic reactions over MIL-100(Sc) were preceded in a heterogeneous way.

**MIL-47(V).** An V(IV)-based MOF MIL-47(V) with the formula of  $\text{V}^{\text{IV}}\text{O}(\text{bdc})$  has been prepared by Férey et al.<sup>31a</sup> MIL-47(V) consists of a porous terephthalate framework built from infinite chains of  $\text{V}^{\text{IV}}\text{O}_6$  octahedra and has a three-dimensional (3D) orthorhombic structure, exhibiting large pore ( $10.5 \times 11.0 \text{ \AA}^2$ ) in the [100] direction. The measured BET and Langmuir surface area are 930(30) and 1320(2)  $\text{m}^2\text{g}^{-1}$ , respectively.

Van Der Voort and Van Speybroeck et al. investigated the catalytic activity of MIL-47(V) in the liquid phase oxidation of cyclohexene (Fig. 9).<sup>31b-c</sup> The catalytic performance of MIL-47(V) in the water and water-free media using TBHP/water and TBHP/decane as oxidant, respectively, has been examined. The major oxidized products were cyclohexene oxide, cyclohexane-1,2-diol, tert-butyl-2-cyclohexenyl-1-peroxide and 2-cyclohexen-1-one, and the conversions were around 80% at the end of the reaction. If the oxidant TBHP was dissolved in water, a significant leaching of V-species into the solution was observed. If, however, the oxidant was dissolved in decane, leaching was negligible and the structural integrity of the MIL-47(V) was maintained during successive runs.

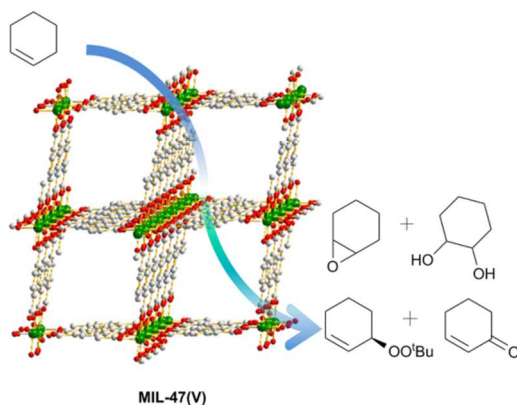


**Fig. 9** Ball-and-stick view of MIL-47(V) and illustration of its catalytic application in oxidation of hydrocarbons. The Co atoms are shown in sea green.

## 2.2 MOF with Commonly Used High Valent Metal Ions (Mn, Co, Cu, Zn, Ag)

**Mn-MOFs.** Long et al. reported the synthesis and crystal structure of  $[\text{Mn}(\text{DMF})_6]_3[(\text{Mn}_4\text{Cl})_3(\text{btt})_8(\text{H}_2\text{O})_{10}]_2$  ( $\text{H}_3\text{btt} = 1,3,5\text{-benzenetristetrazol-5-yl}$ ), obtained from the solvothermal

reaction of  $\text{MnCl}_2$  and  $\text{H}_3\text{btt}$ .<sup>32a</sup> The desolvated form of the compound,  $\text{Mn}_3[(\text{Mn}_4\text{Cl})_3(\text{BTT})_8(\text{CH}_3\text{OH})_{10}]_2$  (Mn-btt), was generated by heating the methanol exchanged crystals at 150 °C under dynamic vacuum for a minimum of 2 h. The X-ray single crystal diffraction revealed a cubic structure in which chloride-centered square-planar  $[\text{Mn}_4\text{Cl}]^{7+}$  units are linked via  $\text{btt}^{3-}$  ligands to form the anionic, 3D framework, containing 7 and 10 Å pores that affords a BET surface area of 2100  $\text{m}^2\text{g}^{-1}$ .  $\text{Mn}^{2+}$  ions were exposed on the surface of the framework, which might serve as potent Lewis acid sites.

They then applied Mn-btt MOF in the cyanosilylation and Mukaiyama-aldol reaction (Fig. 10).<sup>32b</sup> Cyanosilylation of carbonyl-functionalized organic substrates can lead to the formation of cyanohydrins, which are key derivatives in the synthesis of pharmaceuticals. In addition, cyanosilylation can undergo in mild reaction conditions (room temperature). Actually, cyanosilylation of aldehyde has now become a typical reaction to test the Lewis acidity catalysis of CUMs in MOFs. The Mn-btt-catalyzed cyanosilylation of benzaldehyde led to a 98% conversion after 9 h. Meanwhile, the Mukaiyama-aldol reaction between benzaldehyde and methyltrimethylsilyldimethylketene acetal led to aldol product with 63% yield after 99 h. To probe whether the cyanosilylation reaction occurred inside the pores or on the surface of catalyst, substrates 1-naphthaldehyde ( $9.7 \times 8.4 \text{ \AA}^2$ ), 4-phenoxybenzaldehyde ( $13.3 \times 7.3 \text{ \AA}^2$ ) and 4-phenylbenzaldehyde ( $13.1 \times 6.7 \text{ \AA}^2$ ) with increasing molecular dimension were tested, offering corresponding cyanosilylates in 90, 19 and 18%, respectively. The size-selectivity effect suggested that the catalytic reactions might occur in the pores of MOF catalyst. In addition, infrared spectroscopy of the catalyst impregnated with an aliquot of the reaction solution revealed two C–O stretches at 1698 and 1686  $\text{cm}^{-1}$ , corresponding to free and  $\text{Mn}^{\text{II}}$ -bound benzaldehyde, respectively, confirming that activation of the substrate occurred at the unsaturated  $\text{Mn}^{\text{II}}$  sites within the MOF pores.



**Fig. 10** Space-filling view of Mn-btt and illustration of its synthesis and catalytic application in cyanosilylation of aldehydes. The Mn and Cl atoms are shown in orange and bright green, respectively. Hydrogen atoms and the bound MeOH molecules are omitted for clarity.

Wu et al. reported the synthesis and catalytic behaviors of a 3D supramolecular network of  $[\text{Mn}_2(\text{pvia})_2(\text{H}_2\text{O})_2] \cdot 3\text{H}_2\text{O}$  (Mn-pvia,  $\text{H}_2\text{pvia} = E\text{-}5\text{-}(2\text{-}(\text{pyridin-}4\text{-yl)vinyl) \text{isophthalic acid}}$ ) with cavity dimensions of  $7.8 \times 8.9 \text{ \AA}^2$ .<sup>33</sup> The phenylmethanol oxidation was chosen as the model reaction to test the catalytic activity of the desolvated Mn-pvia. The catalytic experiment was performed in acetonitrile at 60 °C with  $\text{NaIO}_4$  as the oxidant and in the presence of the desolvated MOF ambient light. After 18 h, the oxidation product was identified as benzaldehyde in 64% yield.

**Co-MOFs.** Two pyrazolate-based Co-MOFs of  $[\text{Co}^{\text{II}}_4\text{O}(\text{bdpb})_3]$  (MFU-1,  $\text{H}_2\text{bdpb} = 1,4\text{-bis}[(3,5\text{-dimethylpyrazol-4-yl})\text{-benzene}]$ ) and  $[\text{Co}^{\text{II}}(\text{bdpb})]$  (MFU-2), were prepared by Volkmer from the solvothermal reactions of  $\text{H}_2\text{bdpb}$  with  $\text{CoCl}_2$  or  $\text{Co}(\text{NO}_3)_2$ , respectively.<sup>34</sup> The framework of MFU-1 has 3D intersecting channels with an equivalent diameter of 18.1 Å,<sup>34a</sup> whereas the framework of MFU-2 contains quadratic tunnels with the diagonal length of 18.6 Å along the *c* axis. Both of MFU-1 and MFU-2 contain redox-active  $\text{Co}^{\text{II}}$  centers, making them the potentially redox catalysts.<sup>34b</sup> The variable-temperature XRD patterns indicate that the MFU-1 and MFU-2 frameworks were stable up to 270 and 300 °C, respectively, withstanding complete removal of solvent molecules.

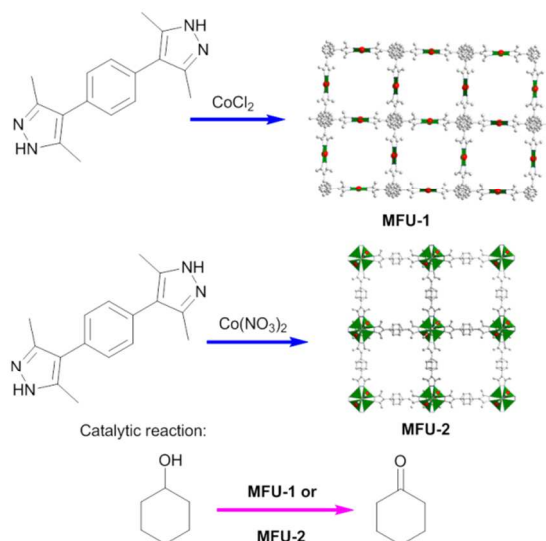


**Fig. 11** Ball-and-stick view of MFU-1 and MFU-2, and illustration of their synthesis and catalytic application in oxidation of hydrocarbons. The Co atoms are shown in red.

To investigate the catalytic activities, the authors employed MFU-1 and MFU-2 in the liquid-phase oxidation of cyclohexene using TBHP as oxidant (Fig. 11). The maximum cyclohexene conversion after 22 h for MFU-1 and MFU-2 were 27.5 and 16%, respectively, and the main reaction products in both of the MOF catalysts were *tert*-butyl-2-cyclohexenyl-1-peroxide, followed by 2-cyclohexen-1-one and cyclohexene oxide. To confirm the heterogeneous nature of the catalytic reaction, the authors performed hot-filtration experiments. Upon reaching a substrate conversion of approximately 50%, the catalyst particles were removed from the hot solution. The filtrate obtained from the test run containing MFU-1 showed no significant catalytic conversion upon catalyst removal, indicating that contributions of soluble species towards catalytic activity were negligible. In contrast, the filtrate from a reaction mixture containing MFU-2 showed only a slightly diminished activity. The different behavior of two MOFs in hot filtration experiments indicated that MFU-1 act as a truly heterogeneous catalyst, whereas the catalytic activity of MFU-2 was mostly due to soluble metal complexes leaching from the framework under catalytic conditions. MFU-1 can be almost completely recovered from the reaction vessel and reused in several catalytic runs. Although there was a loss (around 3%) of catalytic activity after the first run, no further loss in catalytic activity was observed in subsequent runs.

Dietzel and co-workers prepared Co-MOF-74 (also known as CPO-27-Co) with formula  $\text{Co}_2(\text{dhdhc})(\text{H}_2\text{O})$  ( $\text{H}_2\text{dhdhc} = 2,5\text{-dihydroxyisophthalic acid}$ ).<sup>35a</sup> The crystal structure of MOF-74 was built around a 1D honeycomb motif with pores of 11–12 Å diameter. The CUMs in Lewis acidity could be developed upon removal of the solvent molecules attached to the metal sites by heating in vacuum.

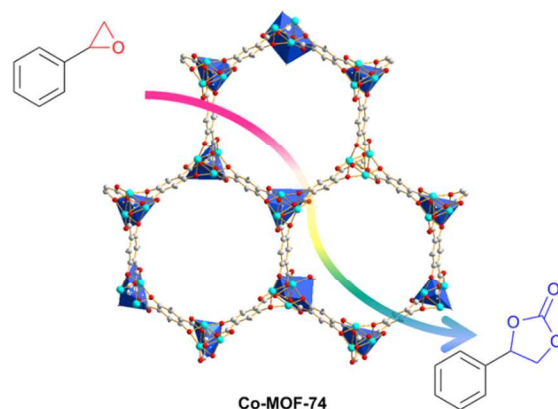


**Fig. 12** Ball-and-stick view of Co-MOF-74 and illustration of its catalytic application in cycloaddition of  $\text{CO}_2$  and epoxides. The Co atoms are shown in light blue polyhedral.

The heterogeneous catalysis of Co-MOF-74 for the cycloaddition of  $\text{CO}_2$  and styrene epoxide was evaluated by Ahn et al (Fig. 12).<sup>35b</sup> Co-MOF-74 catalysts can be reused several times with retention of high catalytic activity with 95% conversion. This result is remarkable since  $\text{CO}_2$  capture has become a worldwide focus because of greenhouse effect. Cycloaddition of  $\text{CO}_2$  and epoxides can transform gaseous  $\text{CO}_2$  to useful cyclic carbonates. Therefore, this reaction has become very popular in MOF catalysis, especially interesting when the porous MOFs have exhibited good  $\text{CO}_2$  adsorption capabilities, and then the reaction might undergo in the cavities.

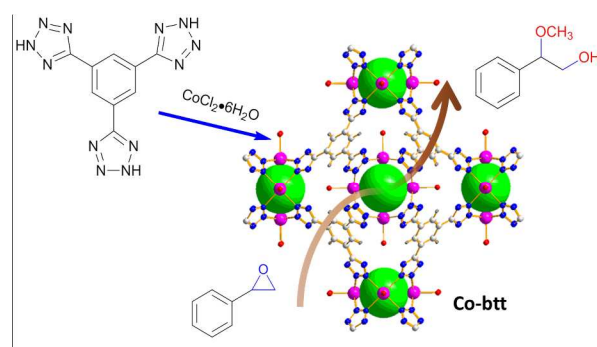


**Fig. 13** Ball-and-stick view of Co-btt and illustration of its synthesis and catalytic application in ring opening of epoxides. The Co and Cl atoms are shown in pink and bright green, respectively.

Stock et al discovered one microporous MOF Co-btt with the formula of  $[\text{Co}(\text{DMA})_6]_3[(\text{Co}_4\text{Cl})_3(\text{btt})_8(\text{H}_2\text{O})_{12}]_2 \cdot 12\text{H}_2\text{O}$  from the solvothermal reaction of  $\text{CoCl}_2 \cdot 6\text{H}_2\text{O}$  and  $\text{H}_3\text{btt}$  in an amide solvent DMA.<sup>36</sup> Co-btt adopts a porous 3D framework of 10.9 and 15.6 Å pores constructed of square-planar  $[\text{Co}_4\text{Cl}]^{7+}$  units interconnected by triangular tritopic  $\text{btt}^{3-}$  bridging ligands. The temperature-dependent XRD analysis showed that the as-synthesized Co-btt was stable up to 350 °C. Co-btt possesses

potentially Lewis acid sites as well as redox-active Co sites. Inspired by the rather high thermal stability, the authors tested Co-btt's catalytic activities in the ring opening of styrene oxide (Fig. 13). Ring opening of epoxides provides a convenient route to 1,2-diols and  $\beta$ -alkoxyalcohols, which can be assisted by mild Lewis acid such as metal cations. Catalytic results showed that Co-btt performed as a better catalyst than the homogeneous catalyst of  $\text{Co}(\text{NO}_3)_2 \cdot 6\text{H}_2\text{O}$ . To testify the heterogeneity of catalysis, they carried out the hot filtration experiment, finding that after Co-btt catalyst was filtered off at 30% conversion, the solution in the absence of solid didn't yield the ring-opening products any more. Furthermore, Co-btt can be recycled, exhibiting very minor decrease of the conversions upon reuse for the second and third runs.

**Cu-MOFs.** As early as in 1999, Williams et al. reported the synthesis and crystal structure of  $\text{Cu}_3(\text{btc})_2$ , also called HKUST-1 (HKUST for Hong Kong University of Science and Technology).<sup>37a</sup> However, its wide applications in catalysis was not explored until several years later. The structure comprises three types of micropores (9.0, 5.0 and 3.5 Å), displaying a cubic network in which  $\text{Cu}_2$ -clusters are coordinated by carboxylate groups to give a so-called paddle-wheel unit. Two  $\text{Cu}^{2+}$  ions are imposed in the vicinity and the residual axial coordination sites are filled by weakly bound water molecules. These loosely bound water molecules point towards the center of the pore. Removal of the copper-bound water molecules are able to yield CUMs, which can be further applied in catalysis. Concerning its catalytic behaviors,  $\text{Cu}_3(\text{btc})_2$  have been used in cyanosilylation of aldehydes, isomerization of terpene derivatives, cyclopropanation of olefins, the Friedländer condensation, Pechmann condensation, and so on (Fig. 14).

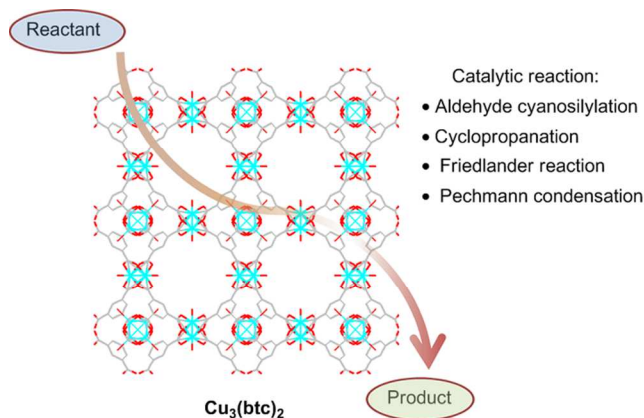


**Fig. 14** Wires and sticks views of  $\text{Cu}_3(\text{btc})_2$  and illustration of its catalytic applications. The Cu atoms are shown in turquoise.

For example, Kaskel et al. used the liquid phase cyanosilylation of benzaldehyde as a test reaction to study selectivity and activity of the porous HKUST-1.<sup>37b</sup> Before the catalytic reactions, the MOF was dehydrated in high vacuum at 373 K in order to remove physically and chemically bound water molecules. Catalytic results showed a cyanosilylation yield of up to 57%. The heterogeneity was proved by filtration experiments at the reaction temperature. Two years later, De Vos et al. found that  $\text{Cu}_3(\text{btc})_2$  can be a highly selective Lewis acid catalyst for the isomerization of terpene derivatives, such as the rearrangement of  $\alpha$ -pinene oxide to campholenic aldehyde and the cyclization of citronellal to isopulegol.<sup>38</sup> The

heterogeneity was also proved by filtration experiments, and  $\text{Cu}_3(\text{btc})_2$  can be used for several runs.

Corma et al. for the first time employed  $\text{Cu}_3(\text{btc})_2$  as catalysts for the cyclopropanation of alkenes with diazoacetates, inducing a carbene transfer reaction from diazo compounds.<sup>39</sup> It is known that in homogeneous catalysis, copper complexes are often applied in carbene formation and transformation process, especially of cyclopropanation with olefins. Moreover, copper complexes have been immobilized in polymers or mesoporous silica such as MCM-41 for heterogeneous catalysis. Corma et al. showed that MOF  $\text{Cu}_3(\text{btc})_2$ , as a heterogeneous catalyst, was active and selective toward the cyclopropanation of alkenes without losing the crystallinity and hence can be reused without further modification. Initially, they studied the reactivity between styrene and ethyl diazoacetate (EDA) in the presence of  $\text{Cu}_3(\text{btc})_2$ . The catalytic reaction yielded cyclopropane with 98% conversion and 71% diastereoselectivity (*trans/cis*). Later, they applied the protocol to other diazo compounds such as ethyl 2-phenyldiazoacetate (PhEDA). The reaction with PhEDA showed much better diastereoselectivity, and only *trans*-diastereoisomer was formed. The crystalline  $\text{Cu}_3(\text{btc})_2$  can be recycled after use. The conversions and yields of the *cis*- and *trans*-cyclopropanation products derived from styrene were maintained within three cycles. A comparison of XRD patterns before and after several reaction runs did not reveal any significant differences. The heterogeneity was confirmed by conventional filtration experiment as well as inductively coupled plasma optical emission spectrometric (ICP-OES) analysis of the filtrate, and little metal leaching was found.

Acting as the efficiently heterogeneous catalyst by  $\text{Cu}_3(\text{btc})_2$  for the Friedländer reaction under mild reaction conditions was discovered by Čejka et al.<sup>40a</sup> The Friedländer reaction between 2-aminobenzophenone and ketone is an important synthesis tool for the formation of quinolone derivations, which can be promoted by both of Bronsted and Lewis acids. MOF  $\text{Cu}_3(\text{btc})_2$  can be recovered after use. XRD evidenced no significant structural changes to  $\text{Cu}_3(\text{btc})_2$  framework after the reaction. They also compared the catalytic activity of  $\text{Cu}_3(\text{btc})_2$  with other heterogeneous catalysts, such as H-BEA and (Al)SBA-15. Under the same experimental conditions, H-BEA and (Al)SBA-15 only yielded the quinolone product in 38 and 36%, respectively, in contrast to 80% conversion over  $\text{Cu}_3(\text{btc})_2$ . In a continuing report, they employed the protocol in the synthesis of polysubstituted quinolines with a wide substrate scope.<sup>40b</sup>

In another report, the same group discovered that  $\text{Cu}_3(\text{btc})_2$  can be also applied to the Pechmann condensation of naphthol and ethyl acetoacetate.<sup>40c</sup> The Pechmann condensation can be used for the synthesis of coumarins, which are important natural substances and have been widely applied in pharmaceutical, agrochemical and fragrance. The condensation was performed under acidic conditions, and almost total transformation of naphthol (93% conversion) to the target product (95% selectivity) was achieved within 20 h. For comparison, the Pechmann condensation with naphthol over BEA and USY zeolites led to the coumarin product in 15 and 23% conversion, respectively. The heterogeneity of the catalysis was also proved by filtration experiments.

Asymmetric catalysis has also been achieved by design of chiral Cu-MOFs. Wu et al. developed a chiral serine-derived ligand (*S*)-3-hydroxy-2-(pyridin-4-ylmethylamino) propanoic acid (papa).<sup>41a</sup> Self-assembly of papa and  $\text{CuCl}_2 \cdot 2\text{H}_2\text{O}$  in a mixed solvent of  $\text{H}_2\text{O}$  and EtOH led to blue crystals of  $\text{Cu}_2(\text{papa})_2\text{Cl}_2$ . The crystal structure is a 3D porous framework containing 1D chiral channels ( $5.1 \times 2.9 \text{ \AA}^2$ ). The cavities are

occupied by water molecule guests, which can be easily removed by heating at 110 °C for several hours. The porous chiral framework of  $\text{Cu}_2(\text{papa})_2\text{Cl}_2$  was maintained after the removal of solvent molecules, and remained stable up to 191 °C. The authors examined the catalytic activities of  $\text{Cu}_2(\text{papa})_2\text{Cl}_2$  in the Biginelli reaction, and addition of Grignard reagent to  $\alpha,\beta$ -unsaturated ketones. The Biginelli reaction is a three-component coupling reaction among ethyl acetoacetate, urea and an aryl aldehyde (e.g. benzaldehyde), catalyzed by Lewis acids such as copper salts, yielding dihydropyrimidinones which are important substances with broad applications in the pharmaceutical industry such as calcium channel blockers and antihypertensive agents. In the presence of  $\text{Cu}_2(\text{papa})_2\text{Cl}_2$ , the Biginelli reaction yielded corresponding dihydropyrimidinone in 90% isolated yield without any enantiomeric excess, whereas 1,2-addition of Grignard reagent gave excellent conversion (up to 98%) as well as good *ee* (up to 99%). The supernatant from  $\text{Cu}_2(\text{papa})_2\text{Cl}_2$  was inactive for neither reaction, which confirmed the heterogeneous behavior of the catalyst system.

Later, this group further reported an interesting 3D MOF  $\text{Cu}_3(\text{pdtc})(\text{pvba})_2(\text{H}_2\text{O})_3$ , which was obtained from the self-assembly of two kinds of pyridine carboxylates pyridine-2,3,5,6-tetracarboxylic acid ( $\text{H}_4\text{pdtc}$ ), (*E*)-4-(2-(pyridin-4-yl)vinyl)benzoic acid (pvba), and  $\text{Cu}(\text{NO}_3)_2$  in a mixed solvent of  $\text{H}_2\text{O}$  and DMF.<sup>41b</sup> The crystal structure showed that pdtc and pvba linked up copper atoms to create a 3D framework with very large 1D opening channels of  $13.8 \times 23.6 \text{ \AA}^2$ , of which one third of the copper sites are exposed on the interior surface, and three of the five copper coordination sites are occupied by volatile water molecules that can be removed with heating. Since the Henry reaction (also referred to as the nitro-aldol reaction), known as one of the most powerful and atom-economic reaction for C-C bond formations with various functionalized structural motifs, can be efficiently promoted by copper complexes, authors evaluate the catalytic activity of this Cu-MOF to the Henry reaction of aromatic aldehydes with nitromethane in solvent free conditions. The reactions generated the corresponding products in excellent yield (up to 85%). The heterogeneity of reactions was confirmed by filtration experiments and the ICP analysis of the filtrate. Only  $6 \times 10^{-3}$  percent of copper ions were released into the solution. Cu-MOF can be simply recovered by filtration, which was subsequently used in the successive five runs without decreasing the catalytic activity. An XRD pattern of the recovered material showed that the structural integrity of the catalyst was maintained during the catalytic process.

A cage-like copper-containing MOF  $\text{Cu}(\text{2-pymo})_2$  (2-pymo = 2-hydroxypyrimidinolate) was obtained by Navarro et al. from the reaction of  $\text{CuX}_2$  salts ( $\text{X} = \text{Cl}, \text{NO}_3$ ) and 2-pymo-HCl in aqueous amine solutions (amine =  $\text{NH}_3, \text{CH}_3\text{NH}_2$ ).<sup>42a</sup> The crystal structure is a distorted 3D sodalite framework, formed by  $\alpha$ -cages accessible through hexagonal windows of about 8 Å. The catalytic activity to 1,3-dipolar cycloaddition reactions ("click" reaction) was demonstrated by Corma et al. for MOF  $\text{Cu}(\text{2-pymo})_2$  (Fig. 15).<sup>42b</sup> The reactions of benzyl azide and phenylacetylene in the presence of  $\text{Cu}(\text{2-pymo})_2$  in ethanol at 70 °C gave the complete conversion of the benzyl azide after 4 h, and yielded the solo 1,4-substituted triazole. After the catalytic reaction, the solid MOF was recovered by filtration and thoroughly washed with ethanol. According to the XRD patterns of  $\text{Cu}(\text{2-pymo})_2$  before and after the catalytic reactions, the crystalline nature of the material was preserved. The Cu-MOF can be reused for at least six consecutive runs without

loss of activity and selectivity. The heterogeneous nature of the catalytic process was demonstrated by a hot filtration test.

Later, the same group found that  $\text{Cu}(\text{2-pymo})_2$  was also an active, stable and reusable solid catalyst for three-component couplings of amines, aldehydes and alkynes to form the corresponding propargylamines (Fig. 15).<sup>42c</sup> After the reaction of propargylamine formation, the solid catalyst was recovered by filtration and washed with dioxane and acetone and dried at room temperature in a desiccator. No significant losses of crystallinity and activity were observed after five runs. No leached Cu was detected in the solution. The hot filtration experiment showed negligible activity in the filtrate.

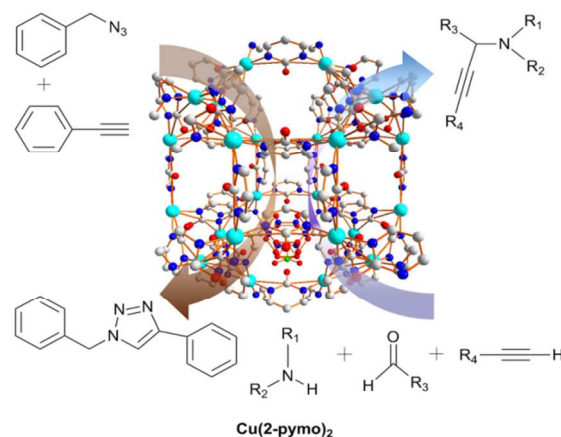


**Fig. 15** Ball-and-stick view of  $\text{Cu}(\text{2-pymo})_2$  and illustration of its catalytic application in click reaction and three-component couplings of amines, aldehydes and alkynes. The Cu atoms are shown in turquoise.

The catalytic activities of the Cu-based MOF in olefin epoxidation reactions was achieved by Jiang et al. with  $\text{Cu}(\text{tcba})(\text{DMA})$  ( $\text{Cu-tcba}$ ,  $\text{tcba} = \text{tris}(4\text{'-carboxybiphenyl)amine}$ ) (Fig. 16).<sup>43a</sup> MOF  $\text{Cu-tcba}$  was obtained from the solvothermal reaction between tcba and  $\text{Cu}(\text{NO}_3)_2$  in DMA and  $\text{H}_2\text{O}$  mixture with 15 drops of 3 M HCl. The crystal structure contains one dimensional channel ( $9.4 \times 9.8 \text{ \AA}^2$ ) in the 3D framework. Desolvated samples have been examined in olefin epoxidation reactions using TBHP as an oxidant at 60°C for 24 h, and the results showed that the epoxide yields were rather high. The heterogeneity of the MOF catalyst has been proved. The matched powder XRD patterns of the used MOF and as-synthesized samples, the negligible loss of copper in the reaction solution, and no further reaction of the filtrate during the filtration experiment all indicated that the desolvated MOF was indeed heterogeneous catalyst.

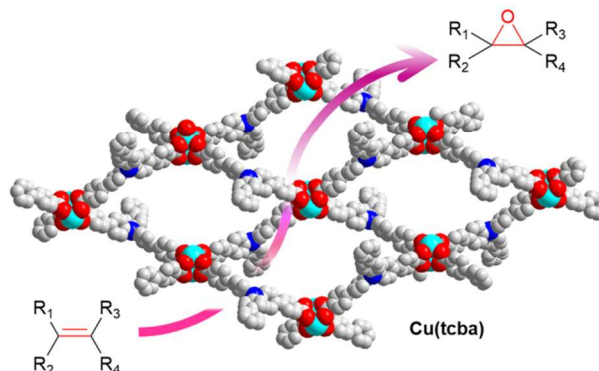


**Fig. 16** Space-filling view of Cu-tcba and illustration of its catalytic application in epoxidation of olefins. The Cu atoms are in turquoise.

Recently, an Cu-MOF  $\text{Cu}_2(\text{bpd})_2(\text{bpy})$  ( $\text{bpd}$  = 4,4'-biphenyldicarboxylic acid;  $\text{bpy}$  = 4,4'-bipyridyl), has been examined in oxidative C-O coupling reactions via C-H activation.<sup>43c</sup> The synthesis and crystal structure of  $\text{Cu}_2(\text{bpd})_2(\text{bpy})$  was reported by James in 2007,<sup>43c</sup> obtained from solvothermal reaction of  $\text{Cu}(\text{NO}_3)_2$ ,  $\text{bpd}$  and  $\text{bpy}$  in DMSO at 125 °C.  $\text{N}_2$  physisorption measurements disclosed that there are three kinds of pores. The pore sizes of two are in the range of 5–15 Å and that of the remaining one is between 15 and 50 Å. Not until in 2013 have Phan et al. examined its catalytic activities.<sup>43b</sup> They found that this Cu-MOF can act as an efficient heterogeneous catalyst for the cross-dehydrogenative coupling reaction of ethers with 2-carbonyl-substituted phenols. The heterogeneity of the catalysis has been confirmed by filtration experiment. In addition, the Cu-MOF catalyst can be recycled and reused for at least 8 runs.

We have developed a series of catalytically active Cu(I)/Cu(II)-MOFs. A robust porous Cu(I)-MOF containing  $\text{Cu}_2\text{I}_2$  subunits,  $\text{Cu}_2\text{I}_2(\text{btp4})$  ( $\text{btp4}$  = benzene-1,3,5-triyl triisonicotinate), was developed as depicted in Fig. 17.<sup>44a</sup> High quality crystals can be readily obtained via the layering of a  $\text{CH}_3\text{CN}$  solution of  $\text{CuI}$  on a  $\text{CHCl}_3$  solution of  $\text{btp4}$ . After thorough structural characterization and gases/vapors adsorption studies of this MOF by means of single-crystal X-ray crystallography, TG and variable-temperature powder XRD, adsorption/desorption isotherms, especially the guest-exchange study through a single-crystal-to-single-crystal manner, we found that MOF  $\text{Cu}_2\text{I}_2(\text{btp4})$  could be a potentially heterogeneous catalysts owing to its large free 1D channels ( $9 \times 12 \text{ \AA}^2$  after considering the van der Waals radii), the ability to facilitate exchange bulky guest molecules, and the availability of coordinatively unsaturated  $\text{Cu}^+$  sites.

Due to its unique feature possessing the  $\text{Cu}_2\text{I}_2$  subunits which are located on the pore surface, we subsequently applied this Cu-MOF in the three-component coupling of sulfonyl azide, alkyne and amine for the first time.<sup>44b</sup> We started the coupling catalysis with tosyl azide ( $\text{TsN}_3$ ). Compared to homogeneous CuI-catalyzed reactions, the  $\text{Cu}_2\text{I}_2(\text{btp4})$ -MOF induced three-component coupling reactions displayed obvious size-selectivity.

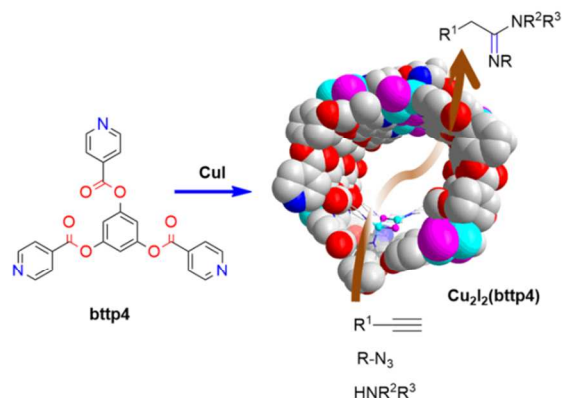


**Fig. 17** Space-filling view of  $\text{Cu}_2\text{I}_2(\text{BTTP4})$  and illustration of its synthesis and catalytic application in three-component coupling of azides, alkynes and amines. The Cu and I atoms are shown in turquoise and pink, respectively.

Afterward, we developed a new family of azide substrates, oxysulfonyl azides, and applied them in the three-component coupling reactions (Fig. 17).<sup>44c</sup> It was found that oxysulfonyl azides showed better reactivities than other azides such as sulfonyl and phosphoryl azides, and we proposed the reactions should undergo in the Cu-MOF pores in such  $\text{Cu}_2\text{I}_2(\text{btp4})$ -catalyzed reactions. To verify this hypothesis, we carried out a series of experiments as well as physical characterizations of the MOF catalyst before and after reactions. Accommodation experiments showed that MOF  $\text{Cu}_2\text{I}_2(\text{btp4})$  selectively adsorbed  $\text{PhCCH}$  over  $\text{CyCCH}$  (cyclohexyl acetylene) and  $t\text{-BuCCH}$ . The IR spectrum disclosed the presence of  $\text{C}=\text{N}$  bonds of the amidine products, and both EDS and XPS confirmed the presence of S in the recycled catalyst sample. XPS also verified that the +1 valence of Cu atoms in  $\text{Cu}_2\text{I}_2(\text{btp4})$  remained unchanged after the catalytic reactions, which was ascertained by observation of the same two intense peaks at  $932.5 \pm 0.2$  and  $952.5 \pm 0.2$  eV assignable to  $\text{Cu}2\text{p}_{3/2}$  and  $\text{Cu}2\text{p}_{1/2}$  components in the  $\text{Cu}_2\text{I}_2(\text{btp4})$  crystallites before and after catalytic reactions. This XPS result also suggested that the recycled  $\text{Cu}_2\text{I}_2(\text{btp4})$  catalyst was still active for further reaction. The heterogeneity of the catalysis has been proved by filtration experiments. The recyclability has also been examined, and  $\text{Cu}_2\text{I}_2(\text{btp4})$  can be reused for at least three runs.

A structurally flexible porous Cu(II)-MOF,  $[\text{Cu}^{\text{II}}(\text{bped})_2(\text{H}_2\text{O})_2(\text{SiF}_6)] \cdot 4\text{H}_2\text{O}$  (Cu-MOF- $\text{SiF}_6$ ) was obtained from *meso*-1,2-bis(4-pyridyl)-1,2-ethanediol and  $\text{CuSiF}_6$  (Fig. 18).<sup>44d</sup> Cu-MOF- $\text{SiF}_6$  is a 3D polycatenated porous framework consisting of 2D (4,4) topological grid networks which display 2-fold inclined interpenetration in the crystal lattice.  $\text{SiF}_6^{2-}$  anions are hosted in the 1D channels of Cu-MOF- $\text{SiF}_6$ . The anion exchange of  $\text{SiF}_6^{2-}$  anions with  $\text{NO}_3^-$  anions led to an isomorphous MOF, Cu-MOF- $\text{NO}_3$ . The 3D polycatenated frameworks show dynamic structural behaviour due to the presence of diol groups and the different anions. For Cu-MOF- $\text{SiF}_6$  with  $\text{SiF}_6^{2-}$  anions, a kinetic trap may be generated for MeOH, but bigger EtOH guest molecules are blocked. In comparison, Cu-MOF- $\text{NO}_3$  with smaller  $\text{NO}_3^-$  anions has enlarged voids and exhibit stepwise MeOH and EtOH sorption. The MOFs efficiently oxidize benzylic compounds to the corresponding carbonyl functionality under mild and convenient reaction condition due to the presence of favourable host-guest interactions and potential coordinatively unsaturated  $\text{Cu}^{2+}$  centers. Their catalytic properties are anion-responsive and Cu-MOF- $\text{NO}_3$  showed better catalytic activity than Cu-MOF- $\text{SiF}_6$ . The catalysts can be reused with the framework intact for at least three times without loss of any activity.

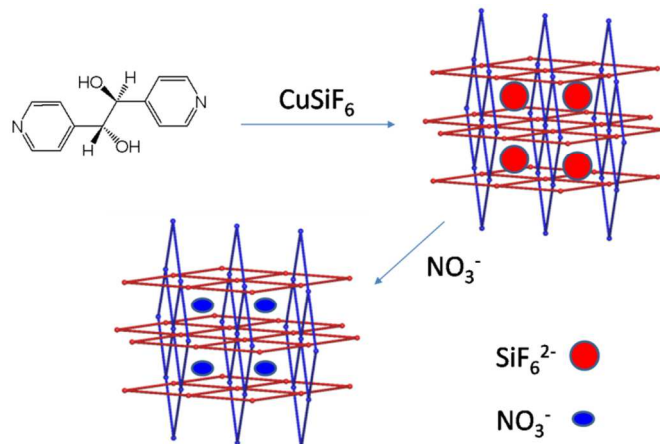


**Fig. 18** Illustration of synthesis of 3D polycatenated Cu-MOF-SiF<sub>6</sub> and its anion-tunable porosity.

Phosphines are excellent ligands for soft transition metal and they are ubiquitous in homogeneous catalysis. With a pyridyl phosphine ligand, 4-(3,5-bis(diphenylphosphino)phenyl)pyridine as ligand, we obtained a series of 3D Cu(I)-MOFs (Fig. 19).<sup>44e</sup> These phosphine-containing MOFs are isostructural based on rigid L<sub>2</sub>M<sub>2</sub> dimeric secondary building block with Br<sup>-</sup> (CuPhos-Br), Cl<sup>-</sup> (CuPhos-Cl) or PF<sub>6</sub><sup>-</sup> (CuPhos-PF<sub>6</sub>) as counteranions. The complexes have a 3-connected 4.12<sup>2</sup> chiral net topology, which can be further simplified to 6<sup>4</sup>.8<sup>2</sup>-qtz. The MOFs contain 1D homochiral channels to host different counteranions. The MOFs show anion-tunable flexible porosity. For example, CuPhos-Br reveals gradual MeOH uptake, while CuPhos-PF<sub>6</sub> exhibits stepwise MeOH sorption. Due to the presence of potential coordinatively unsaturated Cu<sup>+</sup> centers, the MOFs show heterogeneous Lewis acid catalytic activity. The ketalization reactions between ethylene glycol and 2-butanone/cyclohexanone proceeded up to 93% yield with 0.2 mol% catalyst (CuPhos-Br or CuPhos-PF<sub>6</sub>) loading. Profound size selectivity was observed for the MOFs. No reaction happens between ethylene glycol and bulky benzophenone. The MOF catalysts can be reused with the framework left intact for three runs without loss of activity.

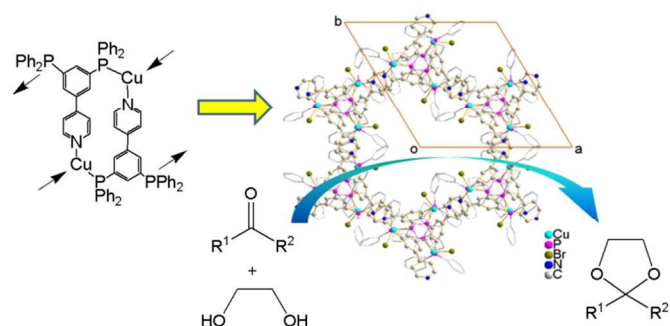


**Fig. 19** Cu(I)-MOFs based on a pyridyl phosphine and their catalytic activity in ketalization reactions.

**Zn-MOFs.** Zn-containing MOFs, which represent one of the most popularly studied MOF materials, also have been utilized as potential candidates in supramolecular heterogeneous catalysis. However, compared to the essential roles of Zn<sup>2+</sup> ion in natural enzymes and wide exploration of its catalytic activities in organic synthesis methodology, Zn-MOF-catalyzed reactions may still wait for further development. Fedin and Kim et al. reported a homochiral MOF [Zn<sub>2</sub>(bdc)(L-lac)(dmf)]·(dmf), which was prepared from the solvothermal reaction of Zn(NO<sub>3</sub>)<sub>2</sub>, L-lactic acid (L-H<sub>2</sub>lac), and 1,4-benzenedicarboxylic acid (H<sub>2</sub>bdc) in DMF at 110 °C for 2 days.<sup>45</sup> Single-crystal X-ray analysis revealed that the Zn<sup>2+</sup> ions and lactate ligands form 1D chiral chains running along the *a* axis. The coordinated DMF ligands and the guest DMF molecules can be readily removed at elevated temperatures without causing structural collapse. The authors found that desolvated samples were capable of mediating highly size- and chemoselective catalytic oxidation of thioethers to sulfoxides by urea hydroperoxide (UHP) or H<sub>2</sub>O<sub>2</sub>. Thioethers with smaller substituents exhibited reasonable conversion (up to 64%) and high selectivity (up to 92%) after 16 h of catalytic reaction, whereas thioethers with bulkier substituents exhibited very poor conversion. The MOF

catalyst can perform at least 30 catalytic cycles without loss of oxidation selectivity.

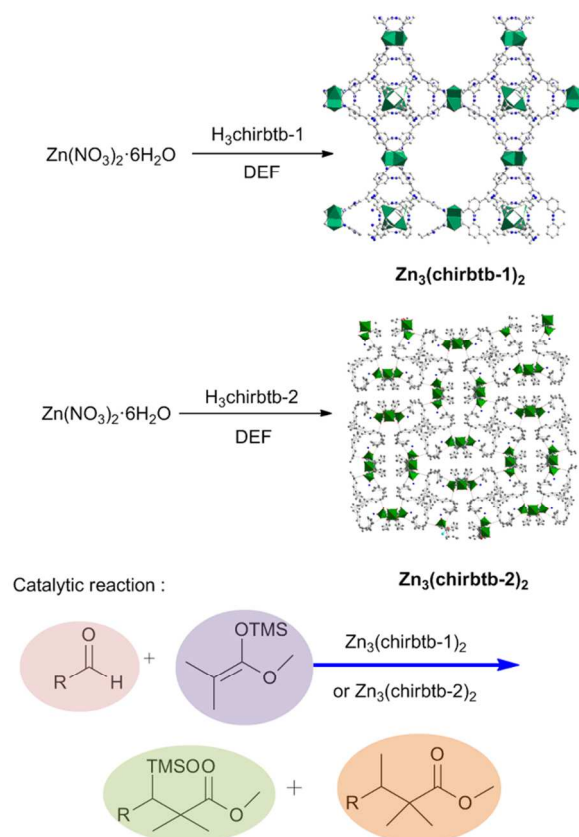


**Fig. 20** Ball-and-stick view of Zn<sub>3</sub>(chirbtb-1)<sub>2</sub> and Zn<sub>3</sub>(chirbtb-2)<sub>2</sub> and illustration of their synthesis and catalytic application in mukaiyama aldol reaction. The Zn atoms are shown in green polyhedra.

Another chiral Zn-MOF applicable in asymmetric catalysis was reported by Glorius and Kaskel et al.<sup>46</sup> They prepared chiral tricarboxylic acids with a btb (btb = 1,3,5-benzenetrisbenzoate) backbone substituted by chiral oxazolidinones (H<sub>3</sub>chirbtb-*n*), namely 1,3,5-tri{4-[2-(4-isopropyl-2-oxooxazolidin-3-yl)]benzoate}benzene (H<sub>3</sub>chirbtb-1) and 1,3,5-tri{4-[2-(4-benzyl-2-oxooxazolidin-3-yl)]benzoate}benzene (H<sub>3</sub>chirbtb-2). Solvothermal reactions of zinc nitrate and H<sub>3</sub>chirbtb-1 and H<sub>3</sub>chirbtb-2 in diethylformamide (DEF) at 100 °C led to crystallization of Zn-MOFs Zn<sub>3</sub>(chirbtb-1)<sub>2</sub> and Zn<sub>3</sub>(chirbtb-2)<sub>2</sub>, respectively. MOF Zn<sub>3</sub>(chirbtb-1)<sub>2</sub> has large-sized pores with approximately 33.7 Å in diameter, whereas MOF Zn<sub>3</sub>(chirbtb-2)<sub>2</sub> possesses rectangular channels of 18 × 18 Å<sup>2</sup> along the *c*-axis. Compared to other Lewis acid catalysis such as cyanosilylation, Mukaiyama aldol reaction required stronger Lewis acid catalysts. In previously mentioned Mukaiyama aldol reactions catalyzed by Mn-btt, the metal nodes were achiral, so the obtained aldol products didn't exhibit any enantiomeric excess. To challenge the MOFs in asymmetric Mukaiyama aldol reaction, both Zn<sub>3</sub>(chirbtb-1)<sub>2</sub> and Zn<sub>3</sub>(chirbtb-2)<sub>2</sub> MOFs were tested (Fig. 20). Zn<sub>3</sub>(chirbtb-1)<sub>2</sub> was found efficient in reaction using benzaldehyde. The enantioselectivity with Zn<sub>3</sub>(chirbtb-1)<sub>2</sub> as asymmetric catalyst during reaction depended on the solvent. If *n*-heptane was used, an enantiomeric excess of 9% was detected, but no influence on the enantioselectivity of the

product could be observed when dichloromethane was used.  $Zn_3(\text{chirbtb}-2)_2$  catalyzed the reaction of benzaldehyde and the silyl enol ether with a decreased reaction rate, and a small but reproducible enantiomeric excess of 6% (*n*-heptane) and 8% (dichloromethane), respectively, was measured.

A series of zeolitic imidazolate frameworks (ZIFs) have been developed and well characterized by Yaghi and others. Among them, ZIF-8 attracted much attention because of its large pores of 11.6 Å that are accessible through small apertures of 3.4 Å<sup>47a</sup>. Furthermore, ZIF-8 is an appealing material to employ as catalyst for CO<sub>2</sub> conversion to cyclic carbonates because of the presence of Lewis acid sites in its framework.

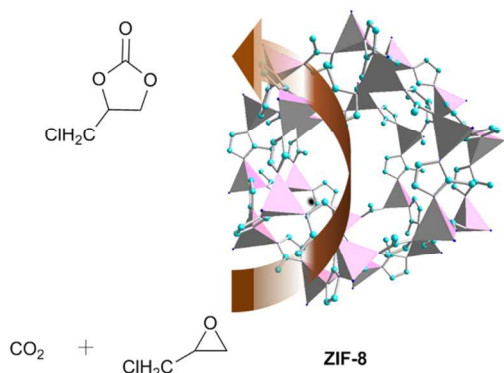


**Fig. 21** Ball-and-stick view of ZIF-8 and illustration of its catalytic application in cycloaddition of CO<sub>2</sub> and epoxides. The Zn atoms are shown in rose polyhedral.

Carreon et al. reported the catalytic performance of ZIF-8 and amino-functionalized ZIF-8 in the synthesis of chloropropene carbonate from CO<sub>2</sub> and epichlorohydrin (Fig. 21).<sup>47b</sup> ZIF-8 was prepared at room temperature from zinc nitrate hexahydrate and 2-methylimidazole, whereas the functionalized ZIF-8 was prepared post-modification of dried ZIF-8 with ethylene diamine. The ZIF-8 catalysts, especially those surface-modified with amines, display high epoxide conversions and moderate to high selectivities to the cyclic carbonate at temperatures even as low as 70 °C. The presence

of both the Zn<sup>II</sup> acid sites and the N basic moieties (in adjacent locations) from the imidazole linker in ZIF-8 probably facilitated the adsorption of the CO<sub>2</sub> on the solid surface and its further conversion to the carbonate. However, the catalytic activity of the recycled catalysts (both nonfunctionalized and amine-functionalized) decreased in the second and third run. As shown in the powder XRD patterns, although ZIF-8 structure was preserved after the first cycle, the recycled catalysts lost their structural features after the second cycle. On the other hand, the BET surface area decreased from 1173 to 772 m<sup>2</sup>/g for the nonfunctionalized ZIF-8 and from 1096 to 915 m<sup>2</sup>/g for the functionalized ZIF-8. This may suggest pore blockage of the recycled ZIF-8 by carbonaceous material formed during the reaction, and may explain in part the lower activity of the recycled catalysts.

**Ag-MOFs.** The application of Ag-MOF in heterogeneous catalysis seems still in its infancy. Duan's group reported a homochiral MOF Ag-tpha (tpha = tris(4-(1-(2-pyridin-2-ylhydrazono)ethyl)-phenyl) amine) with the formula of [Ag<sub>3</sub>(tpha)<sub>2</sub>]-3BF<sub>4</sub>, which was prepared from the self-assembly of tpha and AgBF<sub>4</sub> in methanol.<sup>48</sup> The structure has a 3D framework containing pores of a 7.5 × 8.0 Å<sup>2</sup> cross section. The distorted tetrahedral Ag centers were located within the pores, which were able to react with suitable substrates. Recent research findings show that in the presence of chiral ligands, Ag(I) complexes could promote the asymmetric cycloaddition reactions of azomethine ylides and electron-deficient olefins, leading to the formation of chiral pyrrolidines in good yields and high enantioselectivities. To explore the potential of Ag-MOFs in asymmetric catalysis, homochiral Ag-tpta1 and Ag-tpta2 were prepared from the same procedure as Ag-tpha by using (+)-cinchonine and (-)-cinchonidine as the chiral adducts, respectively. MOFs Ag-tpta1 and Ag-tpta2 were then employed in the 1,3-dipolar cycloaddition of methyl-2(benzylidene amino)-acetate (MBA) and N-methylmaleimide (NMM). Catalytic results showed that the cycloadduct was obtained with 90% and -82% ee in the presence of Ag-tpta1 and Ag-tpta2, respectively (Fig. 22). Recycling experiments also showed that Ag-tpta1 can be used at least three runs and there is no loss of the yields and enantioselectivity.

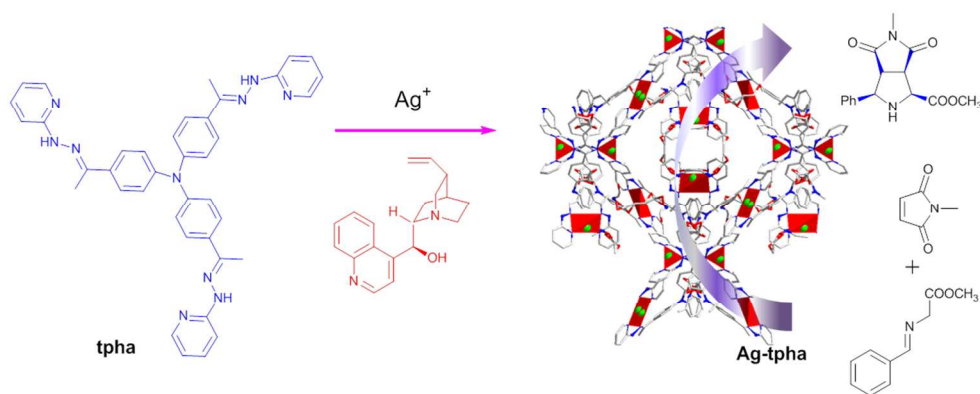


**Fig. 22** Ball-and-stick view of Ag-tpta1 and illustration of its synthesis and catalytic application in 1,3-Dipolar cycloaddition. The Ag atoms are shown in bright green.

### 2.3 MOFs with Other Uncommonly Used Metal Ions (Mg, Zr, Pd, Ce, Bi)

**Mg-MOFs.** Comparing with the commonly used metal ions introduced in Section 2.2, the MOFs constructed from other metals are relatively less. Nevertheless, various catalytic reactions have been investigated by utilizing the MOFs

containing specific metal ions, which, in some cases, may exhibit unique role in heterogeneous catalysis. The uniqueness of Mg-based MOFs may lie in the lightness of Mg atom, which could offer relatively high pore density. Koner et al. have reported a new approach of pH-controlled synthesis of MOFs involving Mg and pyrazole-3,5-dicarboxylic acid ( $H_3pdc1$ ), which allows a progressive increase of dimensionality from zero- to 3D frameworks.<sup>49a</sup> When the pH of the reaction mixture was adjusted to the basic range ( $pH \approx 8$ ), a 3D open framework of  $Mg_3pdc1(OH)_3(H_2O)_2$  (Mg-pdc1) crystallized. Desolvated Mg-MOF was subjected to aldol condensation reactions of various aromatic aldehydes with acetone (Fig. 23). The results showed that nitro-substituted benzaldehydes were converted into their respective  $\beta$ -aldol products as the sole products within 6 h. With benzaldehyde and *p*-methoxybenzaldehyde, however, *trans*-benzylideneacetone was obtained without formation of the  $\beta$ -aldol product. No conversion was observed in the absence of MOF catalyst. To verify that the catalysis was indeed heterogeneous, they performed the hot filtration test. To check the stability of the catalyst, they characterized the recovered material with powder XRD and IR spectral analysis. Comparison of the IR spectra and XRD patterns of the pristine compound and the recovered catalyst convincingly demonstrated that the structural integrity was retained after the aldol condensation reaction. For the recycling study, an aldol condensation reaction was carried out with *p*-methoxybenzaldehyde and *p*-nitrobenzaldehyde for three successive runs. The catalytic efficiency of the recovered catalyst remained almost the same in each run.

Later, they demonstrated the synthesis and catalytic behaviors of another 3D Mg-MOF of  $Mg(pdc2)(H_2O)$  (Mg-pdc2,  $H_2pdc2$  = pyridine-2,5-dicarboxylic acid) with a rectangle type channel ( $12.2 \text{ \AA} \times (3.6 \rightarrow 5.7) \text{ \AA}^2$ ).<sup>49b</sup> They employed this new Mg-MOF in the aldol condensation reactions of aromatic aldehydes and aliphatic ketones such as acetone, cyclohexanone and *tert*-butylcyclohexanone (Fig. 23). Catalytic results showed that the aldehyde substrates are converted to their respective  $\beta$ -aldols as the sole product. In the presence of Mg-pdc2, they noticed that  $\beta$ -aldol products did not undergo further transformation to form unsaturated carbonyl compounds, which were different from Mg-pdc1-catalyzed reactions. Mg-pdc2 can also be recycled and reused several times without significant loss of activity.

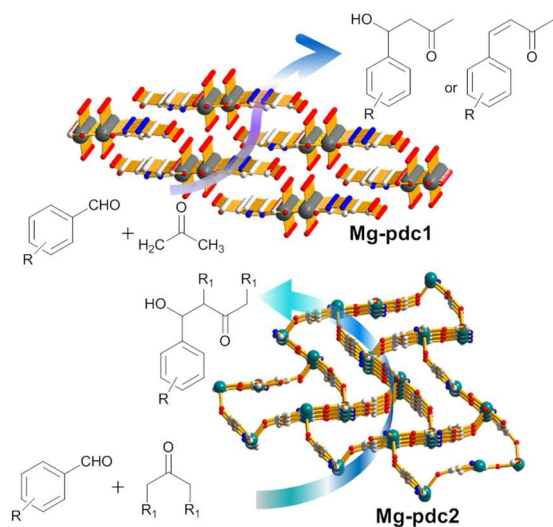


**Fig. 23** Ball-and-stick view of Mg-pdc1 and Mg-pdc2, and illustration of their catalytic application in aldol condensation reactions. The Mg atoms are shown in green.

**Zr-MOFs.** Synthesis of Zr-MOFs seemed to remain a formidable challenge in 1990s at the beginning of MOFs crystal engineering. However, the discovery that the Zr-based MOFs can be prepared and handled conveniently in atmospheric moisture promoted the development and utilization of Zr-MOFs, which was found to possess enhanced stability, compared to Zn-MOFs, probably due to the strong Zr–O bonds within the secondary building unit (SBU) and the high degree of interlinking of these SBUs. The strikingly high thermal stability of the porous framework (up to  $540 \text{ }^\circ\text{C}$ ) and excellent chemical stability make Zr-MOFs superior candidates as heterogeneous catalyst to most of other metal-containing MOFs suffering from low thermal and chemical stability. In 2008, Lillerud group developed a new Zr-MOF UiO-66 (Uio for University of Oslo) with the formula of  $Zr_6O_4(OH)_4(bdc)_{12}$ , which was readily prepared under solvothermal conditions at  $393 \text{ K}$  in DMF starting from  $ZrCl_4$  and terephthalic acid.<sup>50a</sup> The framework comprises tetrahedral and octahedral cages, in a 2 : 1 ratio, of free dimensions close to 8 and 11 Å, respectively. Access to the cages is provided by triangular windows with a free diameter of 6 Å. UiO-66 consists of  $Zr_6O_4(OH)_4(CO_2)_{12}$  clusters in which the triangular faces of the  $Zr_6$ -octahedron are alternatively capped by  $\mu_3$ -O and  $\mu_3$ -OH groups (Fig. 24). Dehydroxylation of the cluster starts at  $250 \text{ }^\circ\text{C}$  and can be completed at  $300 \text{ }^\circ\text{C}$ , and two of the four  $\mu_3$ -OH groups leave together with the hydrogen from the remaining two  $\mu_3$ -OH groups, resulting in a  $Zr_6O_6$  inner cluster. During the process, the overall framework structure is virtually unchanged. This ability to maintain the framework upon dehydroxylation and change in coordination around Zr assisted the application of UiO-66 in catalysis.

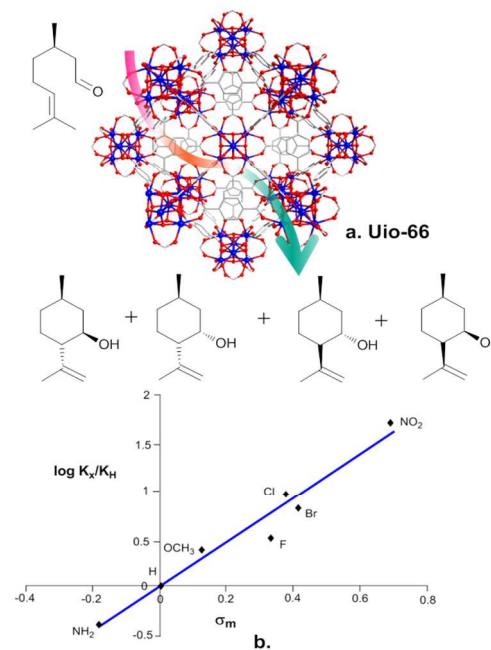


**Fig. 24** (a) Ball-and-stick view of UiO-66 and illustration of its catalytic application in cyclization of citronellal; (b) Hammett plot for cyclization of citronellal with different UiO-66-X ( $X = NH_2, H, OCH_3, F, Br, Cl, NO_2$ ) catalysts.

De Vos et al. studied the catalytic activity of UiO-66 and the amino-modified NH<sub>2</sub>-UiO-66 in cross aldol condensation reaction.<sup>50b</sup> NH<sub>2</sub>-UiO-66 can be prepared by the same procedure as that of NH<sub>2</sub>-UiO-66 with simple replacement of terephthalic acid by 2-aminoterephthalic acid. The UiO-66 materials were evaluated as catalysts in the synthesis of jasminaldehyde (JA, *a*-*n*-amylcinnamaldehyde) from the reaction between heptanal (HA) and benzaldehyde (BA). Before catalytic reactions, both UiO-66 and NH<sub>2</sub>-UiO-66 were pretreated by heating at high temperatures. The results showed that NH<sub>2</sub>-UiO-66 performed better with 10% higher in both activity and selectivity than UiO-66. Hot filtration tests proved the catalytic activity was associated with the solid exclusively other than the liquid phase.

Afterward, Van Speybroeck and De Vos employed a series of UiO-66 MOFs with different benzene-1,4-dicarboxylates (bdc-X; X=H, NH<sub>2</sub>, CH<sub>3</sub>, OCH<sub>3</sub>, F, Cl, Br, NO<sub>2</sub>) in the cyclization of citronellal, and studied the effects of substituents (Fig. 24).<sup>50c</sup> Before reaction, each catalyst was activated at 493 K. Catalytic results showed that the rate was dramatically enhanced by electron-withdrawing groups on the linker (F, Cl, Br, NO<sub>2</sub>), and NO<sub>2</sub>-UiO-66 was by far the most active material, reaching full conversion after only 6 h. They attempted to correlate the activity to electronic effects of the linkers using Hammett's  $\sigma_{\text{meta}}$  values. The strong positive correlation of the  $\log k$  values with  $\sigma_{\text{meta}}$  results in a linear free-energy relationships (LFER,  $\log(k_X/k_H) = \rho\sigma_{\text{meta}}$ ) with  $\rho = 2.35$ . This is the first LFER ever observed for MOF catalysts. Recently, De Vos developed a synthesis method of UiO-66 by adding trifluoroacetic acid (TFA), in which a part of bdc was substituted by trifluoroaceta.<sup>50d</sup> They applied the new Zr-MOF in the "ene"-type cyclization of citronellal to isopulegol. Results showed that the addition of small amounts of TFA could significantly increase the activity.

**Pd-MOFs.** Palladium is an intensively investigated metal atom in a broad range of metal catalyzed reactions; however, the Pd-based MOFs are rarely observed in literature. The difficulty in crystal growth of Pd-MOFs may relate to the specific kinetics of Pd-coordinative bonds; therefore, the potential applications of wide Pd-based catalytic activities in Pd-MOFs are seeking for full growth of Pd-MOFs crystal engineering. Navarro and Mascicchi et al. synthesized a novel, 3D microporous sodalitic network, Pd(2-pymo)<sub>2</sub>, which was thermally stable up to 330 °C in air.<sup>51a</sup> As shown in its crystal structure, Pd(2-pymo)<sub>2</sub> possessed two different hexagonal windows with free openings of 4.8 and 8.8 Å and with a fraction of 42% of the crystal volume available to adsorbed guests.

The catalytic activities of Pd(2-pymo)<sub>2</sub> was tested by Corma et al. in the Suzuki C–C coupling, alcohol oxidation, and olefin hydrogenation (Fig. 25).<sup>51b</sup> In the case of Suzuki C–C cross coupling reaction, the reaction between phenylboronic acid and 4-bromoanisole was chosen as the model reaction. The high values of conversion (85%) and selectivity toward the cross-coupling product (99%) are obtained after 5 h using Pd(2-pymo)<sub>2</sub> at 150 °C. It can be reused without significant diminution of catalyst activity and selectivity. The X-ray diffractograms of used Pd-MOF were almost identical to those of fresh samples. In light of alkene hydrogenation, they chose the reactants to explore the potential shape-selective properties of the material, and compared the hydrogenation rates of 1-octene and cyclododecene. Results showed that 1-octene had very high reactivity whereas cyclododecene didn't work at all, indicating that the active centers located at the internal surface

were accessible through the pore openings for 1-octene, whereas cyclododecene could not diffuse inside the pores.

The liquid-phase hydrogenation of 1-octene and cyclododecene using Pd(2-pymo)<sub>2</sub> as catalyst has also been examined by Klemm et al.<sup>51c,d</sup> They found that in less than 4 h, the size-selectivity was indeed observed; however, when the reaction mixture was exposed to hydrogen for more than 4 h, the hydrogenation of cyclododecene also took place. Through careful studies they concluded that the phenomenon was caused by partial reduction of Pd<sup>2+</sup> centers to Pd<sup>0</sup> nanoparticles. The latter could leach out from the frameworks and then promoted the hydrogenation of larger olefins such as cyclododecene.

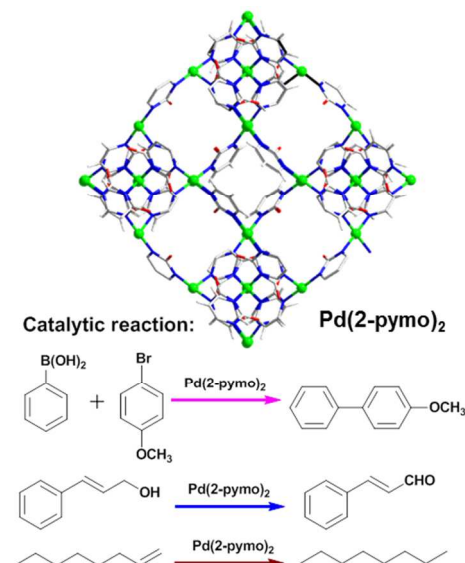


**Fig. 25** Ball-and-stick view of Pd(2-pymo)<sub>2</sub> and illustration of its catalytic application in suzuki coupling, alcohol oxidation, olefin hydrogenation. The Pd atoms are shown in bright green.

**Ce-MOFs.** The lanthanide-containing MOFs (Ln-MOFs) are actually by no means rare compared with Mg-, Zr- or Pd-MOFs. However, endeavor in heterogeneous catalysis by using Ln-MOFs are limited, probably because of the intrinsic attribute of the labile Ln-coordinative bonds. Duan et al. synthesized two homochiral Ln-MOFs Ce-mdip1 and Ce-mdip2 through the solvothermal reactions of methylenediisophthalic acid (H<sub>2</sub>mdip) and Ce(NO<sub>3</sub>)<sub>3</sub>·6H<sub>2</sub>O in the presence of *L*-bcip and *D*-bcip (bcip = *N*-tert-butoxy-carbonyl-2-(imidazole)-1-pyrrolidine), respectively.<sup>52</sup> In compound Ce-mdip1 the mdip ligands linked the metal ions through the carboxyl groups forming a noninterpenetrating 3D network containing chiral channels with a 10.5 × 6.0 Å<sup>2</sup> cross section along the *a*-axis. The Ce ions having removable coordinated water molecules were well-positioned within the channels. The crystal structure of Ce-mdip2 is similar to that of Ce-mdip1, but it exhibits Cotton effects exactly opposite to those of Ce-mdip1. The authors examined the catalytic activities of Ce-mdip1 and Ce-mdip2 in the asymmetric cyanosilylation reactions of aromatic aldehydes and cyanotrimethylsilane (Fig. 26). Results showed that the reactions in the presence of each catalyst can achieve high conversion (>95%) in 24 h and excellent *ee* (up to 98% *ee*), although the reactions led to the formation of opposite major enantiomers. The authors also examined heterogeneity of the reactions. After removal of the catalyst in 4 h, the filtrate afforded only 10% addition conversion upon stirring for

another 7 h. The catalysts can be recycled and reused for three times with a slight decrease in reactivity and enantioselectivity. The powder XRD patterns of recycled catalysts matched with those of as-synthesized catalysts.

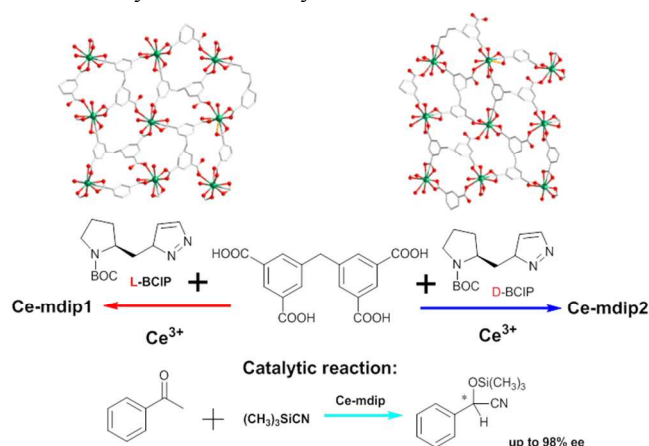


**Fig. 26** Ball-and-stick view of Ce-mdip1 and Ce-mdip2 and illustration of their synthesis and catalytic application in cyanosilylation of aldehydes. The Ce atoms are shown in green.

**Bi-MOFs.** Bismuth is nontoxic, noncarcinogenic and relatively inexpensive metal, and thus Bi compounds are used as green catalyst. Nevertheless, the Bi-based MOFs are rather uncommon either in synthesis or in application study. Kolb and Stock et al. reported a rare Bi-MOF Bi(btbt), which was synthesized by the reaction of  $\text{Bi}(\text{NO}_3)_3 \cdot 5\text{H}_2\text{O}$  with  $\text{H}_3\text{btbt}$  in methanol at 120 °C.<sup>53</sup> Bi(btbt), denoted as CAU-7 (CAU = Christian-Albrechts-Universität). The crystal structure of CAU-7 has 1D channels with the size of approximate 10 Å. The temperature-dependent XRD measurements confirmed the thermal stability of the crystalline framework up to 380 °C. The catalytic activity of CAU-7 was demonstrated in the solvent-free hydroxymethylation of hemicellulose-derived 2-methylfuran to 5-methylfurfuryl alcohol (Fig. 27). Before the catalytic tests, the authors examined the IR spectra of CAU-7 after exposure to acetonitrile, and the IR spectra showed that  $\text{CH}_3\text{CN}$  can chemically adsorbed onto CAU-7, which suggests that CAU-7 possesses mild Lewis acid sites. Due to the presence of such catalytically active sites, CAU-7 performed well at the hydroxymethylation reaction of 2-methylfuran, leading to 75% yield at 90% conversion. The activity of CAU-7 can be comparable to other MOFs with Lewis or Brønsted acidity, such as Uio-66 and MIL-53(Ga).

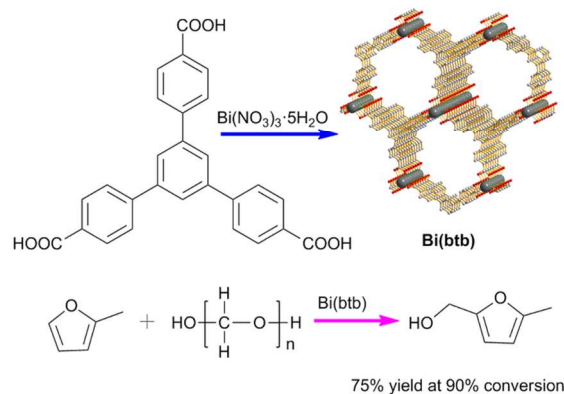


**Fig. 27** Ball-and-stick view of Bi(btbt) and illustration of its synthesis and catalytic application in hydroxymethylation of 2-methylfuran. The Bi atoms are shown in green.

In summary, the organic reactions, which are used to test the catalytic abilities of MILs, are focused on oxidation reactions, whose substrates include unsaturated/saturated hydrocarbons, thiols and sulfides. Cyclohexene oxidation is an especially interesting as it can yield several products such as epoxide, diol, peroxide and enone, depending on the catalyst and the reaction conditions. Both of MIL-47(V)<sup>31b,c</sup> and MIL-101(Cr)<sup>25</sup> can efficiently promote cyclohexene oxidation in the presence of TBHP, yielding enone with high selectivity. Oxidation of secondary C-H bonds, especially in benzylic compounds, could lead to mixtures of alcohols and ketones. When using MIL-100(Fe)<sup>28a</sup> or MIL-101(Cr)<sup>24</sup> as the catalyst, the major products were ketones with the selectivity up to 99%. In the case of sulfide oxidation, MILs again display high selectivity. Only sulfoxide of sulfide was catalyzed by MIL-101(Cr), whereas sulfonation of sulfide couldn't undergo in the presence of MIL-101(Cr). As shown in these examples, MILs can be the first choices for the highly selectively oxidative catalysts.

Pleasantly, MOFs which are constructed with low covalent metal cations such as  $\text{Mn}^{2+}$ ,  $\text{Co}^{2+}$ ,  $\text{Cu}^{1+/2+}$ ,  $\text{Zn}^{2+}$  and  $\text{Ag}^+$ , showed diversity in catalysis. Cyanosilylation of aldehydes, Mukaiyama-aldol reaction and ring-opening epoxides are among the most studied reactions to test the Lewis acidity of CUMs in MOFs.  $\text{Co}^{\text{II}}$  is redox active, and thus  $\text{Co}^{\text{II}}$ -MOFs are usually used for the oxidation catalysts. It is noted that Cu and Ag complexes are good homogeneous catalysts for a lot of valuable organic transformations. As a result, there are more reactions that can be used to examine the catalytic activities of Cu- and Ag-MOFs as heterogeneous catalysts.

In general, although the MOFs in section 2.3 are not common, they could show potentially powerful heterogeneous catalytic activities, especially MOFs that are constructed with  $\text{Pd}^{2+}$  ions, as viewed from the standpoints of methodology. As Pd complexes have been widely applied for C-C cross-coupling reactions as well as C-H bond activation reactions, its versatile potentials in catalytic application may wait for reasonable design and synthesis of more stable Pd-MOF.

### 3. MOFs with Metalloligands

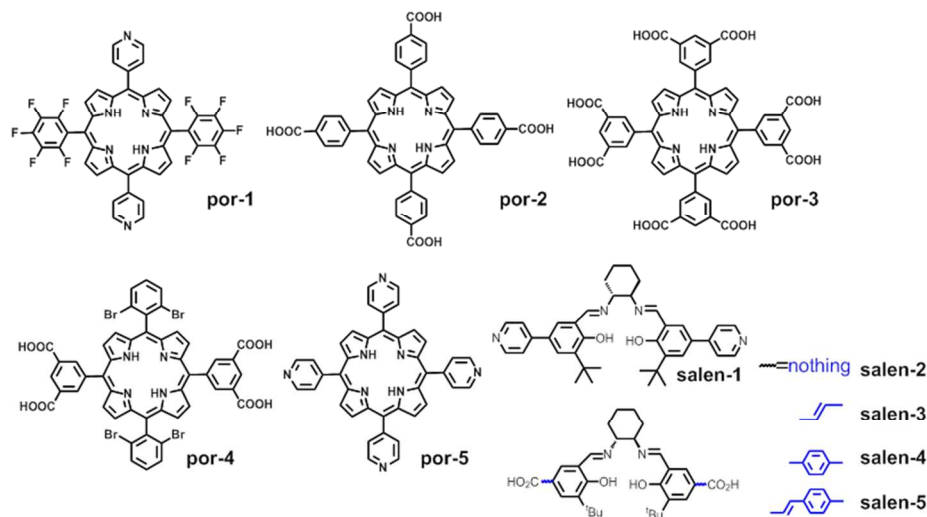
An attractive feature for MOFs as supramolecular heterogeneous catalysts is the potential to incorporating metal complexes that have been proven effective homogeneous catalysts, particularly metallosalens and metalloporphyrins, into the micropores.<sup>54-61</sup> Compared to other immobilized catalysts, the metalloligand-based MOFs can functionalize as heterogeneous asymmetric catalysts with higher catalyst loading and more accessible catalytic centers. Table 2 lists the reported MOFs with metalloligands, the window or channel size, and catalytic reactions. The information about the organic ligands in metalloligand structures are shown in Scheme 1.

Metalloporphyrins should be ideal catalytic struts in MOFs, given their rigidity and well-studied catalytic behavior.<sup>54</sup> One of their important features lies in the characteristic diversity which can be obtained through the addition of a variety of functional peripheral substituents, or via the introduction of functional peripheral substituents. A series of Ru-Mn-Co-porphyrin complexes have displayed excellent activities in asymmetric epoxidation, cyclopropanation and aziridination of olefins, as well as C-H bond activation of carbonhydrogens. Hupp<sup>55</sup>, Ma<sup>56</sup>, Wu<sup>57</sup> and Zhou<sup>58</sup> groups prepared Mn-Co-Pd-Fe-porphyrin-based MOFs, and illustrated their catalytic performances in oxidation reactions.

On the other hand, chiral salen ligands, such as (*R,R*)-1,2-cyclohexanediamino-*N,N'*-bis(3-*tert*-butyl-salicylidene), have

been established as one of the few privileged ligand systems for asymmetric catalysis. Some examples of metallosalen-based catalysis include the asymmetric ring-opening reactions of epoxides and aziridines catalyzed by Co(salen) and Cr(salen) complexes, the enantioselective addition of alkynes to ketones catalyzed by Zn(salen) complexes, and the asymmetric oxidation of sulfides to sulfoxides catalyzed by both Ti(salen) and V(salen) complexes.<sup>54b</sup> Motivated by excellent asymmetric catalytic activities exhibited by homogeneous metallosalen

complexes, MOFs containing chiral metallosalen building blocks have attracted a great deal of recent interest. So far, only a few chiral metallosalen-based MOFs have been examined in asymmetric catalytic reactions. For example, Hupp<sup>59</sup>, Lin<sup>60</sup> and Cui<sup>61</sup> groups constructed chiral MOFs based on Mn-/Ru-/Co-salen-derived bipyridine or bicarboxylate ligands and demonstrated their asymmetric catalytic activity in alkene epoxidation, cyclopropanation and hydrolytic kinetic resolution of epoxides.



**Scheme 1** Structures of porphyrin and salen ligands used in metalloligand-based MOF catalysis.

### 3.1 Metalloporphyrin-Based MOFs

Hupp group developed a porphyrin-based ligand with pyridine terminal groups, 5,15-dipyridyl-10,20-bis(pentafluorophenyl)porphyrin (por-1).<sup>55a</sup> By combining 1,2,4,5-tetrakis(4-carboxyphenyl)-benzene ( $H_4tcbp$ ) and por-1 with a Zn salt, a noninterpenetrated, pillared-paddlewheel MOF was built with the formula  $Zn_2(tcbp)(Zn-por-1)$  (ZnPO-MOF). The structure has large channels in three directions that are occupied by a substantial amount of disordered solvent, including  $15 \times 9 \text{ \AA}^2$  channels along the  $a$  axis,  $11 \times 9 \text{ \AA}^2$  channels along the  $b$  axis, and  $8 \times 9 \text{ \AA}^2$  channels along the  $c$  axis. In the acyl-transfer reaction between  $N$ -acetylimidazole and 3-pyridylcarbinol, a 2420-fold rate enhancement was observed in the presence of ZnPO-MOF relative to the uncatalyzed reaction (Fig. 28).

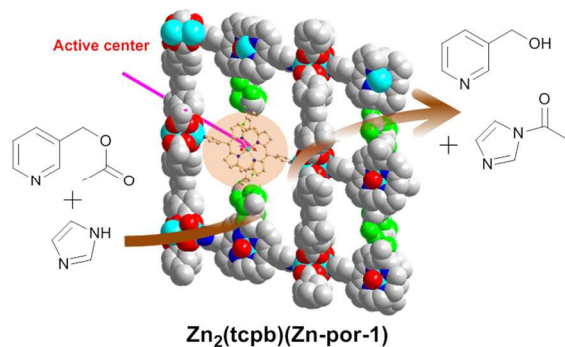


**Fig. 28** Space-filling view of  $Zn_2(tcbp)(Zn-por-1)$  and illustration of its catalytic application in acyl-transfer reaction. The Zn and F atoms are shown in turquoise and bright green.

This group subsequently described a facile synthesis method of MOFs that can incorporate a variety of metalloporphyrins, specifically  $Al^{3+}$ ,  $Zn^{2+}$ ,  $Pd^{2+}$ ,  $Fe^{3+}$ , and  $Mn^{3+}$  complexes.<sup>55b</sup> Reaction of  $Zn(NO_3)_2 \cdot 6H_2O$ , por-1 and 5,10,15,20-tetra(carboxyphenyl)metalloporphyrin (por-2) in the presence of 0.03 M  $HNO_3$  resulted in the metalloporphyrin-based MOF with formula of  $Zn_2(por-1)(por-2)$ . Isostructural materials can be prepared when the free-base porphyrin por-1 was replaced with Mn-por-1 complex, and/or Al-por-2, Pd-por-2, or Fe-por-2 complex was used instead of free ligand por-2. Analysis of single-crystal data revealed noncatenated frameworks of these isostructural materials. The center-to-center distance between cofacial struts derived from por-1 was 16.6  $\text{\AA}$ , while the distance between cofacial por-2's is 22  $\text{\AA}$ .  $Zn_2(Mn-por-1)(Zn-por-2)$  was selected to demonstrate the catalytic activity. Using a soluble analogue of iodobenzene, and the MOF was found to be an effective catalyst for both the epoxidation of styrene and hydroxylation of cyclohexane.

$Zn_2(Zn-por-1)(Zn-por-2)$  can be prepared by a similar procedure.<sup>55c</sup> They found that  $Zn_2(M-por-1)(Zn-por-2)$  ( $M = Al^{3+}$ , none,  $Sn^{4+}$ ,  $Al^{3+}$ ,  $Co^{3+}$ ) could be prepared from solvent-assisted linker exchange reactions between  $Zn_2(Zn-por-1)(Zn-por-2)$  and  $M-por-1$ . Among them,  $Zn_2(Al-por-1)(Zn-por-2)$  displayed good performances in the ring-opening reaction of epoxides with  $TMSN_3$ .

A novel octapic porphyrin ligand, tetrakis(3,5-dicarboxyphenyl)porphine (por-3), was designed by Ma group.<sup>56a</sup> Solvothermal reaction of the por-3 and  $Co(NO_3)_2 \cdot 6H_2O$  in dimethylacetamide (DMA) at 115  $^\circ C$  yielded a porphyrin-based MOF  $\{[Co_3(OH)(H_2O)]_4[Co(por-3)_3] \cdot (H_2O)_{20} \cdot (CH_3OH)_{22} \cdot (DMA)_{25}\}$  (denoted as MMPF-2, MMPF = metal-metalloporphyrin framework). Crystal structure possesses two rectangular channels with a size of  $10 \times$

10 Å<sup>2</sup> along *c* direction. They concurrently designed another porphyrin ligand 5,15-bis(3,5-dicarboxyphenyl)-10,20-bis(2,6-dibromophenyl)porphyrin (por-4).<sup>56b</sup> A new MOF with the formula {[Co<sub>2</sub>(μ<sub>2</sub>-H<sub>2</sub>O)(H<sub>2</sub>O)<sub>4</sub>](Co(por-4))·solvents} (denoted as MMPF-3) was prepared solvothermally from por-4 and Co(NO<sub>3</sub>)<sub>2</sub>. MMPF-3 crystallized in the same space group as **fcu**-MOF-1, which possessed three types of polyhedral cage: a cubohemioctahedron with a window size of ca. 5.9 Å and inner dimensions of about 7.3 Å (atom-to-atom distance), a truncated tetrahedron and a truncated octahedron with a window size of about 9.2 Å and a cavity with an internal volume of about 4000 Å<sup>3</sup>. The catalytic activities of MMPF-2 and MMPF-3 were examined in the epoxidation of *trans*-stilbene using TBHP as oxidant in acetonitrile at 60 °C. Catalytic results disclosed that MMPF-2 converted 67.2% of substrate after 24 h, whereas MMPF-3 demonstrated a highly efficient catalytic activity in terms of both yield (95.7% over 24 h) and selectivity (87.1% epoxide product) (Fig. 29).

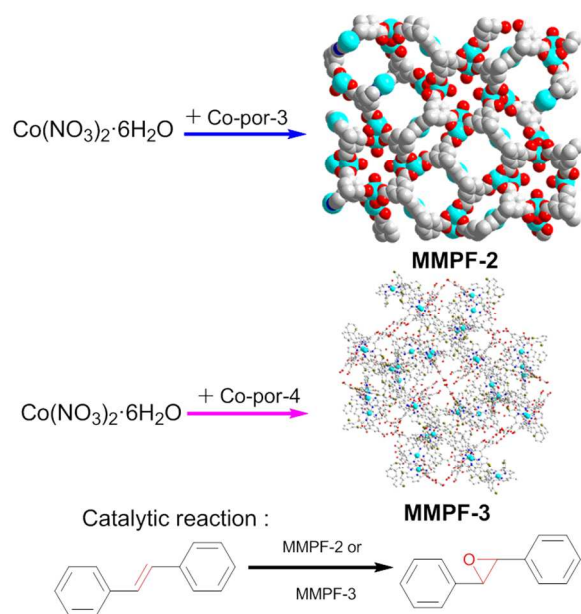


**Fig. 29** Space-filling view of MMPF-2, ball-and-stick view of MMPF-3, their synthesis and catalytic application in epoxidation of olefin. The Co and Br atoms are shown in turquoise and dark yellow.

By employing two porphyrin ligands, tetra(carboxyphenyl)metalloporphyrin (por-2) and tetrapyrrolylporphyrin (por-5), Wu group synthesized new porphyrin-based MOFs.<sup>57</sup> The porous Cd<sub>1.25</sub>(Pd-por-2)(H<sub>2</sub>O) MOF<sup>57a</sup> contains two kinds of channels with dimensions of 4.6 × 12.6 Å<sup>2</sup> and 8.3 × 9.3 Å<sup>2</sup> along the *a* axis, showing significant catalytic activity for styrene oxidation using H<sub>2</sub>O<sub>2</sub> as oxidant (Fig. 30). On the other hand, a reaction of H<sub>3</sub>PW<sub>12</sub>O<sub>40</sub> with Mn<sup>III</sup>Cl(por-5) in DMF yielded the zwitterionic complex {[Mn<sup>III</sup>(DMF)<sub>2</sub>TPyP](PW<sub>12</sub>O<sub>40</sub>)<sup>2-</sup>}, which subsequently reacted with Cd(NO<sub>3</sub>)<sub>2</sub>·4H<sub>2</sub>O in a mixed solvent of DMF and acetic acid at 80 °C, leading to the formation of [Cd(DMF)<sub>2</sub>Mn(DMF)<sub>2</sub>(por-5)](PW<sub>12</sub>O<sub>40</sub>).<sup>57b</sup> The framework of this compound was porous upon the removal of the solvent, displaying large cavities with dimensions of 10 × 10 × 12 Å<sup>3</sup> and 1D channel openings with dimensions of 5 × 12 Å<sup>2</sup> along the [110] direction. MOF [Cd(DMF)<sub>2</sub>Mn(DMF)<sub>2</sub>(por-5)](PW<sub>12</sub>O<sub>40</sub>) displayed excellent capability for highly selective

oxidation of alkylbenzenes using TBHP as the oxidant, giving rise to the corresponding ketones in excellent yields with 100% selectivity.

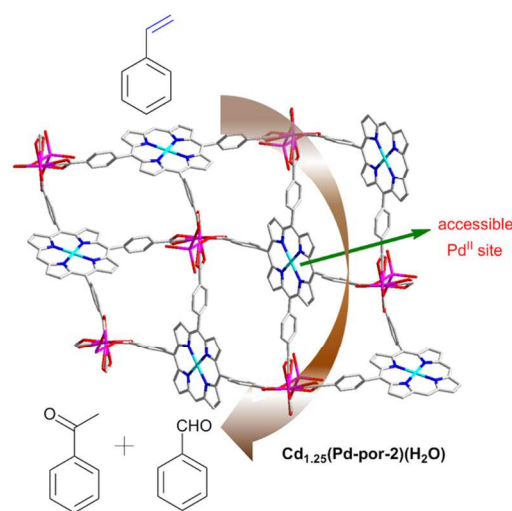


**Fig. 30** Sticks views of Cd<sub>1.25</sub>(Pd-por-2)(H<sub>2</sub>O) and illustration of its catalytic application in oxidation of alkylbenzenes. The Pd and Cd atoms are shown turquoise and pink.

Two more work of Wu's group was published in 2013 about the catalytic MOFs constructed with metalloporphyrin.<sup>57c,d</sup> Porous metalloporphyrinic MOFs M'<sub>2</sub>(HOOC)(M-por-2), (M = Mn<sup>3+</sup> or Fe<sup>3+</sup>; M' = Zn<sup>2+</sup> or Cd<sup>2+</sup>) were prepared from solvothermal reactions of M-por-2 and M'(NO<sub>3</sub>)<sub>2</sub>.<sup>57c</sup> M'<sub>2</sub>(HOOC)(Mn-por-2) can perform as recyclable heterogeneous catalyst in epoxidation of olefins, whereas the Fe-porphyrinic MOFs were much less efficient. This was caused by the deactivation of Fe-porphyrinic MOFs by self-oxidation. M'<sub>2</sub>(HOOC)(Mn-por-2) didn't display size-selectivity in catalysis, since the inner Mn centers were coordinated by format pillars and inaccessible to the substrates. On the other hand, M'<sub>2</sub>(HOOC)(Fe-por-2) still exhibited good performances in intermolecular aldol reaction reaction of aldehydes and ketones. In both catalytic systems, the porphyrinic MOF catalysts displayed better activities than the corresponding homogeneous M(por-2) catalysts.

Another porous Mn-porphyrinic MOF of Zn<sub>2</sub>(MnOH-por-2)(dpni) (dpni = *N,N*-di-(4-pyridyl)-1,4,5,8-naphthalenetetracarboxydiimide) was reported to possess channels with the size of 6.1 × 7.8 Å<sup>2</sup>.<sup>57d</sup> Zn<sub>2</sub>(MnOH-por-2)(dpni) can effectively catalyze the epoxidation of olefins in a heterogeneous manner with size-selectivity. The conversion of styrene in the presence of this Mn-porphyrinic MOF could be as high as 99%. Adsorption experiments also exhibited size-selectivity, and Zn<sub>2</sub>(MnOH-por-2)(dpni) took up 2.5 molecules of styrene, 4.0 molecules of cyclohexene and 2.0 molecules of cyclohexane per formula unit. The crystal structure of the styrene-included Zn<sub>2</sub>(MnOH-por-2)(dpni)·2styrene was obtained. These results suggest that the active catalytic sites should be Mn-por-2 moieties within the pores of framework.

Zhou developed isostructural MOFs Zr<sub>3</sub>(M-por-2) (M = Mn<sup>2+</sup>, Co<sup>3+</sup>, Ni<sup>2+</sup>, Cu<sup>2+</sup>, Zn<sup>2+</sup>) (denoted as PCN-222), which

were produced by solvothermal reactions of M-por-2,  $ZrCl_4$  and benzoic acid in DMF or DEF at  $120^\circ C$ .<sup>58a</sup> The frameworks consisted of  $Zr_6$  clusters linked by M-por-2 ligands. Different from the 12-connected  $Zr_6$  cluster in the Uio-series of MOFs, the  $Zr_6$  cluster was connected to eight porphyrin ligands. PCN-222 contained large 1D open channels with a diameter of up to 3.7 nm. The  $N_2$  adsorption experiment of PCN-222 at 77 K disclosed the typical type IV isotherm, confirming the MOFs with meso pores. In addition, a BET surface area of  $2200\text{ m}^2\text{g}^{-1}$  was determined through the  $N_2$  adsorption. Among these Zr-MOFs, PCN-222(Fe) was exceptionally stable, and can resist in concentrated HCl acid. Catalytic studies showed that PCN-222(Fe) can promote the oxidation of pyrogallol, 3,3,5,5-tetramethylbenzidine and *o*-phenylenediamine with both excellent substrate binding affinity and catalytic activity (Fig. 31). These oxidation reactions are often used to characterize the catalytic performance of heme-like enzyme mimics.

This group further developed a series of highly stable MOFs with the formula of  $Zr_4(M\text{-por-2})$  (denoted as PCN-224; M = no metal, Ni, Co, Fe) with 3D nanochannels (1.9 nm).<sup>58b</sup> The structural difference of PCN-222 and PCN-224 lies in the 8-connected  $Zr_6$  cluster in the former and 6-connected  $Zr_6$  clusters in the latter. The porosity of PCN-224 was examined by  $N_2$  adsorption at 77K, which exhibited a typical type-I isotherm. Based on the  $N_2$  uptake, the BET surface was calculated to be  $2600\text{ m}^2\text{g}^{-1}$ . PCN-224 possesses very high chemical stability, and the frameworks is retained in the wide pH range from 0 to 11. PCN-224(Co) was employed in the cycloaddition reactions of  $CO_2$  and epoxides for three consecutive runs. Results showed that even in the third run, the TON and TOF were 518 and  $129\text{ h}^{-1}$ , respectively, suggesting that PCN-224(Co) was a reusable heterogeneous catalyst for the  $CO_2$ /epoxides cycloaddition reactions. (Fig. 31).

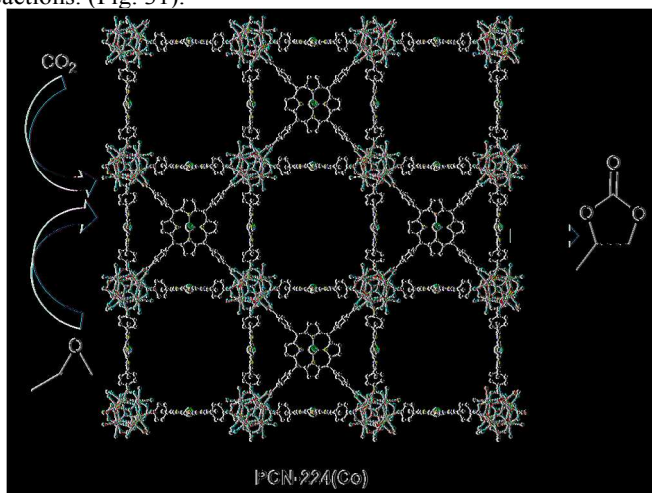


**Fig. 31** Wires and sticks view of PCN-224(Co) and illustration of its catalytic applications. The Fe and Zr atoms are in orange and teal, respectively.

Besides the aforementioned porphyrin-walled MOFs, Eddaoudi et al.<sup>58c</sup> and Zaworotko et al.<sup>58d</sup> have designed and synthesized porphyrin-encapsulated MOFs (porph@MOF) from MOFs containing polyhedral cages, which possess several features such as large cavities and good stability. These porph@MOF materials have showed good catalytic ability in hydrocarbon oxidations.

### 3.2 Metallosalen-Based MOFs

By employing a dipyrindyl  $Mn^{III}(\text{salen-1})Cl$  ( $\text{salen-1} = (R,R)\text{-}(1,2\text{-cyclohexanediamino-}N,N'\text{-bis}(3\text{-tert-butyl-5-(4-pyridyl)salicylidene))$ ) catalyst as a strut in combination with biphenyldicarboxylate (bpdc) or tetrakis(4-carboxyphenyl)benzene (tcpb), Hupp group prepared two zinc paddlewheel MOFs including the catenated  $Zn_2(\text{bpdc})_2(\text{Mn-salen-1})$  and noncatenated  $Zn_2(\text{tcpb})(\text{Mn-salen-1})$ .<sup>59</sup> MOF  $Zn_2(\text{tcpb})(\text{Mn-salen-1})$  consists of a single network with unobstructed channels ( $a \times b = 22.4 \times 11.7\text{ \AA}^2$ )<sup>59b</sup> in comparison to the catenated MOF  $Zn_2(\text{bpdc})_2(\text{Mn-salen-1})$  ( $15.7\text{ \AA} \times 6.2\text{ \AA}^2$ ).<sup>59a</sup> In both frameworks,  $Mn^{III}$  sites were accessible to the channels. Their catalytic activities toward asymmetric epoxidation were examined with 2,2-dimethyl-2H-chromene as substrate and 2-(tertbutylsulfonyl)iodosylbenzene as oxidant (Fig. 32). Epoxide product was obtained with 88% and 80% *ee* in the presence of  $Zn_2(\text{bpdc})_2(\text{Mn-salen-1})$  and  $Zn_2(\text{tcpb})(\text{Mn-salen-1})$ , respectively. The observed enantiomeric excesses (*ee*) rival those of the free molecular catalyst ( $Mn^{III}(\text{salen-1})Cl$ , 90% *ee*) under the same reaction conditions. To determine whether catalysis by  $Zn_2(\text{bpdc})_2(\text{Mn-salen-1})$  occurs predominantly within the channel or instead on the external surface, competitive size selectivity studies were performed. A large porphyrinic substrate, 5,10,15,20-tetraphenylporphyrinato)tin<sup>IV</sup> bis(4-vinyl benzoate, and a small substrate, ethyl 4-vinyl benzoate were mixed in 1 : 1 olefinic unit ratio and reacted with 2-(tertbutylsulfonyl) iodosylbenzene in the presence of the MOF catalyst. The ratio of small to large substrate reactivity increased from 2 to 18 at 45% conversion. In comparison, the homogeneous catalyst  $Mn^{III}(\text{salen-1})Cl$  gave a time-independent 1 : 1 reactivity ratio. The size-selectivity suggested that the MOF-catalyzed reactions mostly underwent in the channels.

A series of isorecticular chiral MOFs (CMOFs) of tunable open channel sizes have been constructed in Lin group, which were assembled from  $Zn_4(\mu_4\text{-O})(O_2CR)_6$  SBUs and Mn-salen-derived dicarboxylic acids composed of the same central unit ( $R,R$ )-1,2-cyclohexanediamino- $N,N'$ -bis(3-*tert*-butyl-salicylidene) $Mn^{III}Cl$  and different terminal groups in the 4,4'-positions (-COOH for salen-2, -CH=CHCOOH for salen-3, - $C_6H_4COOH$  for salen-4, and -CH=CH $C_6H_4COOH$  for salen-5).<sup>60</sup> Reactions of  $Zn(NO_3)_2 \cdot 6H_2O$  with  $Mn^{III}(\text{salen-2})Cl$  and  $Mn^{III}(\text{salen-3})Cl$  in DMF/EtOH led to the formation of two-fold interpenetrated structures of  $[Zn_4(\mu_4\text{-O})(Mn\text{-salen-2})_3] \cdot 20DMF \cdot 2H_2O$  (CMOF-1) and  $[Zn_4(\mu_4\text{-O})(Mn\text{-salen-3})_3] \cdot 42DMF$  (CMOF-2), respectively.<sup>60a</sup> In contrast, the similar reactions in DEF/EtOH gave rise to the non-interpenetrated frameworks of  $[Zn_4(\mu_4\text{-O})(Mn\text{-salen-2})_3] \cdot 22DEF \cdot 4H_2O$  (CMOF-3) and  $[Zn_4(\mu_4\text{-O})(Mn\text{-salen-3})_3] \cdot 37DEF \cdot 23EtOH \cdot 4H_2O$  (CMOF-4). Interestingly, no matter what solvent systems were used, a three-fold interpenetrated framework of  $[Zn_4(\mu_4\text{-O})(Mn\text{-salen-4})_3] \cdot 38DMF \cdot 11EtOH$  (CMOF-5) could be obtained from the reaction of  $Zn(NO_3)_2 \cdot 6H_2O$  and  $Mn^{III}(\text{salen-4})Cl$ . The largest dimension of open channels of these CMOFs were  $8 \times 6\text{ \AA}^2$  (CMOF-1),  $15 \times 7\text{ \AA}^2$  (CMOF-2),  $20 \times 16\text{ \AA}^2$  (CMOF-3),  $25 \times 23\text{ \AA}^2$  (CMOF-4), and  $11 \times 8\text{ \AA}^2$  (CMOF-5), respectively. Catalytic activities of CMOFs 1-5 toward asymmetric epoxidation of unfunctionalized olefins were evaluated with 2,2-dimethyl-2H-chromene as substrate and 2-(*tert*-butylsulfonyl) iodosylbenzene as oxidant, and the conversion rate increases in the order of CMOF-1 < CMOF-5 < CMOF-2 < CMOF-3 < CMOF-4. In addition, CMOFs 4 and 5 are highly effective catalysts for asymmetric epoxidation of chromene to generate

(1*R*,2*S*)-indene oxide in 85% *ee* and 92% *ee*, respectively (Fig. 33). On the other hand, reactions of  $\text{Zn}(\text{NO}_3)_2 \cdot 6\text{H}_2\text{O}$  with  $\text{Mn}^{\text{III}}(\text{salen-5})\text{Cl}$  in DBF/EtOH (DBF = dibutylformamide) yielded  $[\text{Zn}_4(\mu_4\text{-O})(\text{Mn-salen-5})_3] \cdot 4\text{DBF} \cdot 6\text{EtOH} \cdot \text{H}_2\text{O}$  (CMOF-6), whose open channels of triangular shapes with the edge length of 29 Å ran along the  $\langle 001 \rangle$  and  $\langle 1-1-1 \rangle$  directions.<sup>60b</sup> In the presence of CMOF-6, (1*R*,2*S*)-indene oxide was obtained with 84% *ee*.

This group also developed Ru(salen)-based MOFs, the two-fold interpenetrated CMOF-7 with the formula of  $\{\text{Zn}_4(\mu_4\text{-O})[(\text{Ru}^{\text{III}}(\text{salen-2})(\text{py})_2\text{Cl})_3] \cdot (\text{DBF})_7 \cdot (\text{DEF})_7\}$ , and the non-interpenetrated CMOF-8 with the formula of  $\{\text{Zn}_4(\mu_4\text{-O})[(\text{Ru}^{\text{III}}(\text{salen-2})(\text{py})_2\text{Cl})_3] \cdot (\text{DEF})_{19} \cdot (\text{DMF})_5 \cdot (\text{H}_2\text{O})_{17}\}$ , which were prepared by solvothermal reactions of  $[\text{Ru}(\text{salen-2})(\text{py})_2\text{Cl}]$  with  $\text{Zn}(\text{NO}_3)_2 \cdot 6\text{H}_2\text{O}$  in DBF/DEF/EtOH and in DEF/DMF/EtOH, respectively.<sup>60c</sup> The largest cavities in the interpenetrated networks of CMOF-7 were measured to be 8 Å in diameter and were connected to each other by  $4 \times 3$  Å<sup>2</sup> windows, whereas CMOF-8 enjoyed much larger open channel dimensions of  $14 \times 10$  Å<sup>2</sup> and a cavity size of 17 Å. Treatment of CMOF-7 and CMOF-8 with strong reducing agents such as  $\text{LiBeEt}_3\text{H}$  (superhydride) or  $\text{NaB}(\text{OMe})_3\text{H}$  led to CMOF-7' and CMOF-8' in which the  $\text{Ru}^{\text{III}}$  centers had been reduced to  $\text{Ru}^{\text{II}}$

centers. The CMOF-8'-catalyzed asymmetric cyclopropanation of styrene was obtained with very high diastereo- and enantioselectivities (d.r. = 7:1 (*trans/cis*); *ee* = 91% (*trans*) and 84% (*cis*)) in the presence of  $\text{NaBH}(\text{OMe})_3$ . In contrast, a similar cyclopropanation reaction with CMOF-7' as the catalyst gave the desired products in less than 1% yield and with modest *ee* values (33% (*trans*) and 47% (*cis*)). This might be due to the reduced open channels in CMOF-7' relative to those in CMOF-8', thus preventing the diffusion of the reagents into the  $\text{Ru}^{\text{II}}$ /salen active sites in the interior of CMOF-7'.

Similarly, the two-fold interpenetrated MOF  $\{\text{Zn}_4(\mu_4\text{-O})[(\text{Ru}^{\text{III}}(\text{salen-3})(\text{py})_2\text{Cl})_3]_2 \cdot (\text{DBF})_{10} \cdot (\text{DEF})_7\}$  (CMOF-9) and non-interpenetrated  $\{\text{Zn}_4(\mu_4\text{-O})[(\text{Ru}^{\text{III}}(\text{salen-3})(\text{py})_2\text{Cl})_3] \cdot (\text{DEF})_{51}\}$  (CMOF-10) were obtained by the solvothermal reactions in DBF/DEF/EtOH and in DEF/DMF/EtOH, respectively, when salen-3 ligand was used instead.<sup>60d</sup> CMOF-9 and CMOF-10 possessed 3D interconnected channels, with the sizes of  $7 \times 7$  Å<sup>2</sup> and  $19 \times 19$  Å<sup>2</sup>, respectively. The reduced form CMOF-10' displayed better catalytic performances in the cyclopropanation of olefins than CMOF-9'.

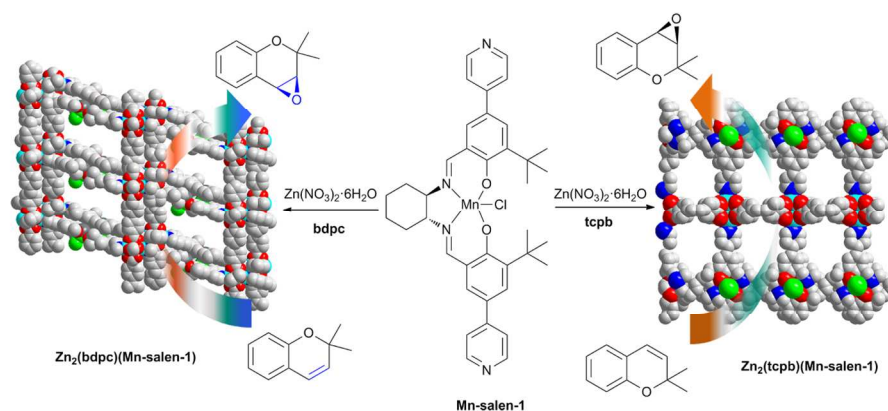


**Fig. 32** Space-filling view of  $\text{Zn}_2(\text{bdpc})(\text{Mn-salen-1})$  and  $\text{Zn}_2(\text{tcpc})(\text{Mn-salen-1})$ , and their synthesis and catalytic application in epoxidation of olefin. The Zn, Mn and Cl atoms are shown in turquoise, teal, and bright green, respectively.

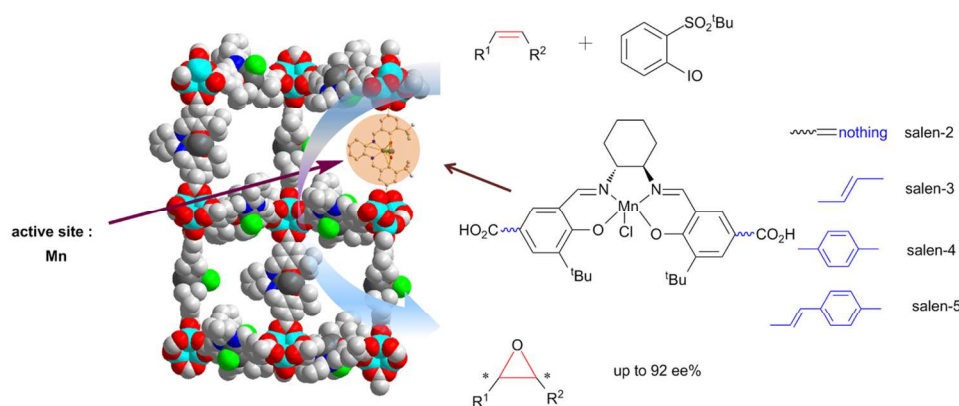


**Fig. 33** Space-filling view of CMOF 1-6 and illustration of their catalytic application in epoxidation of olefin. The Zn, Mn and Cl atoms are shown in turquoise, teal and bright green, respectively.

More recently, Cui group developed a Co(salen)-based MOF,  $[\text{Cd}_4(\text{Co}(\text{salen-2}))_4(\text{DMF})_4(\text{OAc})_4] \cdot 4\text{H}_2\text{O}$ , which was synthesized by heating a 2:1 mixture of  $\text{Cd}(\text{NO}_3)_2 \cdot 6\text{H}_2\text{O}$  and  $\text{Co}(\text{salen-2})(\text{OAc})$  in DMF and  $\text{H}_2\text{O}$ .<sup>61a</sup> MOF  $\text{Cd}_4(\text{Co}(\text{salen-2}))_4(\text{DMF})_4(\text{OAc})_4$  adopted a 3D chiral nanoporous framework that was built from  $\text{Cd}_4$  clusters and  $\text{Co}(\text{salen-2})$  linkers with open channels of  $\sim 12 \times 8$  Å<sup>2</sup> along the *a*-axis. The  $\text{Co}(\text{salen-2})$ -based framework was shown to be an efficient and recyclable

framework. The  $\text{Co}(\text{salen-2})$ -based framework was shown to be an efficient and recyclable

heterogeneous catalyst for hydrolytic kinetic resolution (HKR) of a range of benzyloxy epoxide derivatives bearing both electron-donating and electron-withdrawing substituents with up to 99.5% *ee* (Fig. 34). It was noted that the examined epoxides exhibited good to excellent kinetic resolution selectivities ( $K_{rel} = 13\text{--}43$ , the ratio of relative rates of the two substrate enantiomers). This Co(salen) MOF exhibited size-selective catalysis. While the reaction with the small substrate phenoxy epoxide was in 56% conversion, the one with the sterically more demanding substrate triphenyl glycidyl ether was only in less than 5% conversion under the same reaction conditions. This result suggested that this bulky substrate cannot access the catalytic sites in the porous structure due to its large diameter, and catalytic HKR should occur within the MOF.

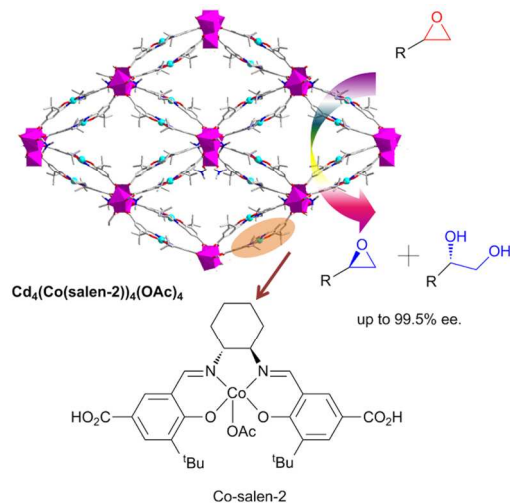


**Fig. 34** Ball-and-stick view of  $\text{Cd}_4(\text{Co}(\text{salen-2}))_4(\text{OAc})_4$  and illustration of its catalytic application in hydrolytic kinetic resolution. The Cd and Co atoms are shown in pink polyhedra and turquoise.

In addition to these porous metallosalenic frameworks, Cao group reported 1D homochiral Ni-salen-1 based coordination polymers, which performed as self-supported heterogeneous catalysts.<sup>61b</sup>

In summary, only five achiral porphyrin ligands have been used so far to construct MOFs, and most of the catalytic applications of these porphyrinic MOFs are related to the oxidation reactions of olefins either of epoxidation or transformations to carbonyl-functionalized substrates. This discipline is rather immature compared to homogeneous metal-porphyrin catalysts, and thus it is in high need to develop more catalytical porphyrinic MOFs, especially containing chiral porphyrin ligands. In comparison, MOFs derived from metallosalen ligands showed richer catalytic chemistry. It might be due to the chiral adduct is easier to be induced to the metallosalen ligand than metalloporphyrin ligand. Chiral salen ligands can be readily prepared by the condensation of aryl aldehyde and commercial available (1*R*,2*R*)-(-)-diaminocyclohexane. As a result, salen-containing MOFs have been applied in asymmetric catalysis such as epoxidation, cyclopropanation and hydrolytic kinetic resolution with excellent *ee* values.

#### 4. MOFs with Functional Organic Sites

As discussed above, studies on the catalytic performance of MOFs with the metal sites taking the essential role in catalysis have been thoroughly studied. However, only a few proofs of concept with regard to the catalytically-active functional organic sites (FOS) in MOF catalysis have been reported.<sup>62-81</sup> The paucity of information on FOS might be because of the difficulty of producing guest-accessible FOS on the pore surface: these organic groups tend to coordinate metal ions via a self-assembly process, resulting in frameworks in which FOS are completely blocked. Nevertheless, three types of strategies have been used to build up catalytic MOFs based on organic functional groups: (a) introduction of these sites in the organic linkers, (b) grafting of these groups on the coordinatively unsaturated metal centers, and (c) post-covalent modification of organic ligands or linker sites. These MOFs containing FOS can not only behave as catalyst themselves but also be used to immobilize catalytic metal complexes through complexation. Selective reports on MOFs containing FOS as well as post-synthetically modified MOFs through complexation of these functional MOFs are listed in Table 3 and 4, respectively.

Concerning base-catalyzed reactions, Kim<sup>62</sup>, Kitagawa<sup>63</sup>, and Gascon<sup>64a</sup> have demonstrated the possibility to use as-synthesized MOFs as basic catalysts by introducing pyridyl, amide and amino groups, respectively, in the organic linkers. In addition, Chang grafted amine onto the unsaturated metal sites of MOFs.<sup>65</sup> These base-type catalysts have been employed in the Knoevenagel condensation and transesterification reactions. Among these areas, the introduction of an amino-group to the MOFs has been particularly effective. Through covalent post-synthesis, Schiff base-containing MOFs can be formed due to the reaction of the amino group and an added aldehyde/ketone reagent, which in turn undergo complexation.<sup>66-70</sup>

In respect of acid-catalyzed reactions, the sulfoxy group ( $-\text{SO}_3\text{H}$ ) has also been introduced through the aromatic linker of MIL-53(Al) and MIL-101(Cr) by Gascon et al<sup>71</sup> and Zhu et al<sup>72</sup>, respectively. These acid catalysts have been employed in esterification of carboxylic acids and alcohols.

As for fine reactions giving rise to more valuable products, organocatalysts such as pyrrolidine, *N*-heterocyclic carbene, urea, binol, bipyridine and catechol have been successfully incorporated into MOFs.<sup>73-81</sup> Kim<sup>73</sup>, Telfer<sup>74</sup> and Duan<sup>75</sup> have prepared pyrrolidine-based MOFs, which can effectively promote the aldol reactions with modest to good *ee* values. Hupp and the co-workers developed NHC-/urea- based MOFs, which can catalyze the addition of alcohols to  $\alpha,\beta$ -unsaturated ketones and Friedel–Crafts reaction, respectively.<sup>76,78</sup> Wu group immobilized Pd onto the NHC-containing MOFs, and the obtained Pd-NHC MOFs effectively promoted the Suzuki–Miyaura cross-coupling reaction of aryl halides with phenylboronic acids.<sup>77</sup> Lin group designed a series of binol-containing ligands to construct functional MOFs, and the latter reacted with Ti(IV) complexes, yielding Ti-binolate MOFs that can perform as active catalysts in the  $\text{ZnEt}_2$  addition reactions with aromatic aldehydes and show excellent *ee* values (up to 93%).<sup>79</sup> Li et al firstly exploited the catalytic activity of the uncoordinated 2,2'-bipyridine in MOF-253 in cross-coupling of aryl halides with inactivated arenes, and further prepared MOF-253-CuI through post-synthetic method and studied its application in the C–O cross-coupling of phenols and alcohols with aryl halides.<sup>80</sup> Hupp et al. grafted catechol to MIL-101(Cr) and then immobilize  $\text{V}^{5+}$  through complexation.<sup>81</sup>

##### 4.1 Pyridyl and Amide Groups

As one of pioneer works in MOF catalysis, in as early as 2000, Kim et al studied the asymmetric catalysis of MOF with pyridyl group behaving as functional organic sites, although only low enantioselectivity was achieved with enantiomeric excess value of 8%. They reported the synthesis of a homochiral MOF, *D*-POST-1 with the formula of  $[Zn_3(\mu_3-O)(dpdc)_6] \cdot 2H_2O \cdot 12H_2O$  (Hdpdc = (4*S*,5*S*)-2,2-dimethyl-5-[(4-pyridinylamino)carbonyl]-1,3-dioxolane-4-carboxylic acid).<sup>62</sup> The structure of *D*-POST-1 features in existence of large chiral 1D channels, the cross-section of which was best described as an equilateral triangle with a side length of 13.4 Å. A half of pyridine groups extrude into the channel without any interactions with the framework, as illustrated in Fig. 35. These exposed pyridyl groups provide the MOF with unique opportunities in heterogeneous catalysis. The catalytic activity of *D*-POST-1 was examined in the transesterification of 2,4-dinitrophenyl acetate. Treatment of 2,4-dinitrophenyl acetate and ethanol with suspension of 0.1 equivalent of the MOF catalyst in carbon tetrachloride for 55 h at 27 °C produced ethyl acetate in 77% yield. However, transesterification of 2,4-dinitrophenyl acetate with bulkier alcohols, for example, isobutanol, neopentanol and 3,3,3-triphenyl-1-propanol, takes place with a much slower or even negligible rate under the same reaction conditions. This size selective observation suggests that the catalysis mainly occurs in the channels. Moreover, *D*-POST-1 manifested enantioselective catalytic activity for the transesterification of 2,4-dinitrophenyl acetate. By using *D*-POST-1 or *L*-POST-1 as catalysts, *S* or *R* enantiomeric ester products were obtained with about 8% enantiomeric excess. In spite of the modest enantioselectivity, such asymmetric catalytic process in MOF pores is believed noteworthy because asymmetric induction has never been observed in reactions mediated by modular porous materials.

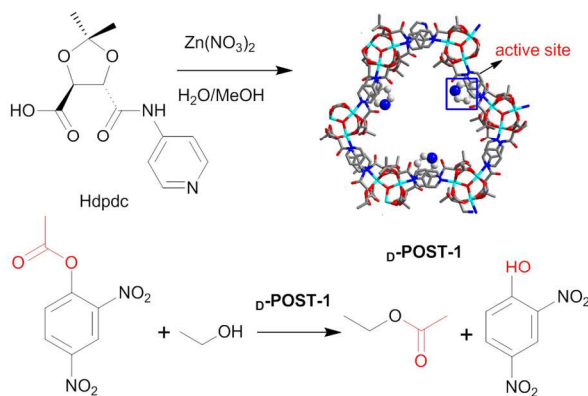


**Fig. 35** Wires and sticks view of *D*-POST-1 and illustration of its synthesis and catalytic application in transesterification.

Kitagawa group for the first time employed a three-connector ligand 4-btapa (*N*<sup>1</sup>,*N*<sup>3</sup>,*N*<sup>5</sup>-tri(pyridin-4-yl)benzene-1,3,5-tricarboxamide) containing three pyridyl groups as coordination sites and three amide groups as guest interaction sites in the self-assembly of a base-type catalytic porous framework,  $\{[Cd(4-btapa)_2(NO_3)_2] \cdot 6H_2O \cdot 2DMF\}_n$  (Cd-btapa) (Fig. 36).<sup>63</sup> The coordination framework was constructed from the Cd(II) center as a six-connected node using 4-btapa as a three-connected linker, producing three-dimensionally running channels with dimensions of  $4.7 \times 7.3 \text{ \AA}^2$ . The zigzag channels were occupied by nitrate anions and  $H_2O$  and DMF molecules. Importantly, the amide groups are highly ordered on the surfaces of the channels, offering a chance to interact with

guest molecules. The TGA data indicated that Cd-btapa was stable up to 250 °C. Taking advantage of these structural characters, they studied the Lewis-base catalysis of Cd-btapa, and examined its catalytic activity in Knoevenagel condensation reactions of benzaldehyde with active methylene compounds, such as malononitrile, ethyl cyanoacetate, and cyano-acetic acid *tert*-butyl ester. It was found that the malononitrile was a good substrate, producing 98% conversion of the adduct, whereas other substrates with larger sizes reacted negligibly. The size-selectivity suggested that the catalytic reactions should occur within the channels. The heterogeneity and recyclability of solid Cd-btapa were examined through filtration and recycling experiments, confirmed by the powder XRD patterns of the catalyst before and after the reactions for high stability of the heterogeneous catalyst. This is the first report on the use of MOFs as heterogeneous catalysts for the Knoevenagel condensation. After this, Knoevenagel condensation has gradually become a benchmark reaction for the test of the Lewis base catalysis of MOFs.

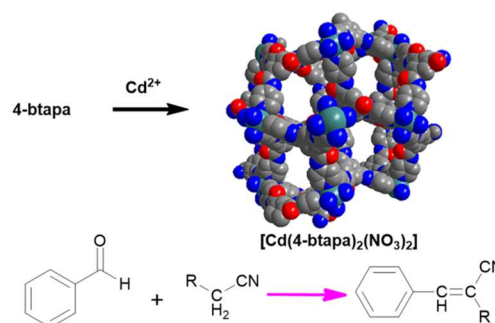


**Fig. 36** Space-filling view of  $Cd(4-btapa)_2(NO_3)_2$  and illustration of its synthesis and catalytic application in Knoevenagel condensation.

#### 4.2 Amino and Aldehyde Groups

Gascon groups showed their interests in the study of the application of amino-functionalized MOFs in Lewis base catalysis by developing an amino-containing MOF,  $NH_2$ -MIL-101(Al), and observed excellent activities and selectivity of these MOFs to the Knoevenagel condensation.<sup>64a</sup> These amino-containing MOFs were stable under the studied reaction conditions, and could be reused without significant loss in activity. More recently, this group developed an oxamate-functionalized MOF, MIL-101(Cr)-PMA (PMA refers to phenylene-mono(oxamate)), which was prepared by the reaction of  $NH_2$ -MIL-101(Cr) and ethyl chlorooxamate at 343 K.<sup>64b</sup> Cu complexes can be incorporated into this oxamate-containing MOF. Two Cu precursors, Cu nitrate and Cu ethylenediamine have been employed, leading to the formation of MIL-100(Cr)-PMA-Cu and MIL-100(Cr)-PMA-CuEDA, respectively. ICP-OES analysis revealed that the Cu contents were about 9 wt% in both cases. The Cu-MOFs exhibits good catalytic performances in 1,3-dipolar cycloaddition reactions of azides and alkynes as well as multicomponent coupling reactions (propargylamine formation).

Another example of amine-functionalized MOF, ED-MIL-101(Cr) (ED = ethylenediamine), was obtained by coordination of ED to the dehydrated MIL-101 framework in Chang group.<sup>65</sup> The synthesis of ED-MIL-101(Cr) was achieved by refluxing ED and dehydrated MIL-101(Cr) framework in toluene. The almost unchanged X-ray diffraction patterns confirmed that the ED grafting occurs with no apparent loss of crystallinity, but with some slight variations of the Bragg intensities. The

catalytic performance of dehydrated ED-MIL-101(Cr) was measured by using the Knoevenagel condensation as a model reaction. In the presence of a catalytic amount of ED-MIL-101(Cr), the condensation of benzaldehyde into *trans*-ethyl cyanocinnamate was accomplished with 97.1% yield and 99.1% *trans* selectivity. Moreover, in terms of turnover frequency (TOF), ED-MIL-101(Cr) showed a remarkably superior activity (TOF = 328 h<sup>-1</sup>). The recyclability test of ED-MIL-101(Cr) clearly supported that it was easily isolated from the reaction suspension by filtration and can be reused without significant loss of activity in the third run.

Yaghi et al. developed IRMOF-3 (isoreticular MOF-3, Zn<sub>4</sub>O(bdc-NH<sub>2</sub>)<sub>3</sub>) with a free diameter of 9.6 Å decorated with pendant amine (-NH<sub>2</sub>) groups, whose crystalline structure is similar to the well-known MOF-5 (or IRMOF-1).<sup>66a</sup> The amine moieties are not intimately involved in the framework backbone, and therefore are available to undergo chemical transformations (Fig. 35).<sup>66-68</sup> A desirable amine transformation via a simple condensation reaction was reported by Rosseinsky et al., producing a salicylidene (sal) moiety IRMOF-3-sal which subsequently undergo metal binding with V(O)(acac)<sub>2</sub>·H<sub>2</sub>O (acac = acetylacetonate) to lead to the formation of IRMOF-3-sal-V (Fig. 37).<sup>66b</sup> Comparable powder XRD patterns for IRMOF-3-sal and IRMOF-3-sal-V with IRMOF-3 verified the persistence of the extended open framework structure. IRMOF-3-sal-V was found to be active for the oxidation of cyclohexene with TBHP (40% conversion of cyclohexene in THF at 60 °C for 72 h). Catalytic behavior was demonstrated to be heterogeneous through the filtration experiment. However, the poor turnover frequencies combined with loss of framework

integrity after catalytic reactions limited its further applicability.

Concurrently, Corma employed the similar covalent post-synthesis methodology to prepare IRMOF-3 containing an Au(III) Schiff base complex.<sup>67</sup> IRMOF-3-sal-Au was prepared through reacting a suitable gold precursor, NaAuCl<sub>4</sub>, with IRMOF-3-sal. According to the elemental analysis of the samples, a maximum functionalization of about 3% of the total -NH<sub>2</sub> groups was accomplished without losing the framework integrity, while gold complexation by the Schiff base complex was almost quantitative. A 3% functionalization of the Schiff base allowed introducing up to 2 wt% of gold in the material. Powder XRD pattern of IRMOF-3-sal-Au remained unaltered when the material was heated up to 300 °C in air, demonstrating that the PSM-MOF is thermally stable. IRMOF-3-SI-Au was then employed to catalyze the multicomponent domino coupling reaction of *N*-tosyl protected ethynylaniline, paraformaldehyde and piperidine (Fig. 37). It was found that the conversion of *N*-tosyl protected ethynylaniline increased continuously up to 93% over IRMOF-3-sal-Au within 14 h. The IRMOF-3-sal-Au exhibited a large substrate scope relating to *N*-protected ethylanilines, aldehydes and amines. Additionally, cyclohexylcarboxaldehyde and octylaldehyde can also take part in this catalysis. The ethynylaniline bearing either an electron-donating methyl group or an electron-withdrawing methoxycarbonyl group performed well in the reactions. Remarkably, the reactions were also successful with chiral amines such as (*s*)-(+)-2-(methoxymethyl)-pyrrolidine and (*s*)-(+)-2-methylpiperidine, giving yields of up to 92%.

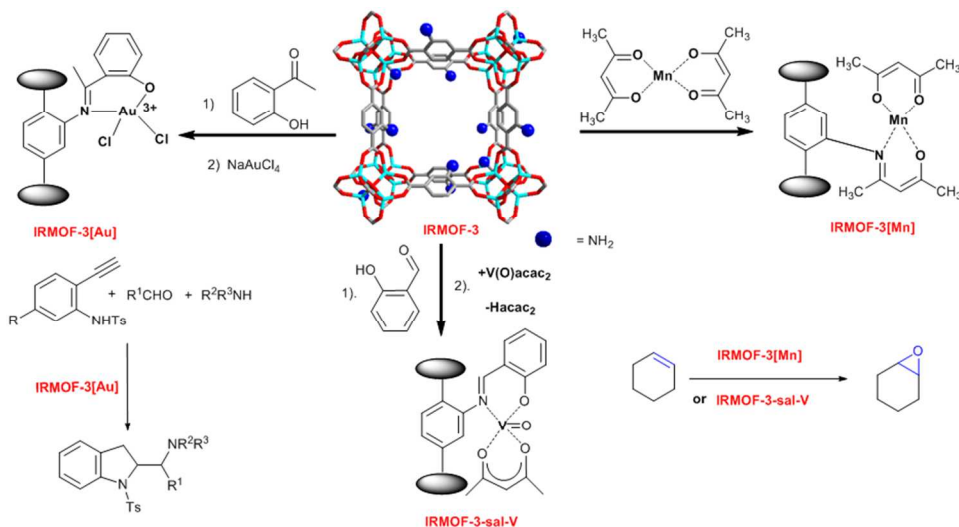


**Fig. 37** Schematic view of post-synthetic modification of IRMOF-3 with three different metal complexes of Au(left), V(middle), Mn(right), and illustration of their catalytic application in epoxidation of olefins (Mn, V) and the three-component coupling reaction (Au).

Ahn et al. prepared an Mn-immobilized MOF via the binding of a manganese(II) acetylacetonate complex to IRMOF-3 through post-synthetic modification, which was accomplished by dissolving Mn(acac)<sub>2</sub> in toluene and treating the resulting solution with IRMOF-3 crystals at 55 °C for 20 h.<sup>68</sup> The obtained IRMOF-3-Mn was stable in an inert atmosphere or in toluene for several months. The powder XRD patterns comparison between IRMOF-3 and IRMOF-3-Mn indicated that the original MOF porous structure was maintained after the post-synthetic reaction. Furthermore, no changes in the type I N<sub>2</sub> adsorption-desorption isotherms were observed after post-

modification of IRMOF-3, again suggesting that the structure of the parent material remained intact after functionalization. Integrating of Mn(acac)<sub>2</sub> into the MOF framework have been verified by means of FT-IR, <sup>1</sup>H NMR and XPS studies. ICP-MS analysis and elemental analysis of IRMOF-3-Mn revealed that the extent of binding of the Mn complex led to a final weight loading of 1.25% Mn in the MOFs. The catalytic activity of IRMOF-3-Mn was tested for the epoxidation of alkenes using molecular oxygen and trimethylacetaldehyde as the oxidant (Fig. 37). The epoxidation of cyclohexene over IRMOF-3-Mn at 40 °C formed cyclohexene oxide with

excellent selectivity (92%) and conversion (68%). It was found that the larger molecule cyclooctene was converted to cyclooctene oxide with lower conversion (60%) and slightly higher selectivity (96%) than cyclohexene under the resembling reaction conditions. The reactivity of the double bond attached to benzylic rings displayed lower conversion and selectivity to epoxide than in the other two cyclic alkenes, cyclohexene and cyclooctene. At 40 °C, styrene was converted to the corresponding epoxide with 52% conversion and 81% selectivity. Recycling experiments confirmed that conversion and selectivity to epoxide were almost identical irrespective of the number of cycles performed. Further confirmation on the stability of Mn in MOF was made through a hot filtering experiment. No Mn in the filtrate after the reaction was detected by ICP measurement. The powder XRD patterns and FTIR spectra of the solid catalyst after reuse were also indistinguishable from those of the fresh catalyst, indicating that no structural deterioration or organic and metal complex decomposition occurred after catalytic reactions.

As mentioned above, the UiO-66 MOF  $Zr_6O_4(OH)_4(bdc)_6$  shows high thermal stability due to the presence of an inner  $Zr_6O_4(OH)_4$  core in which the triangular faces of the  $Zr_6$ -octahedron are alternatively capped with  $\mu_3$ -O and  $\mu_3$ -OH groups. Cohen and Lillerud independently discovered that the UiO-66 motif was very tolerant to functionalized ligands, allowing the synthesis of the amino-functionalized UiO-66-NH<sub>2</sub> with the same topology.<sup>69a,b</sup> Due to the presence of NH<sub>2</sub> groups in the linker, NH<sub>2</sub>-UiO-66 can be further metallated.

A PSM-MOF of UiO-66, NH<sub>2</sub>-UiO-66-damp-Ir (damp = 6-((diisopropylamino)methyl)picolinaldehyde)) was prepared from the reaction between the amino group of NH<sub>2</sub>-UiO-66 and damp by Iglesias and Corma et al., leading to the formation of imino-pincer complex, which further reacted with Ir(I) complex [IrCl(COD)]<sub>2</sub>.<sup>69c</sup> ICP-AES analysis of NH<sub>2</sub>-UiO-66-damp-Ir indicated that the amount of iridium was 3.11 wt%. Catalytic evaluation of the NH<sub>2</sub>-UiO-66-damp-Ir was performed by mixing them with the nitroarenes and carbonyl compounds in isopropanol in a batch reactor. Under the optimized reaction conditions, various aldehydes were reductively aminated with nitrobenzene under 6 bar pressure of molecular hydrogen. T Hot filtration tests for NH<sub>2</sub>-UiO-66-damp-Ir proved that the catalytic activity was associated with the solid exclusively, and no reaction occurred when the catalyst was removed from the reaction mixture. MOF NH<sub>2</sub>-UiO-66-damp-Ir can be recovered by simple filtration in air and reused without noticeable loss of catalytic activity for at least four cycles. The overall framework structure of the material remained intact: the powder XRD patterns and SEM images of both the fresh and the recovered catalysts after catalytic reactions matched very well. TEM images indicated that there was no formation of nanoparticles during the catalytic reactions.

The NH<sub>2</sub>-MIL-101(Fe), which is isostructural to the MIL-101(Cr), is formed by trimeric iron(III) octahedral clusters via linkage of 2-aminoterephthalate ligands.<sup>70a</sup> Canivet et al. reported a PSM-MOF, Ni@NH<sub>2</sub>-MIL-101(Fe), which was prepared via the imine condensation reaction between formyl groups of Ni(PyCHO)Cl<sub>2</sub> and amine groups of NH<sub>2</sub>-MIL-101(Fe).<sup>70b</sup> The condensation yielded 10Ni@NH<sub>2</sub>-MIL-101(Fe) when 1 equiv of PyCHO/NiCl<sub>2</sub> per -NH<sub>2</sub> moiety on the MOF was used, whereas 30Ni@NH<sub>2</sub>-MIL-101(Fe) could be obtained when using 3 equiv of PyCHO/NiCl<sub>2</sub>. Powder XRD analysis confirmed the structural integrity of the solid materials after the functionalization step. As exemplified in Fig. 38, the catalytic activities of Ni@MIL-101(Fe) were examined using the liquid-

phase ethylene dimerization as the benchmark reaction. Typically, Ni@NH<sub>2</sub>-MIL-101(Fe) suspended in heptane was allowed to react in the presence of Et<sub>2</sub>AlCl under 15 bar of ethylene. The Ni@MIL-101(Fe) catalyst was rather active with turnover frequencies up to 3215 h<sup>-1</sup> at 10 °C, and the selectivity for 1-butene product was 94%. Leaching test confirmed that no reaction occurred if the filtrated catalytic solution was again put under catalytic conditions in the presence of Al-based co-catalyst. Powder XRD patterns of 10Ni@MIL-101(Fe) after a catalytic run verified that its crystallinity was kept. Furthermore, after careful washings with anhydrous ethanol and drying, the 10Ni@MIL-101(Fe) can be reused for at least two more catalytic runs without significant loss of activity or selectivity.

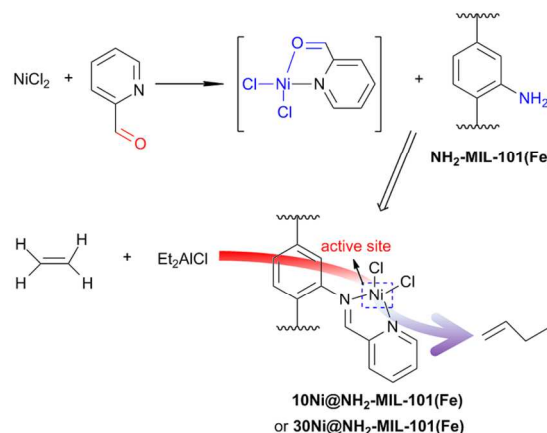


**Fig. 38** Schematic view of the preparation of Ni@NH<sub>2</sub>-MIL-101(Fe) and its catalytic application in ethylene dimerization.

Excellent works demonstrating MOF catalysis in a supramolecular way by using aldehyde-containing MOFs have been done in Farrusseng's group.<sup>70c,d</sup> They functionalized ZIF-type materials to get SIM-1 (Substituted Imidazolate Material), which is isostructural to commercialized ZIF-8 under the name Basolite Z-1200. After grafting C<sub>12</sub> alkyl chains onto the framework, they are able to efficiently control the hydrophilic-hydrophobic balance of the post-modified material, which drives the competitive adsorption of reactants and products.<sup>70c</sup> The introduction of alkyl chains was accomplished by the reaction between the aldehyde group of SIM-1 with dodecylamine. SIM-1 was firstly supported on  $\alpha$ -alumina beads, leading to SIM-1/alumina composites, which were further immersed in a solution of dodecylamine to lead to formation of eggshell SIM-2(C<sub>12</sub>) beads composites. Knoevenagel condensation was used to test the catalytic activity of the SIM on alumina beads. Catalytic results indicated that SIM-2(C<sub>12</sub>)/beads was 3-fold more efficient than SIM-1/beads due to the creation of hydrophobic environment surrounding the catalytic sites in SIM-2(C<sub>12</sub>). Interestingly, it was shown that the contact angle of a catalyst thin layer with water can be directly correlated to the catalytic activity, taking advantage of water that could be produced from Knoevenagel condensation.

#### 4.3 Sulfoxy Group

A strategy to post-synthetically incorporate sulfoxy moieties into MIL-53(Al) was reported by Gascon group.<sup>71</sup> Characterization results demonstrated that, by treating MIL-53(Al) with a mixture of sulfuric acid and triflic anhydride, sulfoxy acid moieties are covalently bonded to the aryl carbons

of the organic linkers (Fig. 39). The acid catalytic property of the resulting functionalized MOF (denoted as S-MIL-53(Al)) was examined using the esterification of a 1:1 molar ratio of acetic acid and *n*-butanol at 343 K. Due to adsorbed  $\text{Ti}_2\text{O}$  or  $\text{H}_2\text{SO}_4$  that were very difficult to eliminate except under reaction conditions, S-MIL-53(Al) showed a high catalytic activity in the first run. Hence, the performance was related to the second use of the catalysts in case of the sulfated MOFs. In the second run, the TOF for S-MIL-53(Al) was around  $1 \text{ min}^{-1}$ . Catalytic experiments with MIL-53(Al) showed the same conversion profile as the blank run, demonstrating that the catalysis can be attributed to the presence of sulfoxy acid groups within the framework pores. Functionalized S-MIL-53(Al) can be recycled without significant loss of activity. This TOF was maintained even after 5 reuses of the S-MIL-53(Al) catalyst.

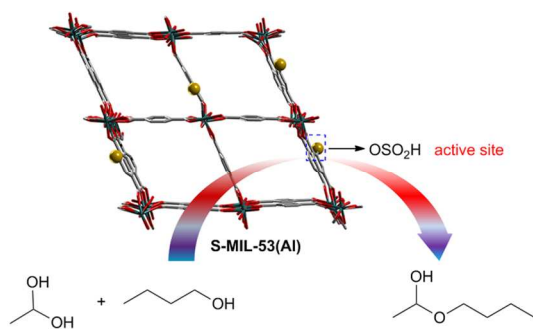


**Fig. 39** Wires and sticks view of S-MIL-53(Al) and illustration of its catalytic application in esterification. The sulfoxy moieties are represented in yellow balls.

On the other hand, a one-pot synthesis of the sulfoxy or sulfonic acid-functionalized MIL-101(Cr) MOF catalyst was presented by Zhang and Zhu et al. The functionalized S-MIL-101(Cr) was obtained from the hydrothermal reaction of  $\text{CrO}_3$ , 2-sulfoterephthalic acid monosodium salt and hydrochloric acid (12 M) at  $180^\circ\text{C}$  for 6 d.<sup>72</sup> The catalytic activities of S-MIL-101(Cr) was tested using the liquid-phase esterification of *n*-hexanol with acetic acid. Over S-MIL-101(Cr), the yield of hexyl acetate was 65.1%. For comparison, MIL-101(Cr) itself did not have any catalytic activity in the esterification. Additionally, S-MIL-101(Cr) showed a much high TOF value of  $2.78 \text{ min}^{-1}$  in the esterification under the optimized conditions. As a heterogeneous catalyst, S-MIL-101(Cr) can be easily recovered after the reaction by filtration and can be reused for 5 runs without significant loss of catalytic activity or selectivity. The results from XRD characterizations for the used S-MIL-101(Cr) catalyst after the 5<sup>th</sup>-run reaction were almost the same as those for the fresh S-MIL-101(Cr), confirming the stability of the prepared S-MIL-101(Cr) catalyst.

#### 4.4 Pyrrolidine

Pyrrolidines as proline-derived compounds have been widely as organocatalysts, and can efficiently promote asymmetric aldol reactions. By postsynthetic modification with chiral ligands (*S*)-*N*-(pyridin-3-yl)-pyrrolidine-2-carboxamide (3-ppc) and (*S*)-*N*-(pyridin-4-yl)-pyrrolidine-2-carboxamide (4-ppc), Kim group reported the synthesis of chiral MOFs possessing pyrrolidine functional group from a pre-assembled achiral MOF, MIL-101(Cr).<sup>73</sup> The chiral ligands can be coordinated to the open metal coordination sites of MIL-101(Cr), leading to the formation of  $[\text{Cr}_3\text{O}(3\text{-ppc})_{1.8}(\text{H}_2\text{O})_{0.25}\text{F}(\text{bdc})_3] \cdot 0.15(\text{H}_2\text{bdc}) \cdot \text{H}_2\text{O}$  (CMIL-1) and  $[\text{Cr}_3\text{O}(4\text{-ppc})_{1.75}(\text{H}_2\text{O})_{0.25}\text{F}(\text{bdc})_3] \cdot 0.15(\text{H}_2\text{bdc}) \cdot \text{H}_2\text{O}$  (CMIL-2). Elemental analysis data indicated that  $\sim 1.8$  ligands per formula were incorporated for both CMILs. Nitrogen adsorption measurements indicated that both chiral MOFs were highly porous even after post modification (BET surface area,  $1420 \text{ m}^2/\text{g}$  for CMIL-1 and  $1375 \text{ m}^2/\text{g}$  for CMIL-2). The catalytic activities of CMILs were tested for asymmetric aldol reactions between various aromatic aldehydes and ketones (Fig. 40). The reactions catalyzed by CMILs produced aldol products in good to excellent yields (60-90%) with fair to good enantioselectivity for *R*-isomers (ee 55-80%). Recycling experiment showed that CMIL-1 can be reused for the asymmetric aldol reaction between *para*-nitrobenzaldehyde and acetone up to three times without significant change in yield and enantioselectivity. A size selectivity study was performed to make sure that the aldol reactions occur mostly in the framework cavities of CMILs. While the reaction between bulky aldehyde 5-formyl-1,3-phenylene-bis-(3,5-di-*tert*-butylbenzoate), which was larger than the window size of CMIL-1, and *para*-nitrobenzaldehyde in the presence of 3-ppc was completed within 36 h, only 5% of the aldol product was observed in the presence of CMIL-1 after the same period of reaction time.

· $\text{H}_2\text{O}$  (CMIL-1) and  $[\text{Cr}_3\text{O}(4\text{-ppc})_{1.75}(\text{H}_2\text{O})_{0.25}\text{F}(\text{bdc})_3] \cdot 0.15(\text{H}_2\text{bdc}) \cdot \text{H}_2\text{O}$  (CMIL-2). Elemental analysis data indicated that  $\sim 1.8$  ligands per formula were incorporated for both CMILs. Nitrogen adsorption measurements indicated that both chiral MOFs were highly porous even after post modification (BET surface area,  $1420 \text{ m}^2/\text{g}$  for CMIL-1 and  $1375 \text{ m}^2/\text{g}$  for CMIL-2). The catalytic activities of CMILs were tested for asymmetric aldol reactions between various aromatic aldehydes and ketones (Fig. 40). The reactions catalyzed by CMILs produced aldol products in good to excellent yields (60-90%) with fair to good enantioselectivity for *R*-isomers (ee 55-80%). Recycling experiment showed that CMIL-1 can be reused for the asymmetric aldol reaction between *para*-nitrobenzaldehyde and acetone up to three times without significant change in yield and enantioselectivity. A size selectivity study was performed to make sure that the aldol reactions occur mostly in the framework cavities of CMILs. While the reaction between bulky aldehyde 5-formyl-1,3-phenylene-bis-(3,5-di-*tert*-butylbenzoate), which was larger than the window size of CMIL-1, and *para*-nitrobenzaldehyde in the presence of 3-ppc was completed within 36 h, only 5% of the aldol product was observed in the presence of CMIL-1 after the same period of reaction time.

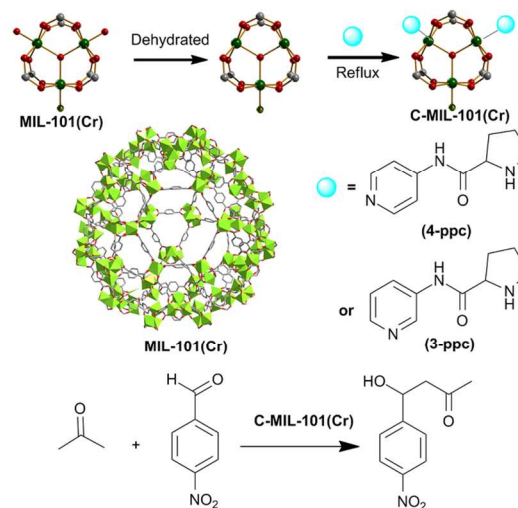


**Fig. 40** Schematic representation of post-modification of the dehydrated MIL-101(Cr) with *L*-proline-derived ligands (e.g. 3-ppc and 4-ppc) and illustration of the catalytic application in aldol reaction.

Telfer group also presented a strategy for incorporating pyrrolidine to MOFs,<sup>74</sup> in which the functional MOFs were built on the fact that biphenyl-4,4'-dicarboxylic acid ligands, including those substituted at the 2 and/or 2' positions, can react with zinc(II) to form IRMOFs. They chose (*S*)-2-(1-(*tert*-butoxycarbonyl)pyrrolidine-2-carboxamido)-[1,1'-biphenyl]-4,4'-dicarboxylic acid ((*S*)-pro-boc) as the building block. The solvothermal reaction of (*S*)-pro-boc with  $\text{Zn}(\text{NO}_3)_2$  in *N,N*-diethylformamide (DEF) produced well-faceted, colorless, cubic crystals of IRMOF-pro-boc. The crystal structure closely resembles other members of the IRMOF series. IRMOF-pro-boc can be converted to IRMOF-pro in a single-crystal-to-single-crystal manner by heating to  $165^\circ\text{C}$  in DMF under microwave irradiation (Fig. 41). IRMOF-Pro was then employed as heterogeneous catalyst in aldol reactions. Reaction of acetone and 4-nitrobenzaldehyde gave the aldol product 4-

hydroxy-4-(4-nitrophenyl)-pentan-2-one with 29% *ee*. The aldol reaction of cyclopentanone and 4-nitrobenzaldehyde to give hydroxy(4-nitrophenyl)methylcyclopentanone was also tested. The diastereomeric ratio (*dr*) of the *anti* to the *syn* products was determined to be 75:25, with *ee*'s of 14% for the *anti* isomer and 3% for the *syn* isomer, respectively.

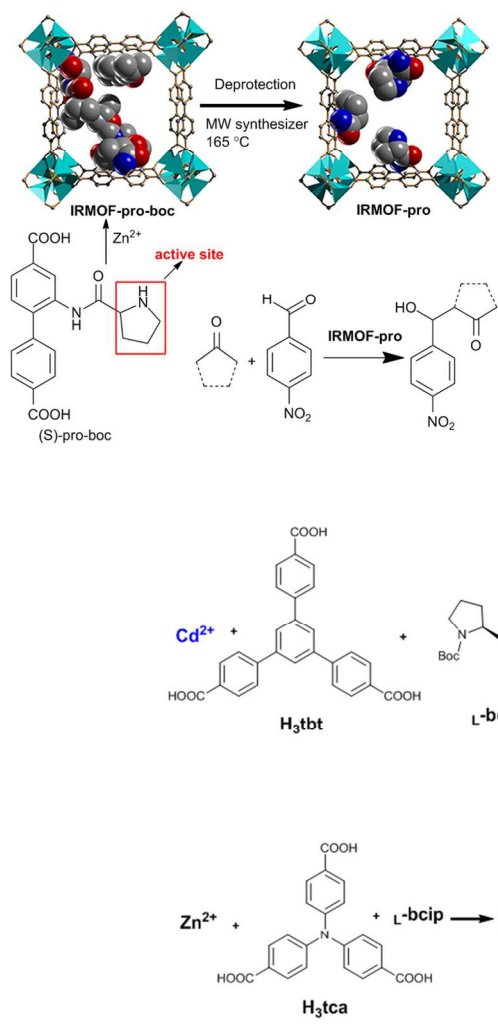


**Fig. 41** Structures of IRMOF-pro-boc and the deprotected form IRMOF-pro and illustration of catalytic application in aldol reaction of the latter

Two homochiral MOFs of Cd-tbt and Zn-pyi containing pyrrolidine units were synthesized in Duan group.<sup>75</sup> Cd-tbt was produced by a hydrothermal reaction using cadmium perchlorate, 1,3,5-tris(4-carboxyphenyl)benzene ( $H_3tbt$ ) and *L*-*N*-*tert*-butoxy-carbonyl-2-(imidazole)-1-pyrrolidine (*L*-bcip) as the reactants.<sup>75a</sup> In the coordination framework of Cd-tbt, the rhombus channels with dimensions of  $4.0 \times 6.5 \text{ \AA}^2$  were constructed through tumbling one 2D sheet to another in an interpenetration fashion, and molecules of *L*-pyrrolidine-2-yl-imidazole (*L*-pyi) were located above or beneath the 2D interpenetration layer with the potential catalytic active sites N-H of pyrrolidine exposed (Fig. 42). The catalytic ability of Cd-tbt was tested using the asymmetric aldol reactions between aromatic aldehydes and cyclohexanone. The reaction with the heterogeneous catalyst Cd-tbt achieved with 30% higher *ee* than the one with the homogeneous catalyst *L*-pyi. The better catalytic performances of Cd-tbt might partially originate from the restricted movement of the substrate on the MOF's exterior coupled with multiple chiral inductions, since the channel of Cd-tbt was not large enough to encapsulate molecules of *L*-pyi and the substrates.

**Fig. 42** Crystal structures of Cd-tbt and Zn-pyi and illustrations of their syntheses and catalytic applications in aldol reaction and  $\alpha$ -Alkylation of aldehyde, respectively.

On the other hand, the precursor Zn-bcip was formed from the solvothermal reaction of 4,4',4''-tricarboxyltriphenylamine ( $H_3tca$ ) and  $Zn(NO_3)_2 \cdot 6H_2O$  in the presence of *L*-bcip in a mixed solvent of DMF and ethanol.<sup>75b</sup> In the coordination framework of Zn-bcip, 1D channels of  $12 \times 16 \text{ \AA}^2$  were formed along the [100] direction with *L*-bcip molecules located within the channels. Zn-pyi was then obtained after heating Zn-bcip in DMF at 165 °C using microwave irradiation for about 4 h. Zn-pyi was employed to prompt the asymmetric  $\alpha$ -alkylation of aliphatic aldehydes (Fig. 42) using a common fluorescent lamp (26 W) as the light source. Under the optimized condition, the reaction between phenylpropylaldehyde and diethyl 2-bromomalonate finished with a high reaction efficiency (74% in yield) and an excellent enantioselectivity (92% *ee*). In the presence of bulky aldehyde 3-(3-oxopropyl)phenyl 3,5-di-*tert*-butylbenzoate, whose size ( $17.4 \times 13.8 \text{ \AA}^2$ ) was larger than the pore size of Zn-pyi as the aldehyde substrate, the photocatalytic  $\alpha$ -alkylation reaction only gave 7% of product under the same reaction

conditions. The size selectivity of the substrate suggested that the alkylation reactions occurred mostly in the channel of the catalyst, not on the external surface. Zn-pyi can be easily isolated from the reaction suspension by simple filtration alone and can be reused at least three times with a slight decrease in its reactivity and selectivity (yield decreasing from 74% to 70% with the *ee* value decreasing from 92% to 88%).

#### 4.5 N-heterocyclic carbene

N-heterocyclic carbenes (NHCs) are most frequently prepared via deprotonation of the corresponding azolium salts such as imidazolium. NHCs are powerful organocatalysts, and will react with  $\alpha,\beta$ -unsaturated ketones to form enone intermediates, which then take part in a broad range of transformations. On the other hand, NHCs are electron-rich, neutral  $\sigma$ -donor ligands, and can form very strong bonds with the majority of metals.

And thus, NHCs have mostly been used as ancillary ligands for the preparation of transition metal-based catalysts. Incorporation of catalytically active NHCs in MOFs is an interesting topic.<sup>76</sup> Farha, Scheidt and Hupp et al. reported their work about converting Willans' tripodal imidazolate framework-1 (TIF-1,  $\text{Co}_3\text{Cl}_3(\text{tmtb})_2$ ,  $\text{tmtb} = 1,3,5$ -Trimethyl imidazole-2,4,6-triethyl benzene) to carbene-like species through deprotonation of coordinated imidazoles (Fig. 43).<sup>77a</sup> MOF TIF-1 possesses one-dimensional channels with the pore diameter at its smallest measures 8.5 Å. TIF-1 displayed high thermal stability, and retained crystallinity after heating under vacuum at 200 °C for two days. One notable feature of TIF-1 was that the C4/C5 sites of the imidazoles, rather than C2 sites, protruded into the framework pores. The space-filling model of TIF-1 crystal structure indicated that the C2 carbon was completely inaccessible to atoms or molecules entering the pores. As a result, under special circumstances, NHCs was deprotonated at C4 or C5, forming abnormal, or,  $\alpha$ -NHCs within the pores of TIF-1. The catalytic activity of deprotonated TIF-1 was examined using the addition of alcohols to  $\alpha,\beta$ -unsaturated ketones. In the presence of TIF-1 solids, the conjugate addition of methanol and benzyl alcohol to (*E*)-hex-4-ene-3-one yielded the corresponding ethers with 65% and 83% conversion, respectively. Powder X-ray diffraction of TIF-1 before and after catalysis suggested retention of crystallinity. Competition reactions of a 1:1 molar ratio of benzyl alcohol and methanol were conducted to probe whether catalysis occurred primarily on the surface of the MOF or within the pores. No significant differences in reactivity were noted, suggesting that catalysis occurred chiefly on the surface of the MOF rather than inside the MOF pores.

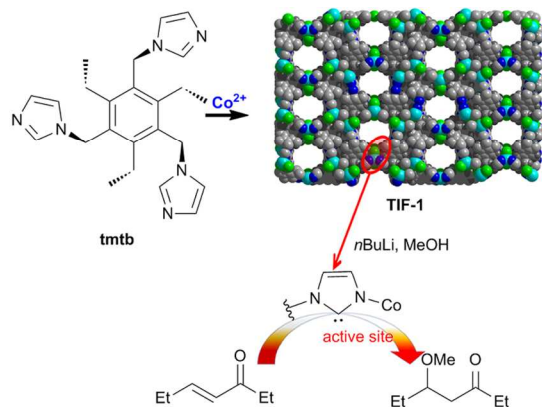


**Fig. 43** Space-filling view of TIF-1 and illustration of its synthesis and catalytic application in nucleophilic conjugate addition.

NHCs can also be generated in Zwitterionic organic ligands. Wu et al. designed two imidazolium-based ligands, 1,1'-methylenebis-(3-(4-carboxyphenyl)-1*H*-imidazol-3-ium) (mcpi) and 1,1'-methylenebis-(3-(4-carboxy-2-methylphenyl)-1*H*-imidazol-3-ium) (mcpiMe).<sup>77b,c</sup> They used these two ligands to construct novel MOFs of  $[\text{Cu}_2(\text{mcpi})_2(\text{MeOH})_2] \cdot 4\text{NO}_3 \cdot \text{H}_2\text{O}$  (Cu-mcpi) and  $[\text{Zn}(\text{mcpiMe})\text{Cl}_2] \cdot 8\text{H}_2\text{O}$  (Zn-mcpiMe). On one hand, Cu-mcpi was prepared by heating a mixture of  $\text{H}_2(\text{mcpi})\text{Cl}_2$  and  $\text{Cu}(\text{NO}_3)_2 \cdot 3\text{H}_2\text{O}$  in a mixed solvent of MeOH and EtOH at 65 °C for one day.<sup>77b</sup> Single-crystal structure analysis of Cu-mcpi revealed large cavities with the cross dimensions of  $18 \times 34 \text{ \AA}^2$ . On the other hand, Zn-mcpiMe was synthesized from the reaction of  $\text{H}_2(\text{mcpi-Me})\text{Cl}_2$  and  $\text{Zn}(\text{NO}_3)_2 \cdot 6\text{H}_2\text{O}$  in a mixed solvent of  $\text{H}_2\text{O}$  and EtOH at room temperature for three days (Fig. 44).<sup>77c</sup> Zn-mcpiMe had a very large exterior wall diameter of 4.91 nm and an interior channel diameter of 3.32 nm. Interlocking of the nanotubes gave rise to a 3D chiral framework containing 1D helical cylinder-like channels with diameter of 2.0 nm. It is noted that the imidazolium moieties in both MOFs are readily available to be deprotonated for the formation of NHCs, which can bind with catalytic metal ions to form metallocarbenes (e.g. Pd-NHC). This can be conveniently performed by treating the MOFs with  $\text{Pd}(\text{OAc})_2$  in THF solvent. ICP-MS showed that around 11.0 and 7.8% palladium could be immobilized in the porous frameworks of Cu-mcpi and Zn-mcpiMe, respectively. The Suzuki–Miyaura cross-coupling reaction of aryl halides with phenylboronic acids was carried out to evaluate the catalytic activity of the  $\text{Pd}^{\text{II}}$ -immobilized porous materials (Fig. 44). Catalytic results showed that the PSM-MOFs (e.g. Pd/Cu-mcpi and Pd/Zn-mcpiMe) can catalyze the coupling reaction of a variety of phenylbromides or phenyliodides with phenylboronic acids in toluene at 70 °C in the presence of  $\text{K}_2\text{CO}_3$ . The hot filtration experiments showed that no reaction occurred in the absence of the solid catalyst. The  $\text{Pd}^{\text{II}}$ -immobilized material can be recycled and reused for six successive runs without deteriorating the catalytic activity. A powder XRD pattern for the recovered solid catalyst showed that the structural integrity of the catalyst was maintained during the catalytic process.

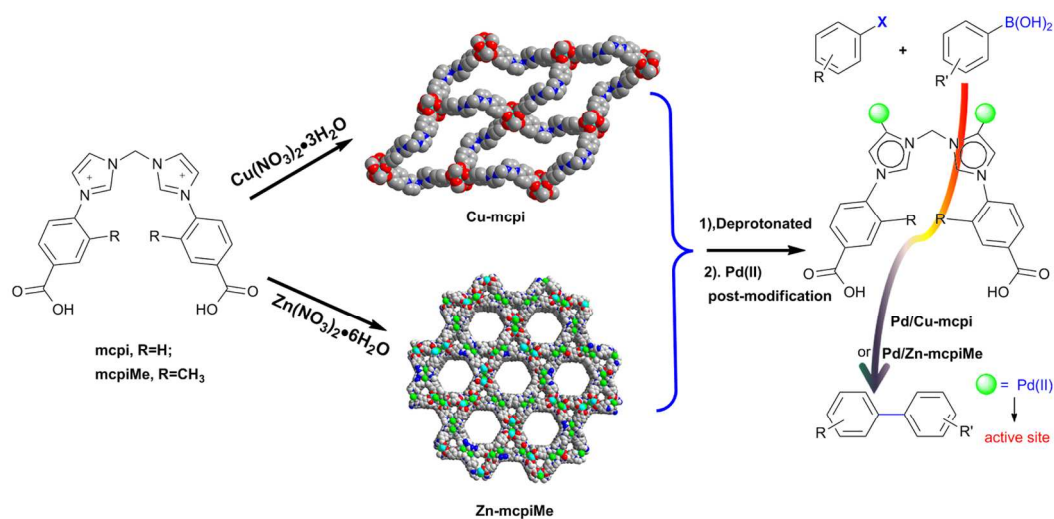


**Fig. 44** Illustration of the syntheses of Pd/Cu-mcpi and Pd/Zn-mcpiMe and their catalytic application in Suzuki–Miyaura cross-coupling.

#### 4.6 Urea

The heterogeneous catalysis of MOFs with ureas as functional group has been seldom explored in literature. Farha, Scheidt and Hupp et al. developed a urea-containing MOF,  $Zn_2(\text{bipy})_2(\text{cada})$  (NU-601; bipy = 4,4'-bipyridine;  $H_4\text{cada} = 5,5'$ -(carbonylbis(azanediyl))diisophthalic acid).<sup>78</sup> MOF NU-601 possessed large channels in all directions (*a* axis,  $12.05 \times 13.95 \text{ \AA}^2$ , *b* axis,  $11.38 \times 13.69 \text{ \AA}^2$ , and *c* axis,  $11.38 \times 4.87 \text{ \AA}^2$ ; atom-to-atom separations) with N–H urea bonds projecting into the pores. The catalytic activity of activated NU-601 was examined for the Friedel–Crafts reaction between pyrroles and nitroalkenes (Fig. 45). The reaction between *N*-methylpyrrole and (*E*)-1-nitroprop-1-ene with 10 mol% NU-601 in 1:1 MeNO<sub>2</sub>/THF at 60 °C finished with 98% consumption of (*E*)-1-nitroprop-1-ene after 36 h. To confirm that the active catalyst species did not leach into solution, filtration experiments were performed. After the removal of NU-601, the reaction of the filtrate shut down rapidly, suggesting that the reaction was heterogeneous in nature. NU-601 was reusable, maintaining its reactivity after one cycle of use and experiencing only a slight degradation of reactivity after five cycles. The solid MOF catalyst retained its crystallinity as determined by powder XRD. To investigate whether the catalysis took place on the surface or within the pores of MOF NU-601, larger substrates were used as steric probes. Toward this end, when 1-phenethyl-1H-pyrrole and/or (*E*)-(4-nitrobut-3-en-1-yl)-benzene were employed, the substrate consumption and reaction yield decreased rapidly. Such reagent size selectivity provided evidence that the catalytic reactions most occurred within the cavities of the MOFs catalyst.

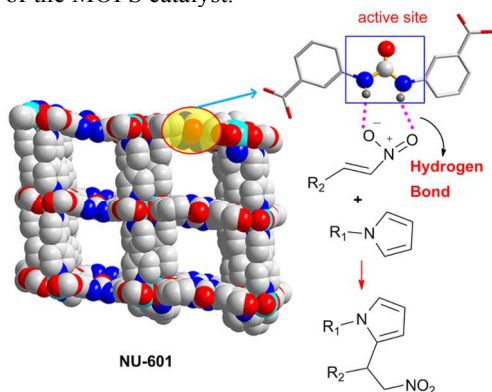


**Fig. 45** Space-filling view of NU-601 and illustration of its catalytic application in Friedel–Crafts reaction.

#### 4.7 Binol

As a type of specific organic ligand that can generate intrinsically chiral MOFs, the binol-type ligands have been early developed by Lin group to synthesize homochiral MOFs in purpose of asymmetric catalysis. They designed two chiral ligands derived from 1,1'-bi-2-naphthol (binol), namely (*R*)-6,6'-dichloro-2,2'-dihydroxy-1,1'-binaphthyl-4,4'-bipyridine (binol-1) and (*R*)-2,2'-dihydroxy-1,1'-binaphthyl-4,4',6,6'-tetrabenzoate (binol-2).<sup>79a-c</sup> Self-assembly of the two ligands and different salts resulted in the formation of MOFs of  $[\text{Cd}_3\text{Cl}_6(\text{binol-1})_3] \cdot 4\text{DMF} \cdot 6\text{MeOH} \cdot 3\text{H}_2\text{O}$  ( $\text{CdCl}_2$ -binol-1),  $[\text{Cd}_3(\text{binol-1})_4(\text{NO}_3)_6] \cdot 7\text{MeOH} \cdot 5\text{H}_2\text{O}$  ( $\text{Cd}(\text{NO}_3)_2$ -binol-1),  $[\text{Zn}_2(\text{binol-2})(\text{dmf})(\text{H}_2\text{O})] \cdot 2\text{EtOH} \cdot 4.3\text{DMF} \cdot 4\text{H}_2\text{O}$  ( $\text{Zn}$ -binol-2) and  $[(\text{binol-2})\text{Cu}_2(\text{solvents})_2]$  ( $\text{Cu}$ -binol-2), which possess large channels with the size of  $16 \times 18 \text{ \AA}^2$ ,  $14 \times 14 \text{ \AA}^2$ ,  $15 \times 20 \text{ \AA}^2$ ,

and  $30 \times 20 \text{ \AA}^2$ , respectively. Treatment of these homochiral MOFs with excess  $\text{Ti}(\text{O}i\text{Pr})_4$  produced Ti-containing MOFs in which the dihydroxy groups of binol were coordinated with Ti(IV) salts (Fig. 46). These Ti-containing MOFs was found to be able to perform as active catalysts in the  $\text{ZnEt}_2$  addition reactions with aromatic aldehydes. In the case of 1-naphthaldehyde, the product (*R*)-1-(1-naphthyl)propanol was obtained with high yields and excellent *ee* values in the presence of the Ti-containing MOFs derived from  $\text{CdCl}_2$ -binol-1 (93%),  $\text{Cd}(\text{NO}_3)_2$ -binol-1 (90%) and  $\text{Cu}$ -binol-2 (91%). However, only 22% *ee* was obtained in the reaction catalyzed by the post-synthesized catalyst from  $\text{Zn}$ -binol-2. In order to study the dependence of the enantiomeric excesses on the open channel sizes, they prepared later a series of isorecticular chiral MOFs of  $\text{Cu}$ -binol-2 based on tetracarboxylate bridging ligands with different length derived from 1,1'-bi-2-naphthol (binol) and copper paddle-wheel secondary building units (SBUs).<sup>79d</sup> Catalytic results showed that the enantiomeric excesses of 1-phenyl-1-propanol that resulted from the addition of diethylzinc to benzaldehyde were indeed dependent on the CMOF channel sizes.

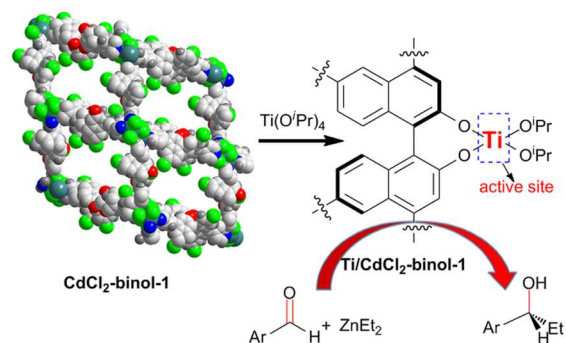


**Fig. 46** Schematic view of the preparation of  $\text{Ti}/\text{CdCl}_2$ -binol-1 and its catalytic application in  $\text{ZnEt}_2$  addition.

#### 4.8 Bipyridyl

A representative example of heterogeneous catalysis utilizing bipyridyl functional group in MOF materials was established on the basis of porous MOFs containing free uncoordinative Bipyridyl organic sites. Yaghi et al. prepared MOF-253 ( $\text{Al}(\text{OH})(\text{bpydc})$ ; bpydc = 2,2'-bipyridine-5,5'-dicarboxylate) in which the 2,2'-bipyridine (bpy) moieties are not coordinated with any metal ions.<sup>80a</sup> Considering that organic molecules that contain bidentate chelating centers, such as *N,N'*-dimethylethane-1,2-diamine, 1,10-phenanthroline, and quinoline-1-amino-2-carboxylic acid could catalyze the direct arylation of arenes, Li et al. then tested the catalytic activity of MOF-253 in the similar reactions (Fig. 47).<sup>80b</sup> For initial optimization, the cross-coupling of 4-iodoanisole with benzene was selected as the model reaction. When three equivalents of KO*t*Bu was used in the presence of 30 mol% of MOF-253, the reaction furnished the product in 99% yield after 36 h. Surprisingly, the efficiency was dramatically decreased when the same amount of H<sub>2</sub>bpydc was used to replace MOF-253. These results indicated that the catalytic efficiency of bpydc ligands in the cross-couplings could be improved significantly by assembling them within a MOF structure.

Later, Li et al. further used MOF-253 for the immobilization of CuI.<sup>80c</sup> The activated MOF-253 was soaked in an acetonitrile solution of CuI to give rise to MOF-253-0.5CuI (8.3 wt% Cu), which as determined by elemental analysis. As depicted in Fig.

47, thus functionalized MOF-253-0.5CuI was then employed in the C–O cross-coupling of phenols and alcohols with aryl halides. Under the optimized reaction conditions, the reactions between phenols and aryl halides could lead to the ethers with up to 97% yield. The reusability of the catalyst system was also tested, and no significant efficiency loss was observed after three runs. The powder XRD experiments of the catalyst after the third run displayed no significant changes in the crystalline structure of the MOF after reactions, and the AAS experiments on the reaction mixture showed that a very low Cu leaching amount (<0.1% of the total Cu) was detected in solution.

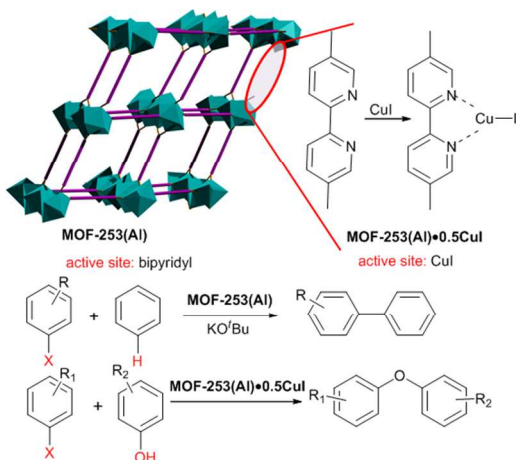


**Fig. 47** Illustration of the structure of MOF-253 and the preparation of MOF-253-0.5CuI, and their catalytic applications.

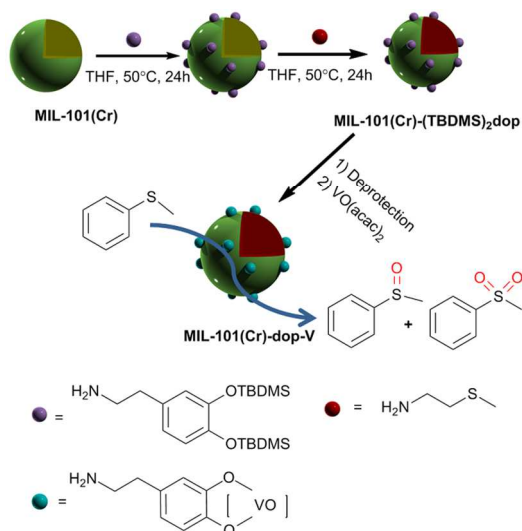


**Fig. 48** Schematic representation of the preparation of MIL-101(Cr)-dop-V and its catalytic application in oxidation of thioanisole.

#### 4.9 Catechol

A judicious strategy to incorporate catechol into MOF skeleton as the functional organic group for heterogeneous catalysis has been proposed by Farha, Hupp and Nguyen et al.<sup>81</sup> They used MIL-101(Cr) for the post-synthesis incorporation of catechols that can then be further metallated with VO(acac)<sub>2</sub> as illustrated in Fig. 48. They chose dopamine (dop) as the catechol-bearing

grafting agent, and successful dopamine grafting was achieved by exposing the dehydrated MIL-101(Cr) to a suspension of free-base dopamine in anhydrous THF at 50 °C for 24 h. To get a better handle on dopamine loading, they protected its two hydroxyl functionalities with *tert*-butyldimethyl silyl (TBDMS) groups prior to grafting, and then used ICP-OES to determine the molar ratio of Si to Cr. ICP analysis indicated a Si/Cr ratio of ~ 0.10 (equivalent to only 5% dopamine loading). These results pointed to modification being limited to Cr<sup>III</sup> sites at or near the MOF external surface. Thus the obtained MIL-101(Cr)-(TBDMS)<sub>2</sub>dop was then exposed to a considerably smaller amine 2-(methylthio)ethylamine as a secondary modifier, which might access the internal surfaces of the porous MOF. After deprotection, MIL-101(Cr)-(TBDMS)<sub>2</sub>dop converted to MIL-101(Cr)-dop, which can be readily metallated with VO(acac)<sub>2</sub> to give a material with a V/Cr ratio of ~0.05, the maximum possible for a stoichiometry of one catechol per vanadium. They then evaluated the catalytic activity of MIL-101(Cr)-dop-V in oxidation of thioanisole. In the presence of TBHP, MIL-101(Cr)-dop-V was capable to catalyze the oxidation of thioanisole to the corresponding sulfoxide and sulfone with 57 and 26% yield, respectively. Furthermore, the MIL-101(Cr)-dop-V catalyst can be recovered and re-used without any loss in total sulfide conversion.

In summary, functional organic sites in MOFs have developed from simple functional groups such as pyridyl, amine and amide in early work to relatively complex and more valuable FOS such as proline and derivatives, NHCs and urea, all of which are perfect organocatalysts. L-Proline is natural substance, and thus homochiral MOFs derived from it or its derivatives can be well designed and synthesized. Although there is an extensive repertoire of chiral NHCs and ureas, they haven't been incorporated to MOFs. As shown in the available reports, NHCs in MOFs are merely based on imidazolium salts. Other NHCs sources such as triazolium, tetrazolium, pyrazolium, oxazolium and thiazolium salts have not been used for the synthesis of NHCs-containing MOFs. On the other hand, FOS can be used for the immobilization of metal catalysts, of which amino groups are most studied. This might be ascribed to a variety of amino-containing MOFs such as amino-substituted IRMOFs, Uios and MILs available. As exemplified here, bipyrindyl, NHCs, catechol, etc. can well bond with metal complexes. To explore the rich catalysis of MOFs, efforts might be driven to the design of more suitable ligands with these valuable functional groups for MOF synthesis.

#### 5. MNPs@MOF

The inherent host-guest chemistry of porous MOF materials allows the implementation of desired properties by filling the framework cavities with various guest molecules and clusters. In particular, the doping of MOFs with metal nanoparticles (MNPs) is of interest for heterogeneous catalysis.<sup>82-95</sup> It is expected that the crystalline porous structures of MOFs can limit the migration and aggregation of MNPs, considering that the typical synthesis of MNPs inside MOFs (MNPs@MOF) is through a stepwise process, that is, precursor infiltration and subsequent decomposition that converts the precursor into nanoparticles inside the framework cavity. Until now, a few catalytically active metals (e.g., Cu, Ru, Au, Pd, Pt) have been finely dispersed into the MOF cavities (e.g. MOF-5, MOF-177, MIL-101(Cr), ZIF-8, ZIF-90), among which Au@MOF and Pd@MOF have been largely studied compared to others.

The widely used approach to prepare MNPs@MOFs (or sometimes denoted as MNPs/MOFs) is to use MOFs as

stabilizing host material providing a confined space for nucleation, which includes techniques such as chemical vapor deposition, solution infiltration, and solid grinding for introducing the metal precursor (e.g.  $ML_n$ ). The intermediates, namely precursor loaded materials  $[ML_n]_m@MOF$ , are subsequently converted to  $MNPs@MOFs$  in hydrogen or with other reducing agents such as  $NaBH_4$ . It is mandatory to choose precursors with decomposition conditions that will be tolerated by the host MOF framework. Therefore, the thermal stability of the MOF framework should match the corresponding decomposition temperature of the precursor in order to obtain nanoparticles in an unchanged host matrix. In the case of impregnation of MOFs in solution, metal complexes or salts are diluted in adequate solvents and subsequently used for impregnation. After removal of the solvents, the metal precursors can decompose to the metal by further treatment.

The concept of solvent-free gas-phase infiltration to yield precursor loaded MOF materials has been introduced by Fischer in 2005.<sup>82b</sup> In comparison to the impregnation of MOFs in solution and similar to the solid-grinding method, this gas-phase infiltration benefits from the absence of competition between solvent and metal precursor molecules, and therefore allows a much wider range of metal loadings, even above 40 wt.% metal in a single step. On the other hand, the solution based synthesis strategy for the deposition of metals inside MOFs can avoid the use of highly reactive and air sensitive precursors, which are usually applied in solvent-free gas-phase infiltration method. In Table 5 are summarized the selective literatures relevant to the loading of metal nanoparticles on MOFs. Early works focused on the use of the well-known MOF-5 as the scaffold, while more recent work extended to MIL-101(Cr). The excellent chemical and thermal stability of the latter MOF has facilitated the fair evaluation of the new properties of the composites.  $MNPs@MOFs$  have been employed in heterogeneous catalysis such as methanol synthesis, hydrogenation of hydrocarbons, reduction of ketones, oxidation of alcohols, CO oxidation, C-C bond formation and indole formation reaction. Especially,  $Au@MOF$  catalyzed alcohol oxidation and  $Pd@MOF$  (usually  $Pd@MIL-101(Cr)$ ) catalyzed C-C bond formation reactions have attracted a great deal of attention.

### 5.1 Cu@MOF and Ru@MOFs

MOF-5 ( $IRMOF-1$ ,  $Zn_4O(bdc)_3$ ), which was developed by Yaghi et al., is a suitable host for various types of loading studies due to its facile synthesis even in larger scales, temperature stability up to 400 °C in argon, the relatively large pore opening of 7.8 Å, and high Langmuir surface area of up to 4500  $m^2 g^{-1}$ .<sup>82a</sup> Depending on the tilting of the *bdc* linkers, MOF-5 can be considered to exhibit two kinds of pore diameters with 11.0 and 15.1 Å.

By way of metal organic chemical vapor deposition (MOCVD), Fischer group successfully loaded the porous framework of MOF-5 with volatile complexes such as  $CpCu(PMe_3)$ ,  $CpCu(CN^iBu)$  and  $Ru(cod)(cot)$ , leading to the formation of  $[CpCu(PMe_3)]_2@MOF-5$ ,  $[CpCu(CN^iBu)]@MOF-5$ , and  $[Ru(cod)(cot)]_{3.5}@MOF-5$ , respectively.<sup>82-83</sup> The intermediates  $[CpCu(PMe_3)]_2@MOF-5$  and  $[CpCu(CN^iBu)]@MOF-5$  have been found to be able to convert into the respective materials  $Cu@MOF-5$  by a variety of methods, such as photoassisted thermolysis at 90-100 °C under inert gas, purely thermal hydrogenolysis at 200-220 °C, or photoassisted hydrogenolysis.<sup>82c,d</sup> A loading of about 10-11 wt % Cu is obtained in the final material  $Cu@MOF-5$  within

one loading cycle. The  $N_2$  absorption studies revealed type I isotherms and gave values of 1000-1100  $m^2 g^{-1}$  for the equivalent Langmuir surface, providing evidence that the resulting materials  $Cu@MOF-5$  are still highly porous. Comparison of the powder XRD patterns of desolvated MOF-5 with  $Cu@MOF-5$  verified that the characteristic reflection pattern of the crystalline MOF-5 host material is nicely retained. Transmission electron micrographs of the obtained  $Cu@MOF-5$  materials proved presence of Cu particles of 1-3 nm that were homogeneously distributed over the MOF matrix. No particles or agglomerates outside the MOF matrix were observed. The measured X-ray absorption near edge structure (XANES) and extended X-ray absorption fine structure (EXAFS) were compared with reference samples of bulk Cu,  $CuO$ , and  $Cu_2O$ , revealing that  $Cu@MOF-5$  contains mainly Cu(0). The  $Cu@MOF-5$  samples have been tested as heterogeneous catalysts for methanol synthesis (Fig. 49), and the catalytic results afforded stable values of 70  $\mu mol MeOH \cdot g^{-1} cat \cdot h^{-1}$  for  $Cu@MOF-5$ .

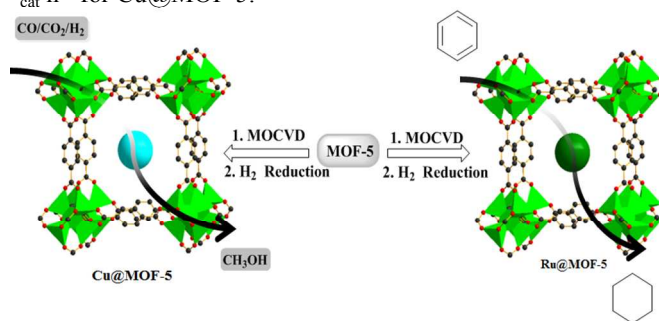


**Fig. 49** Illustration of the preparation of  $Cu@MOF-5$  and  $Ru@MOF-5$  and their catalytic applications. The Zn atoms are shown in bright green octahedral. The blue and green balls in MOF-5 represent Cu and Ru nanoparticles, respectively.

Furthermore, hydrogenolysis of  $[Ru(cod)(cot)]_{3.5}@MOF-5$  yielded  $Ru@MOF-5$  with ruthenium nanoparticles (30 wt % of Ru) in a typical size range of 1.5 – 1.7 nm, embedded in the intact MOF-5 matrix, which has been confirmed by transmission electron microscopy (TEM) and powder XRD measurements.<sup>83</sup> From the type I isotherms of the  $N_2$  sorption measurements of the composite, an equivalent Langmuir surface area of 860  $m^2 g^{-1}$  was calculated. The resulting  $Ru@MOF-5$  was tested as a catalyst in the hydrogenation of benzene, and the reaction was performed under 3 bar  $H_2$  at 75 °C (Fig. 49). It was found that the reaction was complete in 20 h, and the conversion of benzene to cyclohexane was detected to be approximately 25%.

### 5.2 Au@MOFs

Haruta group developed an effective method for the direct deposition of Au clusters onto MOFs, such as CPL-1 ( $[Cu_2(pzdc)_2(py_2)]_n$ , *pzdc* = pyrazine-2,3-dicarboxylate, *pyz* = pyrazine), CPL-2 ( $[Cu_2(pzdc)_2(bpy)]_n$ ), MIL-53(Al), MOF-5, and HKUST-1, by a solid grinding process with a volatile organogold complex,  $Me_2Au(acac)$ .<sup>84</sup> The Au/PCPs were prepared via the following procedure:  $Me_2Au(acac)$  (*acac* = acetylacetonate) and PCPs were ground in an agate mortar in air for 20 min at room temperature, and then the mixture was treated in a stream of 10 vol%  $H_2$  in  $N_2$  at 120 °C for 2 h, thus obtaining Au/PCPs by simply solid grinding. From TEM observations, Au clusters were found to be larger than the pore

size and were mostly placed on the outer surfaces of PCPs. Au/PCPs exhibited moderate to high catalytic activity for the aerobic oxidation of alcohols in the liquid phase. In the presence of the base of  $K_2CO_3$ , benzyl alcohol oxidation in methanol with Au/CPL-1, Au/CPL-2 and Au/HKUST-1 yielded

benzaldehyde as the major product, whereas the same reaction with Au/MIL-53(Al) and Au/MOF-5 gave methyl benzoate as the major product (Fig. 50). Since the catalytic Au clusters are actually attached on the surface of MOF materials, these catalytic reactions may not take use of their porous properties.

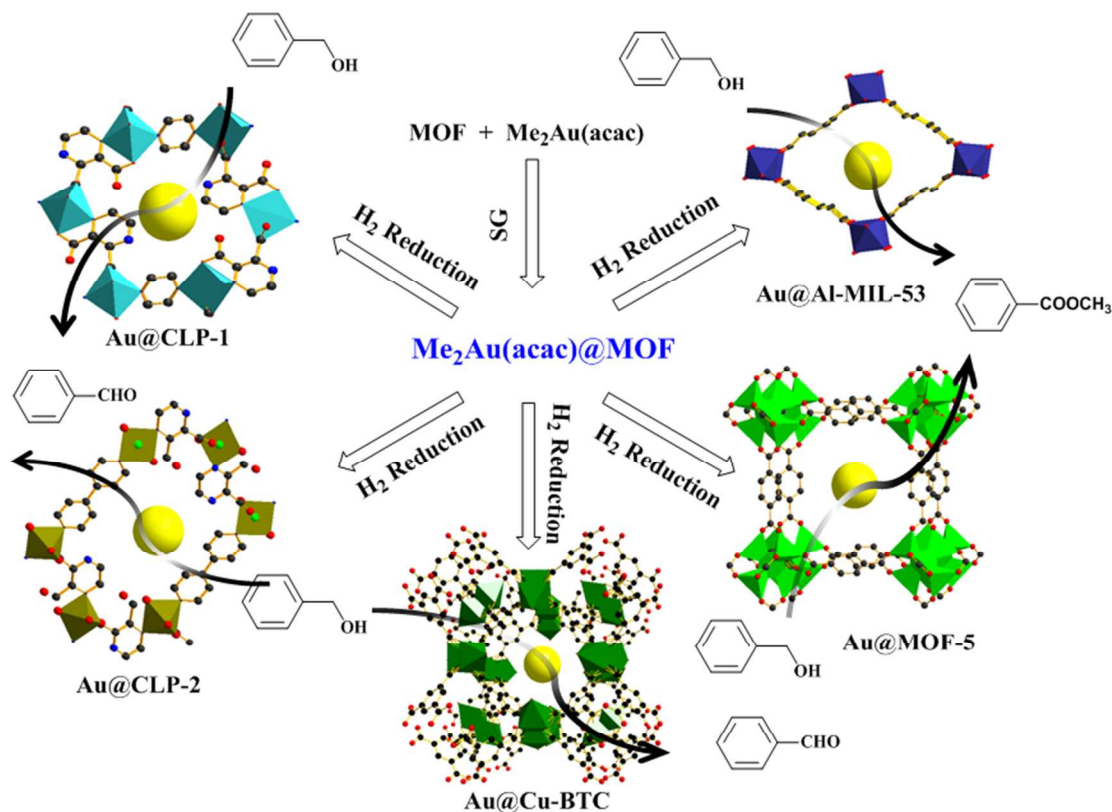


**Fig. 50** Illustration of the preparation of Au@MOFs via different methods and their catalytic applications. The gold ball in the MOF represents Au nanoparticles.

Alternatively, ZIF-8 is desirable for depositing metal nanoparticles into the framework pores because it holds an intersecting 3D structural feature, high thermal stability (over 500 °C), large pore size (diameter of 11.6 Å), and large surface area (BET, 1413 m<sup>2</sup>g<sup>-1</sup>).<sup>47a</sup>

By a simple solid grinding method, Xu groups supported Au NPs with ZIF-8.<sup>85</sup> The Au@ZIF-8 was prepared by grinding the pretreated ZIF-8 and desired quantitative volatile organogold complex (to give 0.5, 1.0, 2.0, and 5.0 wt % Au loadings, respectively)  $Me_2Au(acac)$  uniformly in an agate mortar in air for ~35 min at room temperature. Then the as-prepared sample was treated in a stream of 10 vol% H<sub>2</sub> in He at 230 °C for 2.5 h. The Au@ZIF-8 samples were catalytically active in CO oxidation (Fig. 51). TEM images showed that the mean diameters are 3.4 ± 1.4 and 3.1 ± 0.9 nm for 1.0 wt % Au@ZIF-8 before and after reaction, respectively, whereas the average diameters are 4.2 ± 2.6 and 3.5 ± 2.4 nm or 5.0 wt % Au@ZIF-8 before and after catalysis, respectively. The crystalline order of the ZIF-8 host matrix mostly remains unchanged after loading Au NPs and several runs of reactions, which has been confirmed by the comparison of the powder XRD patterns. There were no obvious diffractions characteristic of Au NPs observed from the patterns of Au@ZIF-8 after catalysis, which agrees with TEM observation.

By means of solvent free gas-phase infiltration (MOCVD) method, Fischer group successfully synthesized Au@ZIF-8 and

Au@ZIF-90, which were prepared by the sublimation of the volatile gold complex  $Au(CO)Cl$  into the activated MOFs in static vacuum (0.5 bar) at 60 °C for 72 h and the subsequent hydrogenation of the obtained  $[Au(CO)Cl]@MOF$  materials under hydrogen (2 bar) with temperatures varying from 100 °C (Au@ZIF-8) to 130 °C (Au@ZIF-90).<sup>86</sup> The loading was varied between 5 and 30 wt.% (i.e., up to 33 mol %). The powder XRD data reveal intact MOF frameworks after the incorporation of gold. Neither the peak positions nor the line shapes were altered significantly. The resulting BET surface areas obtained by standard nitrogen adsorption measurements are between 1334 and 787 m<sup>2</sup>g<sup>-1</sup> for Au@ZIF-8 (10 and 30 wt% Au) and 1004 and 632 m<sup>2</sup>g<sup>-1</sup> for Au@ZIF-90 (10 and 30 wt% Au). High-resolution TEM imaging indicated that a broad size distribution of 1-5 nm and a narrower size regime of 1-2 were obtained for Au@ZIF-8 and Au@ZIF-90, respectively. The catalytic activities of Au@ZIFs were tested in the oxidation of alcohols, and the results showed that Au@ZIF-8 had a very high activity whereas Au@ZIF-90 was inactive (Fig. 51). Similar to Au/MIL-53(Al) and Au/MOF-5 prepared by solid grinding method,<sup>3</sup> Au@ZIF-8 catalyzed oxidation reaction of benzyl alcohol to produce methyl benzoate as the major product.

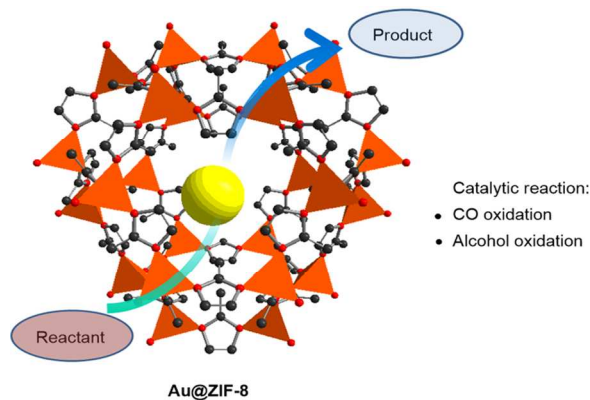


**Fig. 51** Catalytic applications of Au@ZIF-8. The Zn atoms are shown in orange octahedral. The gold ball in ZIF-8 represents Au nanoparticles.

Compared to other MOFs, MIL-101(Cr) represents probably the most widely used catalyst support for deposition of MNPs due to its high chemical and thermal stability, large surface area, and huge cavities. By employing a simple colloidal method with polyvinylpyrrolidone (PVP) as protecting agent, Li and coworkers developed a highly efficient heterogeneous gold catalyst of Au/MIL-101(Cr).<sup>87</sup> After the mixture of an aqueous solution of  $\text{HAuCl}_4$  and PVP was vigorously stirred in an ice bath for 1 h, an aqueous solution of  $\text{NaBH}_4$  was added to the mixture, giving rise to the formation of the Au:PVP colloids, which were immediately deposited onto the MIL-101(Cr) support. The Au/MIL-101(Cr) was obtained by the hydrogenation of the performed Au:PVP composites at 200 °C in  $\text{H}_2$  for 2 h. After the loading of Au and  $\text{H}_2$  reduction, there was no apparent loss of crystallinity as testified by the powder XRD patterns, indicating that the framework of MIL-101(Cr) was mostly retained. The gold content was estimated about 0.5 wt %, measured by AAS analysis. The HRTEM image of the obtained Au/MIL-101(Cr) demonstrated that small gold particles (<3 nm) could be encapsulated inside the pores of MIL-101(Cr). Au/MIL-101(Cr) displayed extremely high catalytic activities in liquid-phase aerobic oxidation of a wide range of alcohols (Fig. 52).

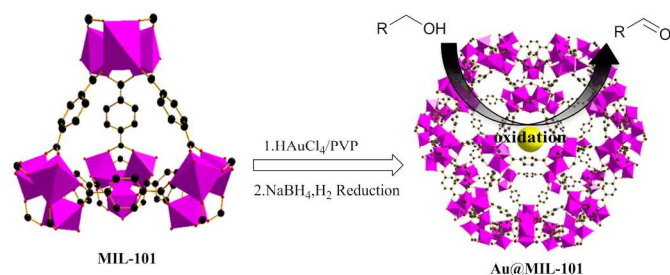


**Fig. 52** The preparation of Au@MIL-101 with  $\text{HAuCl}_4/\text{PVP}$  and the application in oxidation reaction of alcohols. The Cr atoms are shown in pink octahedral, the gold ball inside the MIL-101 pore represents Au nanoparticles.

### 5.3 Pd@MOFs

By an incipient wetness infiltration of  $\text{Pd}(\text{acac})_2$  ( $\text{acac}$  = acetylacetonate) precursor followed by reduction under vacuum or using hydrogen flow at different temperatures, Kaskel group prepared Pd nanoparticles loaded MOF-5.<sup>88a</sup> With this incipient

wetness technique, the precursor was dissolved in solvent (e.g.  $\text{CHCl}_3$ ), and the volume of the solvent applied in the loading procedure was estimated from the free volume of the porous material used. The metal loading was determined to be 1 wt% by elemental analysis. The BET surface area of the composite material was found to be reduced in comparison to the starting material, from 2,885 to 958  $\text{m}^2\text{g}^{-1}$ . The catalytic activity of Pd/MOF-5 has been tested for styrene, 1-octene and *cis*-cyclooctene in a static hydrogen atmosphere. The catalytic evaluation showed that the palladium loaded MOF-5 had a high catalytic activity in styrene hydrogenation comparable to that of palladium on activated carbon, but *cis*-cyclooctene hydrogenation was considerably slower. However, the as-prepared Pd/MOF-5 was unstable in contact with water or humid air, which is due to the low hydrothermal stability of the MOF-5 support.

Pd/MOF-5 has also been prepared by Seayad group through a modified procedure.<sup>88c</sup>  $\text{K}_2\text{PdCl}_4$  and  $\text{NaBH}_4$  were employed as precursor and reducing agent, respectively. The Pd contents vary from 0.25 to 3 wt%. The HR-TEM images showed that the sizes of the Pd nanoparticles were in the range of 3 to 12 nm. The Pd NPs were well dispersed on the surface of MOF-5. The obtained Pd/MOF-5 were used as catalyst in the aminocarbonylation reaction. Results indicated that Pd/MOF was a renewable heterogeneous catalyst for aminocarbonylation among aryl iodides, amines and CO, with a wide substrate scope related to both of aryl iodides and amines.

To develop an air-stable Pd/MOF catalyst, Kaskel group further tested to support palladium in MIL-101(Cr) via the similar incipient wetness impregnation method.<sup>88b</sup> The dispersion of palladium in the fresh Pd/MIL-101 material was analysed via hydrogen chemisorption, suggesting that the diameter of the palladium particles was around 1.5 nm. Compared to Pd/MOF-5, Pd/MIL-101(Cr) (1 wt% Pd) manifested a better catalytic performance in the hydrogenation of olefins.

Alternatively, Li group prepared Pd nanoparticles supported in MOF by impregnation of activated MIL-101 with a  $\text{Pd}(\text{NO}_3)_2$  precursor diluted in DMF at room temperature, followed by placing under a stream of  $\text{H}_2$  at 200 °C for 2 hours to yield Pd/MIL-101(Cr).<sup>89</sup> The powder XRD measurements confirmed that the palladium loading (ca. 1 wt%) did not result in any apparent loss of MOF crystallinity, indicating that the framework integrity of the MIL-101(Cr) was well maintained. The TEM image showed that the palladium NPs were highly dispersed, with a mean diameter of  $(1.9 \pm 0.7)$  nm. The XPS investigation of Pd/MIL-101(Cr) at the palladium 3d level indicated that most of the palladium was in the reduced form. The Pd/MIL-101(Cr) catalyst was found effective in Suzuki–Miyaura and Ullmann coupling reactions of aryl chlorides as well as the one-step synthesis of methyl isobutyl ketone (Fig. 52). However, the unreduced  $\text{Pd}^{\text{II}}/\text{MIL-101(Cr)}$  was ineffective in the reactions, suggesting that palladium in the reduced form should act as the active site.

Cao group demonstrated that Pd/MIL-101(Cr), which was prepared through solution infiltration of activated MIL-101(Cr) with  $\text{Pd}(\text{NO}_3)_2$  as precursor and subsequent hydrogenation with  $\text{H}_2$  at 200 °C for 4 h, exhibited extremely high catalytic activities in the direct C2 arylation of substituted indoles with iodobenzenes at 120 °C (Fig. 53).<sup>90a</sup> The powder XRD patterns showed that the frameworks of MIL-101(Cr) did not alter after the Pd loading (ca. 0.5 wt%). TEM images of Pd/MIL-101(Cr) indicated that most of the dispersed Pd NPs were successfully encapsulated in the cages of the MIL-101(Cr), with a mean

diameter of (2.6 ± 0.5) nm. The XPS and energy-dispersive X-ray spectroscopy (EDS) data revealed that Pd<sup>0</sup> and Cr<sup>III</sup> metal sites coexisted in the Pd/MIL-101(Cr) doped materials. In the XPS traces, the 3d<sup>5/2</sup> and 3d<sup>3/2</sup> peaks of Pd<sup>0</sup> were observed at 336.2 and 341.4 eV and no obvious peaks corresponding to Pd<sup>II</sup> ions were detected. More recently, they modified the procedure of the Pd/MIL-101(Cr)-catalyzed C2 arylation, employing arylboronic acids instead of iodobenzenes.<sup>90c</sup> With the modified procedure, the indole formation reaction can undergo in a milder reaction condition, and doesn't require high temperature.

The same group also used NH<sub>2</sub>-MIL-101(Cr) as catalyst support, and successfully encapsulated Pd nanoparticles by ionic reaction of ammonium groups with [PdCl<sub>4</sub>]<sup>2-</sup> and a subsequent reduction with NaBH<sub>4</sub>.<sup>90b</sup> Based on inductively coupled plasma atomic emission spectroscopy (ICP-AES) data, they estimated that a 0.62 wt % of palladium was loaded in the porous Pd/NH<sub>2</sub>-MIL-101(Cr) framework. The bright-field and dark-field TEM images suggested that most of the dispersed Pd NPs were included in the cages of the NH<sub>2</sub>-MIL-101(Cr) MOF framework, with a mean diameter of 2.49 nm. The XPS and EDS data revealed that most of the palladium atoms were in the reduced form. The doped Pd/NH<sub>2</sub>-MIL-101(Cr) MOF was effective in the dehalogenation of aryl chlorides in water with HCOONH<sub>4</sub>. With a similar ion-exchanged method, Cao group also prepared Pd nanoparticles supported on amine-functionalized, mixed-linker MOFs (MIXMOFs) based on MIL-53(Al).<sup>90d</sup> The mean diameter of Pd NPs was about 3.2 nm. The Pd/MIXMOF displayed highly catalytic activity for Heck reaction and can be easily recovered and reused.

On the other hand, Li group embedded Pd nanoparticles within MIL-101(Cr) via an incipient wetting procedure with Pd(acac)<sub>2</sub> (0.5 ~ 4 wt% Pd) as the precursor, followed by the reduction in a 10% H<sub>2</sub>/Ar flow at 493 K for 2 h.<sup>91</sup> The almost unchanged XRD patterns of 3%-Pd/MIL-101 suggested that the Pd incorporation occurred with no apparent loss of MOF structural integrity. Through the measurement of CO chemisorption, the Pd nanoparticle size was calculated to be around 2.6 nm for Pd/MIL-101(Cr) (3 wt% Pd). This conclusion was further verified by STEM images of 3%-doped Pd/MIL-101(Cr) MOF, which suggested that the mean diameter of Pd nanoparticles was 2.1 nm. The catalytic properties of the resulting Pd/MIL-101(Cr) samples were evaluated in an atom-economy synthesis of indole in water. In the presence of Pd/MIL-101(Cr) catalyst (1.0 mol% Pd), 2-iodoaniline as well as a variety of substituted 2-iodoaniline could react with phenylacetylene to produce the corresponding indoles with high yields (up to 98%) (Fig. 53).

In contrast to the works mentioned above, Kempe group reported the synthesis of Pd@MIL-101(Cr) by means of the metal-organic chemical vapor deposition method. The volatile complex (η<sup>5</sup>-C<sub>5</sub>H<sub>5</sub>)Pd(η<sup>3</sup>-C<sub>3</sub>H<sub>5</sub>) was chosen as the precursor, and the loading of the complex in MIL-101(Cr) framework was identified to be higher than 50 wt%.<sup>92</sup> Quantitative reduction of the Pd precursor complex with H<sub>2</sub> gave rise to Pd NPs inside the MIL-101(Cr) pores (Pd@MIL-101(Cr)). The generation of Pd@MIL-101(Cr) at low temperatures (21 °C) and low H<sub>2</sub> pressure (5 bar) led to the Pd nanoparticles with around 2.7 nm size, whereas the nanoparticles with smaller size (about 1.7 nm) were formed within MIL-101 when adjusting the conditions to elevated temperature (70 °C) and higher pressure (70 bar). The synthesized Pd@MIL-101 samples were investigated as heterogeneous catalysts in the solvent-free reduction of ketones (Fig. 53). Both of Pd@MIL-101 materials prepared in high and low temperatures can effectively promote the reduction of

aromatic ketones. In general, Pd@MIL-101 showed higher conversions for smaller substrates while lower conversions for bigger substrates.

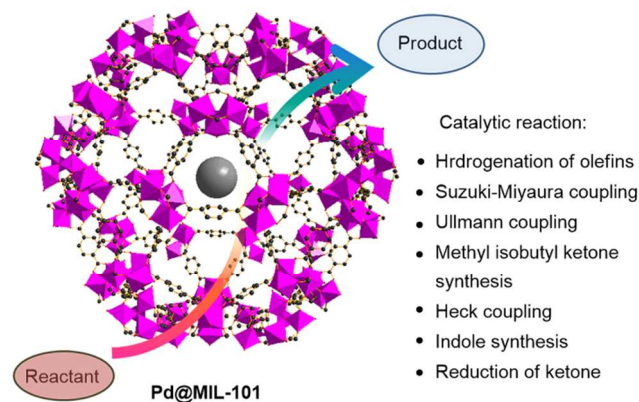


**Fig. 53** Catalytic applications of Pd@MIL-101. The Cr atoms are shown in pink octahedral. The gray ball in the MIL-101 pore represents Pd nanoparticles.

#### 5.4 Pt@MOFs

Similar to Pd atom with wide catalytic potentials in organic reactions, Pt atom is also interested to chemists and has been applied in MOF catalysis through integration as nanoparticles. The larger pore opening and pore volume of MOF-177 (10.8 Å and 1.59 m<sup>2</sup>g<sup>-1</sup>), in comparison to MOF-5 (7.8 Å and 1.04 m<sup>2</sup>g<sup>-1</sup>), allows the diffusion of larger molecules into the MOF cavities, as well as the overall absorption of more molecules per cavity than in MOF-5.<sup>93a</sup> By means of MOCVD method, Kempe group successfully accomplished the gas-phase loading of MOF-177 with the volatile platinum precursor Me<sub>3</sub>PtCp' (Cp' = methylcyclopentadienyl).<sup>93b</sup> Subsequent reduction of the inclusion compound [Me<sub>3</sub>PtCp']<sub>4</sub>@MOF-177 by hydrogen at 100 bar and 100 °C for 24 h gave rise to the formation of platinum nanoparticles in MOF-177 host lattice (Pt@MOF-177). TEM images of the Pt-loaded Pt@MOF-177 hybrid materials showed that the size of the platinum nanoparticles was mainly between 2 and 3 nm. An ICP-MS measurement indicated that 43 wt% of platinum was loaded in MOF-177 framework. Such Pt@MOF-177 has been tested in the oxidation reaction of alcohols. Under the optimized reaction conditions, allylic alcohols were oxidized smoothly with high selectivity.

More recently, Xu group used the “double solvents” method to introduce ultrafine Pt nanoparticles into MIL-101(Cr) pores without Pt nanoparticles aggregation on the external surface of framework.<sup>94</sup> The “double solvents” included a hydrophilic solvent (water) and a hydrophobic solvent (hexane), the former containing the metal precursor (H<sub>2</sub>PtCl<sub>6</sub>) whereas the latter playing an important role to suspend the adsorbent and facilitate the impregnation process. There was no loss of crystallinity in the powder XRD patterns after H<sub>2</sub> reduction, suggesting that the integrity of the MIL-101(Cr) framework was maintained after the host Pt@MIL-101(Cr) loading Pt up to 5 wt %. The TEM and electron tomographic measurements clearly demonstrated the uniform 3D distribution of the ultrafine Pt nanoparticles was achieved with the average size of 1.8 ± 0.2 nm throughout the interior cavities of MIL-101(Cr) pores. The synthesized Pt@MIL-101(Cr) displayed excellent catalytic activities for reactions in all three phases, including

liquid-phase ammonia borane hydrolysis, solid-phase ammonia borane thermal dehydrogenation and gas-phase CO oxidation reactions (Fig. 54).



**Fig. 54** Catalytic applications of Pt@MIL-101. The Cr atoms are shown in pink octahedral. The gray boll in the MIL-101 pores represents Pt nanoparticles.

Another example of Pt-doped MOF catalysis comes from Gascon group, who developed the synthetic strategy by encapsulation of the Pt-supported phosphotungstic acid (PTA) in NH<sub>2</sub>-MIL-101(Al) framework.<sup>95</sup> The grafting of platinum was performed by mixing an ethanolic solution of H<sub>2</sub>PtCl<sub>6</sub> with a suspension of PTA-NH<sub>2</sub>-MIL-101(Al) in ethanol for 1 h. Indicated by the XPS and ICP-OES data of Pt/PTA-NH<sub>2</sub>-MIL-101(Al), the atomic ratios of Pt/Al, W/Al and Pt/W were estimated to be 0.33, 2.02 and 0.165, respectively. After reduction with hydrogen, the resulting hybrid catalysts have been tested in the oxidation of CO, the preferential oxidation of CO in the presence of H<sub>2</sub>, and the hydrogenation of toluene. The catalytic results showed that the Pt/PTA-MOF catalyst was more active than a commercial Pt/Al<sub>2</sub>O<sub>3</sub> reference catalyst.

In general, different metal nanoparticles can be formed in the cavities or the surfaces of MOFs, and exhibited rich catalytic behaviors. Different preparation methods, including gas phase infiltration, impregnation, solid grinding and colloidal, have profound influences on the metal loading as well as the size/shape of the nanoparticles. As far as catalytic results are concerned, MOFs, as the hosts, play an important role on the selectivity of the products. As exemplified in Au/MOFs catalyzed benzyl alcohol oxidation, Au/CPL-1, Au/CPL-2 and Au/HKUST-1 provided benzaldehyde as the major product, whereas Au/MIL-53(Al), Au/MOF-5 and Au@ZIF-8 yielded methyl benzoate as the major one.

## 6. MOFs for Photo- and Biomimetic Catalysis

In more specific sense, supramolecular catalysis by way of porous MOFs as heterogeneous catalysts has been elegantly demonstrated by recent state-of-art progress in MOF-based biomimetic catalysis and photocatalysis.<sup>14e,17c,22</sup> To learn ideas from nature to incorporate biomimetic effect and photochemical transformation into MOF catalysts provide novel perspectives on tackling some long-lasting problems, such as inefficient enzyme-mimic catalysis, and ever-increasing global energy and environmental crisis. In these aspects, excellent reviews have been presented by Zhou<sup>22a</sup> and Wu<sup>22b</sup> to introduce MOFs as heterogenous biomimetic catalysts in the applications of

peroxidase, cytochromes P450 and hemoglobin biomimicry, and by Lin<sup>17c</sup> and García<sup>14e</sup> to introduce MOF-catalyzed and photodriven proton reduction, CO<sub>2</sub> reduction, and organic transformations. Herein, we only discuss a few examples to highlight their catalytic applications in aqueous environment.

Implantation of biomimetic active sites, such as metalloporphyrin motifs, into thermal and chemical stable MOF frameworks are able to stabilize the catalytic centers, creat reactive pockets and diffusion-favored hierarchical structures, thus facilitating substrates recognition, enchancing catalytic efficiency, and increasing shape- and size-selectivity superior to the homogeneous counterparts. In nature, metalloporphyrins are well known for performing many biological functions in aqueous media, such as light harvesting, oxygen transportation, and forming cofactors for many enzyme/protein families. We have introduced relevant research works on porous MOFs containing metalloporphyrinic frameworks<sup>55-58</sup> as biomimetic catalysts In section 3.1.

In general, the porous MOFs integrating metalloporphyrinic frameworks as SBUs are not always suitable for biomimetic catalysis, in case they are constructed from carboxylate liangds and Zn<sup>2+</sup>, Cd<sup>2+</sup> and Co<sup>2+</sup> cations.<sup>55-57</sup> This is because these ions show higher affinities for water molecules than the carboxylate ligands, and thus the corresponding frameworks are inevitably instable in aqueous media. However, the high valent metal ions, such as Cr<sup>3+</sup>, Fe<sup>3+</sup>, Al<sup>3+</sup>, Sc<sup>4+</sup>, V<sup>4+</sup> and Zr<sup>4+</sup>, are more reactive to carboxylate ligands, affording porous MOFs with satisfactory thermal, chemical and moist stability. Excellent examples include MIL and Uio series MOFs.

Encouraged by this finding, Zhou et al endeavored to synthesize Zr-porphyrinic MOFs with the attempt to obtain catalytic MOFs in aqueous conditions.<sup>58</sup> For example, they prepared PCN-222(Fe) which is related to cytochromes P450 in structural nature.<sup>58a</sup> The prosthetic group of P450 consists of an iron protoporphyrin IX, which is protected by polypeptides. These enzymes are potent oxidants capable of catalyzing many useful oxidation reactions. All cytochrome P450 enzymes are involved in a complex multienzymatic system, which hampers their industrial applications. The newly-developed PCN-222(Fe) was an ideal synthetic platform for mimicking cytochrome P450 enzymes owing to its stability, mesoporosity and high density of metalloporphyrin centers, and exhibited excellent peroxidase-like catalytic activity (Fig. 55). For the pyrogallol oxidation reaction, the  $K_{cat}$  of PCN-222(Fe) was seven times higher than that of free hemin, indicating that PCN-222(Fe) was a much more powerful catalyst than free hemin. Moreover, the  $K_m$  value of PCN-222(Fe) was lower than that of natural horseradish peroxidase enzyme, suggesting that PCN-222(Fe) had a better affinity of the substrate. The excellent catalytic performances of PCN-222(Fe) was due to the large open channels (3.7 nm), which effectively prevented the self-dimerization of porphyrin centers and made it easy for substrates to enter the pores and bind to the catalytic centers.

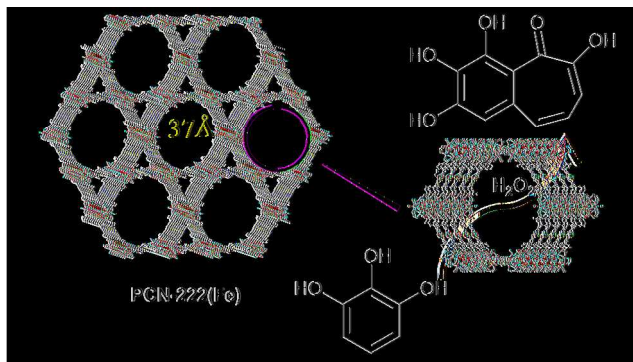


**Fig. 55** Wires and sticks view of PCN-222(Fe) and illustration of its catalytic applications. The Fe and Zr atoms are in orange and teal, respectively.

On the other hand, natural photosynthesis is well-known to be utilized by green plants to achieve various photochemical transformations, such as water splitting and carbon dioxide reduction. These light-driven photochemical reactions can convert sunlight energy to chemical energy. To make use of MOFs for light harvesting and photocatalysis may take the advantages to easily integrate multiple functional components into the hierarchically organized MOF framework to accomplish highly efficient photocatalysts. Moreover, tailorable MOF frameworks readily allow incorporation of varied chromophores to utilize the full solar spectrum, especially visible region, with high efficiency. Three current strategies to develop MOF photocatalysts have been outlined and introduced in detail by Lin<sup>17c</sup> and García,<sup>14e</sup> which include: (1) employing MOF as a host for the encapsulation of a chromophore, (2) choosing photo-responsive organic ligands/metalloligands, and (3) exploring the semiconducting quantum dots properties of the metal nodes or encapsulated nanoparticles. It is proposed that the future trend for MOF photocatalysts is to develop MOFs possessing resistibility against water, since the modest hydrolytic and thermal stabilities of most MOFs prevent them from practical applications in solar energy utilization. We herein introduce two recent reports about stable MOF photocatalysts and their catalytic applications in aqueous solution.<sup>96</sup>

Ott and Cohen have successfully incorporated an effective proton reduction catalyst  $[\text{FeFe}](\text{bdt})(\text{CO})_6$  (bdt = benzenedithiolate) to MOFs.<sup>96a</sup> 2,3-Dimercaptoterephthalic acid was prepared firstly and then complexed with  $\text{Fe}_3(\text{CO})_{12}$ , yielding the complex  $[\text{FeFe}](\text{dcbdt})(\text{CO})_6$  (dcbdt = 1,4-dicarboxybenzene-2,3-dithiolate). This metalloligand reacted with Zr(IV) salts directly failed to produce crystalline materials, resulting in the decomposition of the cluster. Instead, Uio-66- $[\text{FeFe}]\text{dcbdt}(\text{CO})_6$  was obtained through the ligand exchange of  $[\text{FeFe}](\text{dcbdt})(\text{CO})_6$  with bdc in Uio-66. A series of physical characterization such as EDX, EA, TGA and  $^1\text{H}$  NMR showed that 14% of bdc in was exchanged for  $[\text{FeFe}](\text{dcbdt})(\text{CO})_6$ . In conjunction with  $[\text{Ru}(\text{bpy})_3]^{2+}$  as a photosensitizer and ascorbate as an electron donor, Uio-66- $[\text{FeFe}]\text{dcbdt}(\text{CO})_6$  catalyzed photochemical hydrogen evolution in water at pH 5, and exhibited higher performances than that of the free

complex  $[\text{FeFe}]\text{dcbdt}(\text{CO})_6$  in terms of rate and total hydrogen production yield. The superior catalytic performance of MOF might be due to the stabilization of the catalyst located within the framework.

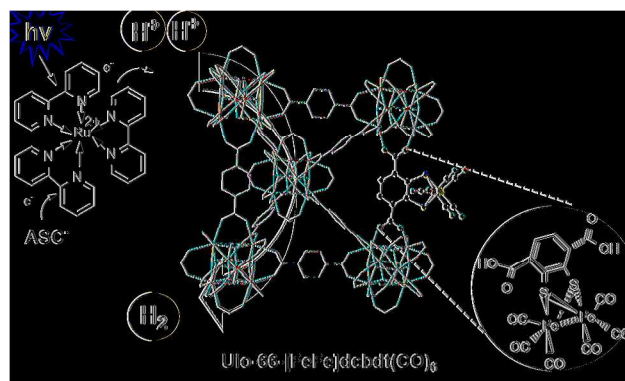


**Fig. 56** Wires and sticks view of Uio-66- $[\text{FeFe}]\text{dcbdt}(\text{CO})_6$  and illustration of its catalytic applications in photochemical hydrogen evolution in water at pH 5.

$\text{Fe}_2\text{O}_3$  is a promising visible light photocatalysts due to their small band gap. However, its photocatalytic performance is limited by the high recombination rate of the photogenerated charge carriers. This can be overcome by reducing the particle dimensions. MOFs containing  $\text{Fe}^{\text{III}}$ -oxide clusters linked together in three dimensions by organic linkers can be promising photocatalysts. Roeffaers et al. examined the catalytic activities of several Fe-based MOFs such as MIL-100(Fe),  $\text{NH}_2$ -MIL-101(Fe), MIL-88B(Fe) and  $\text{NH}_2$ -MIL-88B(Fe) in degradation of Rhodamine 6G in aqueous solution under visible light illumination (350-850 nm).<sup>96b</sup> Results showed that all of these  $\text{Fe}^{\text{III}}$  oxide based MOFs displayed remarkable visible light photocatalytic activity, and MIL-88B(Fe) exhibited the highest efficiency. In comparison, homogeneous iron(III) acetate clusters were also employed in the same reaction, however, no photocatalytic activity was measured under similar conditions. This might be due to the low stability of such clusters in water, whereas incorporating them to the MOF resulted in higher cluster stability.

## 7. Conclusion and Perspective

This review makes an endeavor to outline the main advances and developments of MOFs for applications in heterogeneous supramolecular catalysis. After a brief introduction of unique porous attributes of MOFs on the background of MOFs self-assembly and crystal engineering, as well as their catalytic relevance and studying techniques, we start with catalytic applications of the well-known MILs series, such as MIL-101, MIL-100, MIL-53 and MIL-47 that have shown unusual thermal and chemical stability, and other purposely designed MOFs with CUMs with varied synthetic methodologies and catalytic activities. Afterwards, the functionalized MOFs for the purpose of heterogeneous catalysis have been classified and selectively introduced. The practical routes for functionalization of MOFs as heterogeneous catalyst include direct synthesis, incorporating linkers with homogeneous catalysts, post-synthetic functionalization like either grafting of active groups on the open metal sites of certain structures or binding metal complexes to the free functional groups within frameworks, and

encapsulation of metal nanoparticles inside the MOF pores. Finally, applications of MOFs in photo- and biomimetic catalysis are briefly introduced. Among various synthetic strategies proposed for MOF catalysis, the approach to loading metal nanoparticles, as well as active POMs and classic metal complex catalysts, into the porous matrices of MOFs may represent a newly developed and promising field of research in MOF catalysis that complements other extensively explored catalytic studies in which the catalytic activities are mainly based on the pure MOFs.

On the basis of abundant examples reported to use MOFs as heterogeneous catalysts under various conditions, it can be concluded that the crystalline and porous MOFs are good candidates as active and selective catalysts, or as catalyst host framework, for a wide variety of chemical reactions, varying from acid–base, redox to transition metal catalysis including C–C and C–X (X = halide) formation. Especially, homochiral MOFs catalyzed reactions can give rise to enantioselective compounds, which might have important potential in drug design and fine chemicals synthesis. In addition, many of these works demonstrated that the reasonable stability, heterogeneity and selectivity could be achieved by the coordination frameworks of MOFs. For example, MOF catalysis has been proved to be applicable even in the gas phase reactions like CO oxidation, which may help to get rid of the concerns about practically catalytic applications of MOF materials.

In this context, MOFs materials should have a bright future in the catalytic synthesis of some important and valuable organic molecules because, for example, (1) they can be pre-designed on a rational basis according to a specific requirement of catalytic reaction, or deliberately tailored and modified to suit for a specific catalytic purpose, (2) the well-defined crystal structure of MOFs on the atomic level allows the explicit assessment of structure–activity relationships and application of the catalytic mechanism to a demanding reaction, (3) the uniform catalytic sites arrangement and their well isolation in three-dimensionality make them readily accessible by the substrates, which offers great advantages in light of the catalytic efficiency and economy in contrast to the bulky heterogeneous catalysts of which only the active sites on the solid surface are useful in catalytic reactions, and most important, (4) the intrinsic porous nature of the MOFs imposes a special confinement of the coordination space with the catalytic reactions taking place in a chemically and sterically tunable and modular microenvironment, which is of significance in a supramolecular sense for artificial synthesis mimicking natural enzymes that is difficult to accomplish by the small molecular catalysts.

Over the past ten years, more and more excellent works about MOF catalysis have appeared. Such fast advances in the field of MOF catalysis may benefit from: (1) several well-established MOFs materials are commercially available, such as Fe(BTC) (Basolite F 300), HKUST-1 (Basolite C 300) and MIL-53(Al) (Basolite A 100). This liberates the MOF materials from synthetic chemists, and largely expands and speeds up their applications in catalytic study, (2) more and more thermally and chemically stable MOFs have been prepared, for example, Zr-containing MOFs which have been testified to be highly stable up to 540 °C and proven to be adequately stable against acid and moisture conditions, which have encouraged researchers to investigate more chemical reactions in a wider scope, (3) MOF catalysis starts to be interested to organic chemists who will help to advance this burgeoning field to mature in a more rational and critical sense, and (4) rapid

interdisciplinary study has appeared, for example, MOF catalysis has extended into the fields of nanoscience, photochemistry, biochemistry and medicine. This may booster some new research topics and open the doors to the broad scientific community.

Moreover, it may be expectable that MOF catalysis will continuously expand into more catalytic fields, such as photocatalysis, electrocatalysis, and even biocatalysis, because the self-assembly process of MOFs endows this kind of porous solid materials with versatile properties with regard to photochemistry, electrochemistry, supramolecular chemistry and biochemistry. As classified in the Introduction of this review, 2<sup>nd</sup> to 4<sup>th</sup> generations of MOFs can all be utilized in MOF catalysis; however, understanding of the fact that the MOF structures can undergo a variable of post-processing procedures may put the MOF materials on a platform that new catalytic concepts and strategies could be created. The 3<sup>rd</sup> generation of MOFs should be paid more attention in-depth in catalytic sense, since their ability to be responsive to various external stimuli may generate more extensive catalytic skills with regard to environmental heat, light, pressure, mechanics, as well as chemical, physical, photo and magnetic induces. If the initial research interest in MOF catalysis is considered to start from the pure MOF materials containing active sites, the stage nowadays appreciate their ability to act as catalyst support. The next step of MOF catalysis can move further to utilize MOF materials as catalyst precursors and base materials, for example, to grow MOF crystals in nanosize to form colloids, gels, and other hybrid materials that are suitable for catalytic study.<sup>5d??</sup> Using MOF structures as precursors to generate metal oxide nanoparticles, metal-containing carbon materials, as well as hybrid polymeric and mesoporous solid materials, have been explored recently. These investigations may afford more chances for applications of MOF catalysis in extended conditions.

On the other hand, it is unlikely that MOF materials will replace other porous materials such as microporous zeolites and mesoporous silica, considering that MOFs are inferior to them in thermal and chemical stability. In addition, just as MOF can behave as hosts for metal complexes, metal ions substituting silicon atoms in the frameworks of zeolite and mesoporous silica can act as acid or redox active sites and may be used for different classes of catalytic reactions. Comparison among ZSM-5, MCM-41 and MIL-101(Cr), which represent the typical zeolite, mesoporous silica and MOF materials, respectively, are shown in Table 6. Upon evaluation of these three porous solid materials from different aspects (e.g. structure feature, surface area, stability and catalysis features), it can be concluded that these three porous solids possess rich catalysis chemistry and can supplement one another in heterogeneous catalysis. For instance, zeolites have the highest stability and hence can be readily used in gas phase catalysis, especially in industry catalysis, mesoporous silica enjoy the largest cavities and therefore allow large substrates to enter the pores, while MOF materials possess the biggest surface areas, i.e. a densest amount of active sites.<sup>97-99</sup>

To take advantage of catalytic behavior that is unique to MOFs, more attention might be paid to explore the application of MOF catalyst in more valuable organic molecules formation reactions, which can carry out under relatively mild conditions. It is delight to see more and more organic chemists have gotten involved in the field of MOF catalysis to open up new orientations of MOF catalysis. Some reactions, which cannot occur in the presence of free homogeneous catalysts, can work

well after these homogeneous catalysts are incorporated/assembled within the MOF skeleton or pores due to the difference of electron configuration and steric environment of the constituent ligands (or metalloligands) in confined spaces and the single molecule scattering in solution. Besides, they bring up challenges towards MOF catalysis. In the ligand-assisted transition metal catalyzed reactions, subtle modification of the ligand might give rise to a huge improvement on the activity and selectivities including chemo-, regio- and enantio- selectivity. The same situation is suitable for catalytic reactions in the presence of organocatalysts. However, there are some practical difficulties to assemble/incorporate these high-valued ligands/organocatalysts within MOFs. This might account for the fact that the concepts of MOF catalysis have been set up for around twenty years; nevertheless, MOF materials may still have a long way to be considered as reliable heterogeneous catalysts in practical and industrial applications in general.

### List of Acronyms and Abbreviations Used

acac	Acetylacetonate
AAS	atomic absorption spectroscopy
BA	benzaldehyde
bcip	<i>N</i> -tert-butoxy-carbonyl-2-(imidazole)-1-pyrrolidine
binol	1,1'-bi-2-naphthol
binol-1	( <i>R</i> )-6,6'-dichloro-2,2'-dihydroxy-1,1'-binaphthyl-4,4'-bipyridine
binol-2	( <i>R</i> )-2,2'-diethoxy-1,1'-binaphthyl-4,4',6,6'-tetrabenzoate
bipy	4,4'-bipyridine
bpdc	1,4-biphenyldicarboxylate
bpy	2,2'-bipyridine
bpydc	2,2'-bipyridine-5,5'-dicarboxylate
btp4	benzene-1,3,5-triyl triisocotinate
CAU	Christian-Albrechts-Universität
cod	1,5-cyclooctadiene
cot	1,3,5-cyclooctatriene
CUM	coordinatively unsaturated metal sites
CyH	cyclohexene
damp	6-((diisopropylamino)methyl)picolinaldehyde
DBF	dibutylformamide
dcbdt	1,4-dicarboxybenzene-2,3-dithiolate
bdt	benzenedithiolate
DEF	diethylformamide
DMF	<i>N,N</i> -Dimethylformamide
DMA	<i>N,N'</i> -dimethylacetamide
dop	dopamine
dpni	<i>N,N</i> -di-(4-pyridyl)-1,4,5,8-naphthalenetetracarboxydiimide
ED	ethylenediamine
EDA	ethyl diazoacetate
EDS	Energy-dispersive X-ray spectroscopy
EXAFS	X-ray absorption fine structure
FOS	functional organic sites
HA	heptanal
Hdpdc	(4 <i>S</i> ,5 <i>S</i> )-2,2-dimethyl-5-[(4-pyridinylamino)carbonyl]-1,3-dioxolane-4-carboxylic acid
HKR	hydrolytic kinetic resolution
HKUST	Hong Kong University of Science and Technology
Hpapa	( <i>S</i> )-3-hydroxy-2-((pyridin-4-ylmethyl)amino)propanoic acid
Hpvba	( <i>E</i> )-4-(2-(pyridin-4-yl)vinyl)benzoic acid
Hpymo	pyrimidin-2(1 <i>H</i> )-one
H <sub>2</sub> bdc	terephthalic acid
H <sub>2</sub> bdc-NH	2-aminoterephthalic acid
H <sub>2</sub> bdpb	1,4-bis[(3,5-dimethyl)pyrazol-4-yl]-benzene
H <sub>2</sub> bpdb	1,4-bis[(3,5-dimethyl-1 <i>H</i> -pyrazol-4-yl)]benzene
H <sub>2</sub> dhbdc	2,5-dihydroxyisophthalic acid
H <sub>2</sub> (pdc-2)	pyridine-2,5-dicarboxylic acid
H <sub>3</sub> btb	5'-(4-carboxyphenyl)-[1,1':3',1''-terphenyl]-4,4''-dicarboxylic acid
H <sub>3</sub> btc	benzene-1,3,5-tricarboxylic acid
H <sub>3</sub> btt	1,3,5-tri(2 <i>H</i> -tetrazol-5-yl)benzene
H <sub>3</sub> chirbtb-n	chiral oxazolidinones

H <sub>3</sub> ChirBTB-1	5'-(4-carboxy-3-(( <i>S</i> )-4-isopropyl-2-oxooxazolidin-3-yl)phenyl)-3-(( <i>S</i> )-4-isopropyl-2-oxooxazolidin-3-yl)-3''-(3-isopropyl-5-oxooxazolidin-4-yl)-[1,1':3',1''-terphenyl]-4,4''-dicarboxylic acid
H <sub>3</sub> ChirBTB-2	3,3''-bis(( <i>S</i> )-4-benzyl-2-oxooxazolidin-3-yl)-5'-(3-(3-benzyl-5-oxooxazolidin-4-yl)-4-carboxyphenyl)-[1,1':3',1''-terphenyl]-4,4''-dicarboxylic acid; Meim = 2-methyl-1 <i>H</i> -imidazole
H <sub>3</sub> pdc-1	pyrazole-3,5-dicarboxylic acid
H <sub>3</sub> ibt	1,3,5-tris(4-carboxyphenyl)benzene
H <sub>3</sub> tca	4,4',4''-tricarboxyltriphenylamine
H <sub>3</sub> tcbca	4',4'',4''''-nitrotritolris([1,1'-biphenyl]-4-carboxylic acid)
H <sub>3</sub> cada	5,5'-(carbonylbis(azanediyl))diisophthalic acid
H <sub>3</sub> mdip	5,5'-methylenediisophthalic acid
H <sub>3</sub> pdte	pyridine carboxylates pyridine-2,3,5,6-tetracarboxylic acid
H <sub>3</sub> ptdc	pyridine-2,3,5,6-tetracarboxylic
H <sub>3</sub> tcpb	1,2,4,5-tetrakis(4-carboxyphenyl)-benzene
ICP-OES	Inductively coupled plasma optical emission spectrometry
IR	Infrared spectroscopy
JA	<i>a</i> - <i>m</i> -amylcinnamaldehyde
1-bcip	1- <i>N</i> - <i>tert</i> -butoxy-carbonyl-2-(imidazole)-1-pyrrolidine
LFER	linear free-energy relationship
1-H <sub>2</sub> lac	1-lactic acid
1-lac	1-lactic acid
1-pyi	1-pyrrolidine-2-yl-imidazole
MeIM	2-methylimidazole
MBA	methyl-2(benzylidene amino
mcpi	1,1'-methylenebis-(3-(4-carboxyphenyl)-1 <i>H</i> -imidazol-3-ium)
mcpiMe	1,1'-methylenebis-(3-(4-carboxy-2-methylphenyl)-1 <i>H</i> -imidazol-3-ium)
MILs	materials of institute Lavoisier
MMPF	metal-metalloporphyrin framework
MNPs	metal nanoparticles
MOCs	Metal-Organic Containers
MOCVD	metal organic chemical vapor deposition
MOFs	Metal-Organic Frameworks
MOGs	Metal-Organic Gels
MOMs	Metal-Organic Molecules
NMM	<i>N</i> -methylmaleimide
NMR	Nuclear magnetic resonance
PhEDA	ethyl 2-phenyldiazoacetate
por-1	5,15-dipyridyl-10,20-bis(pentafluorophenyl)-porphyrin
por-2	5,10,15,20-tetra(carboxyphenyl)metalloporphyrin
por-3	tetrakis(3,5-dicarboxyphenyl)-porphine
por-4	5,15-bis(3,5-dicarboxyphenyl)-10,20-bis(2,6-dibromophenyl)porphyrin
Pro	( <i>S</i> )-2-(pyrrolidine-2-carboxamido)-[1,1'-biphenyl]-4,4''-dicarboxylic acid
PSM	post-synthetic modifications
PTA	phosphotungstic acid
PVP	polyvinylpyrrolidone
PXRD	Powder X-ray diffraction
pyz	pyrazine
pzdc	pyrazine-2,3-dicarboxylate
sal	salicylidene
salen-1	( <i>R,R</i> )-(2)-1,2-cyclohexanediamino- <i>N,N'</i> -bis(3- <i>tert</i> -butyl-5-(4-pyridyl)salicylidene)
salen-2	5,5'-((1 <i>E</i> ,1' <i>E</i> )-((1 <i>R</i> )-cyclohexane-1,2-diylbis(azanilylidene))bis(methanylylidene))bis(3-( <i>tert</i> -butyl)-4-hydroxybenzoic acid)
salen-3	(2 <i>E</i> ,2' <i>E</i> )-3,3'-((1 <i>E</i> ,1' <i>E</i> )-((1 <i>R</i> )-cyclohexane-1,2-diylbis(azanilylidene))bis(methanylylidene))bis(3-( <i>tert</i> -butyl)-4-hydroxy-5,1-phenylene)diacrylic acid
salen-4	5',5''-((1 <i>E</i> ,1' <i>E</i> )-((1 <i>R</i> )-cyclohexane-1,2-diylbis(azanilylidene))bis(methanylylidene))bis(3'-( <i>tert</i> -butyl)-4'-hydroxy-[1,1'-biphenyl]-4-carboxylic acid)
salen-5	4,4'-((1 <i>E</i> ,1' <i>E</i> )-((1 <i>E</i> ,1' <i>E</i> )-((1 <i>R</i> )-cyclohexane-1,2-diylbis(azanilylidene))bis(methanylylidene))bis(3-( <i>tert</i> -butyl)-4-hydroxy-5,1-phenylene) bis(ethen <i>e</i> -2,1-diy)) dibenzoic acid
SBU	secondary building units
SEM	Scanning electron microscope
( <i>S</i> )-pro-boc	( <i>S</i> )-2-(1-( <i>tert</i> -butoxycarbonyl)pyrrolidine-2-carboxamido)-[1,1'-biphenyl]-4,4''-dicarboxylic acid
TBAb	tetrabutylammonium bromide
TBDMS	<i>tert</i> -butyldimethyl silyl
TBHP	<i>tert</i> -butylhydroperoxide
tcpb	tetrakis(4-carboxyphenyl)benzene
TDXRPD	temperature-dependent XRPD
TEM	transmission electron microscope
TGA	Thermogravimetric Analysis
TIF-1	tripodal imidazolate framework-1
tmb	1,3,5-Trimethyl imidazole-2,4,6-triethyl benzene
TOF	turnover frequency

Tpha	tris(4-(1-(2-pyridin-2-ylhydrazono)ethyl)-phenyl) amine
TsN <sub>3</sub>	tosyl azide
UHP	urea hydroperoxide
UiO	University of Oslo
VTXRPD	variable-temperature X-ray powder diffraction
XANES	X-ray absorption near edge structure
XFS	X-ray fluorescent spectroscopy
XPS	X-ray photoelectron spectroscopy
ZIFs	zeolitic imidazolate frameworks
2-pymo	2-hydroxypyrimidinolate
3-ppc	(S)-N-(pyridin-3-yl)-pyrrolidine-2-carboxamide
4-btapa	(1,3,5-benzene tricarboxylic acid tris[N-(4-pyridyl)amide
4-ppc	(S)-N-(pyridin-4-yl)-pyrrolidine-2-carboxamide

## Acknowledgements

This work was supported by the 973 Program (2012CB821701) and NSF Projects (21373278, 21102186, 91222201, 21121061 and 21173272) of China, the NSF of Guangdong (S2013030013474), the FRF for the Central Universities and the RFDP of Higher Education of China.

## Notes and references

MOE Laboratory of Bioinorganic and Synthetic Chemistry, State Key Laboratory of Optoelectronic Materials and Technologies, Lehn Institute of Functional Materials, School of Chemistry and Chemical Engineering, Sun Yat-sen University, Guangzhou 510275, P.R. China

E-mail: zhli99@mail.sysu.edu.cn (L. Zhang); cecscy@mail.sysu.edu.cn (C.-Y. Su).

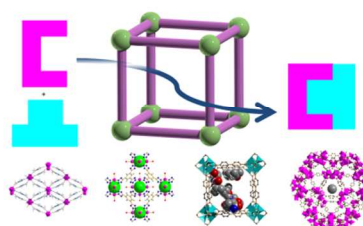
- (a) J. Elemans, J. Cornelissen, M. Feiters, A. Rowman, R. Nolte, in *Supramolecular Catalysis*, ed. van Leeuwen, P.W. N. M. Ch. 6; (b) Z. Wang, K. Clary, R. Bergman, K. Raymond and F. Toste, *Nat. Chem.*, 2013, **5**, 100; (c) R. Breslow, L. Overman, *J. Am. Chem. Soc.*, 1970, **92**, 1075-1077; (d) J. Meeuwissen, J. Reek, *Nat. Chem.*, 2010, **2**, 615.
- (a) M. Yoshizawa, J. Klosterman, M. Fujita, *Angew. Chem. Int. Ed.*, 2009, **48**, 3418-3438; (b) S. Seidel, P. Stang, *Acc. Chem. Res.* 2002, **35**, 972-983; (c) S. Leininger, B. Olenyuk, P. Stang, *Chem. Rev.*, 2000, **100**, 853-908; (d) M. Wiester, P. Ulmann, C. Mirkin, *Angew. Chem. Int. Ed.*, 2011, **50**, 114-137; (e) D. Fiedler, D. Leung, R. Bergman, K. Raymond, *Acc. Chem. Res.*, 2005, **38**, 351-360; (f) R. Saalfrank, H. Maid, A. Scheurer, *Angew. Chem. Int. Ed.*, 2008, **47**, 8794-8824; (g) C. Chen, J. Zhang, C. Su, *Eur. J. Inorg. Chem.*, 2007, 2997.
- M. Ranocchiari and J. A. van Bokhoven, *Phys. Chem. Chem. Phys.*, 2011, **13**, 6388-6396.
- (a) J. Perry IV, J. Perman and M. Zaworotko, *Chem. Soc. Rev.*, 2009, **38**, 1400-1417; (b) Q. Zhang, J. Zhang, Q. Yu, M. Pan, C. Su, *Cryst. Growth Des.* 2010, **10**, 4076-4084; (d) S. Xiang, J. Shi and J. Zhang, *Global J. Inorg. Chem.*, 2010, **1**, 42-64; (e) Z. Wang, G. Chen and K. Ding, *Chem. Rev.*, 2009, **109**, 322-359.
- (a) M. Piepenbrock, G. Lloyd, N. Clarke, and J. Steed, *Chem. Rev.*, 2010, **110**, 1960-2004; (b) A. Tam and V. Yam, *Chem. Soc. Rev.*, 2013, **42**, 1540-1567; (c) D. Díaz, D. Kühbeck and R. Koopmans, *Chem. Soc. Rev.*, 2011, **40**, 427-448; (d) L. Li, S. Xiang, S. Cao, J. Zhang, G. Ouyang, C. Chen and C. Su, *Nat. Commun.*, 2012, **4**, 1774; (e) J. Zhang, C. Su, *Coord. Chem. Rev.*, 2013, **257**, 1373-1408; (f) J. Zhang and S. L. James, in *Homogeneous Catalysts: Types, Reactions and Applications*, Nova Science Publishers, Inc., New York, 2011, ch. 5, pp 155-184.
- (a) Transition Metals for Organic Synthesis (Eds.: M. Beller, C. Bolm), Wiley-VCH, Weinheim, 2004; (b) P.W. N. M. van Leeuwen, *Homogeneous Catalysis: Understanding the Art*, Kluwer Academic Publishers, Dordrecht, 2004; (c) P. Dydio, W. I. Dzik, M. Lutz, B. de Bruin and J. N. H. Reek, *Angew. Chem. Int. Ed.*, 2011, **50**, 396-400; (d) K. S. Joya, Y. F. Joya, K. Ocakoglu and R. van de Krol, *Angew. Chem. Int. Ed.*, 2013, **52**, 10426-10437.
- (a) D. Bradshaw, J. B. Claridge, E. J. Cussen, T. J. Prior and M. J. Rosseinsky, *Acc. Chem. Res.*, 2005, **38**, 273-282; (b) S. Kitagawa and K. Uemura, *Chem. Soc. Rev.*, 2005, **34**, 109-119; (c) H. Deng, M. A. Olson, J. F. Stoddart and O. M. Yaghi, *Nat Chem*, 2010, **2**, 439-443; (d) S. Horike, S. Shimomura and S. Kitagawa, *Nat Chem*, 2009, **1**, 695-704; (e) R. Matsuda, R. Kitaura, S. Kitagawa, Y. Kubota, R. V. Belosludov, T. C. Kobayashi, H. Sakamoto, T. Chiba, M. Takata, Y. Kawazoe and Y. Mita, *Nature*, 2005, **436**, 238-241.
- (a) A. J. Blake, N. R. Champness, P. Hubberstey, W.-S. Li, M. A. Withersby and M. Schröder, *Coord. Chem. Rev.*, 1999, **183**, 117-138; (b) B. Moulton and M. J. Zaworotko, *Chem. Rev.*, 2001, **101**, 1629-1658; (c) C. Janiak, *Dalton Transactions*, 2003, 2781-2804; (d) K. Biradha, C.-Y. Su and J. J. Vittal, *Crystal Growth & Design*, 2011, **11**, 875-886; (e) M. O'Keeffe, *Chem. Soc. Rev.*, 2009, **38**, 1215-1217.
- S. Kitagawa and M. Kondo, *Bull. Chem. Soc. Jpn.*, 1998, **71**, 1739-1753.
- (a) Z. Wang and S. M. Cohen, *Chem. Soc. Rev.*, 2009, **38**, 1315-1329; (b) S. M. Cohen, *Chem. Rev.*, 2011, **112**, 970-1000.
- D. Farrusseng, S. Aguado and C. Pinel, *Angew. Chem. Int. Ed.*, 2009, **48**, 7502-7513.
- (a) J. Lee, O. K. Farha, J. Roberts, K. A. Scheidt, S. T. Nguyen and J. T. Hupp, *Chem. Soc. Rev.*, 2009, **38**, 1450-1459; (b) J. E. Mondloch, O. K. Farha, J. T. Hupp, *RSC Catalysis Series*, 2013 (12), 289-309.
- A. Corma, H. Garcia and F. X. Llabres i Xamena, *Chem. Rev.*, 2010, **110**, 4606-4655.
- (a) A. Dhakshinamoorthy, M. Alvaro and H. Garcia, *Catal. Sci. Technol.*, 2011, **1**, 856-867; (b) A. Dhakshinamoorthy, M. Alvaro and H. Garcia, *Chem. Commun.*, 2012, **48**, 11275-11288; (c) A. Dhakshinamoorthy, M. Opanasenko, J. Čejka and H. Garcia, *Adv. Synth. Catal.*, 2013, **355**, 247-268; (d) A. Dhakshinamoorthy and H. Garcia, *Chem. Soc. Rev.*, 2012, **41**, 5262-5284; (e) H. Garcia and B. Ferrer, *RSC Catalysis Series*, 2013 (12), 365-383.
- J. Kim, H.-Y. Cho and W.-S. Ahn, *Catal Surv Asia.*, 2012, **16**, 106-119.
- (a) P. Valvekens, F. Vermoortele and D. De Vos, *Catal. Sci. Technol.*, 2013, **3**, 1435-1445; (b) F. Vermoortele, P. Valvekens, D. De Vos, *RSC Catalysis Series*, 2013 (12), 268-288.
- (a) L. Ma, C. Abney and W. Lin, *Chem. Soc., Rev.*, 2009, **38**, 1248-1256; (b) J. M. Falkowski, S. Liu, W. Lin, *RSC Catalysis Series*, 2013 (12), 344-364; (c) J. -L. Wang, C. Wang, W. Lin, *ACS Catal.*, 2012, **2**, 2630-2640.
- (a) K. Kim, *Top Curr Chem.*, 2010, 293, 115-153; (b) M. Yoon, R. Srirambalaji and K. Kim, *Chem. Rev.*, 2012, **112**, 1196-1231.
- G. Nickerl, A. Henschel, R. Grunker, K. Gedrich and S. Kaskel, *Chem. Ing. Tech.*, 2011, **83**, 90-103.
- Roland A. Fischer, *Top Curr Chem.*, 2010, **293**, 77-113.
- (a) J. Juan-Alcañiz, J. Gascon and F. Kapteijn, *J. Mater. Chem.*, 2012, **22**, 10102; (b) J. Juan-Alcañiz, E. V. Ramos-Fernandez, F.

- Kapteijn, J. Gascon, *RSC Catalysis Series*, 2013 (12), 310-343; (c) F. X. Llabres i Xamena, I. Luz, F. G. Cirujano, *RSC Catalysis Series*, 2013 (12), 237-267; (d) J. Gascon, A. Corma, F. Kapteijn, F. X. Llabres i Xamena, *ACS Catal.*, 2014, **4**, 361-378.
- 22 (a) Z.-Y. Gu, J. Park, A. Raiff, Z. Wei, H.-C. Zhou, *ChemCatChem.*, 2014, **6**, 67-75; (b) M. Zhao, S. Ou, C.-D. Wu, *Acc. Chem. Res.* 2014, **47**, 1199-1207; (c) N.V. Maksimchuk, M. N. Timofeeva, M. S. Melgunov, A.N. Shmakov, Yu. A. Chesalov, D. N. Dybtsev, V. P. Fedin, O. A. Kholdeev, *J. Catal.*, 2008, **257**, 315-323; (d) J. Song, Z. Luo, D. K. Britt, H. Furukawa, O. M. Yaghi, K. I. Hardcastle, C. L. Hill, *J. Am. Chem. Soc.*, 2011, **133**, 16839-16846; (e) Q. Han, C. He, M. Zhao, B. Qi, J. Y. Niu, C. Y. Duan, *J. Am. Chem. Soc.* 2013, **135**, 10186-10189; (f) D. T. Genna, A. G. Wong-Foy, A. J. Matzger, M. S. Sanford, *J. Am. Chem. Soc.*, 2013, **135**, 10586-10589; (g) N. V. Maksimchuk, K. A. Kovalenko, S. S. Arzumanov, U. A. Chesalov, M. S. Melgunov, A. G. Stepanov, V. P. Fedin, O. A. Kholdeeva, *Inorg. Chem.*, 2010, 2920-2930.
- 23 (a) G. Férey, C. Mellot-Draznieks, C. Serre, F. Millange, J. Dutour, S. Surble and I. Margiolaki, *Science*, 2005, **309**, 2040-2042; (b) A. Henschel, K. Gedrich, R. Kraehnert and S. Kaskel, *Chem. Commun.*, 2008, 4192-4194; (c) Kim, S. Bhattacharjee, K. E. Jeong, S. Y. Jeong and W. S. Ahn, *Chem. Commun.*, 2009, 3904-3906.
- 24 Y. K. Hwang, D.-Y. Hong, J.-S. Chang, H. Seo, M. Yoon, J. Kim, S. H. Jung, C. Serre and G. Férey, *Appl. Catal., A*, 2010, **358**, 249-253.
- 25 N. V. Maksimchuk, K. A. Kovalenko, V. P. Fedin and O. A. Kholdeeva, *Adv. Synth. Catal.*, 2010, **352**, 2943-2948.
- 26 O. V. Zalomaeva, A. M. Chibiryaev, K. A. Kovalenko, O. A. Kholdeeva, B. S. Balzhinimaev and V. P. Fedin, *J. Catal.*, 2013, **298**, 179-185.
- 27 P. Horcajada, S. Surble, C. Serre, D. Y. Hong, Y. K. Seo, J. S. Chang, J. M. Greneche, I. Margiolaki and G. Férey, *Chem. Commun.*, 2007, 2820-2822.
- 28 (a) A. Dhakshinamoorthy, M. Alvaro and H. Garcia, *J. Catal.*, 2009, **267**, 1-4; (b) A. Dhakshinamoorthy, M. Alvaro and H. Garcia, *Adv. Synth. Catal.*, 2010, **352**, 711-717; (c) A. Dhakshinamoorthy, M. Alvaro and H. Garcia, *Chem. Commun.*, 2010, **46**, 6476-6478; (d) A. Dhakshinamoorthy, M. Alvaro and H. Garcia, *Chem. -Eur. J.* 2010, **16**, 8530-8536; (e) A. Dhakshinamoorthy, M. Alvaro, H. Chevreau, P. Horcajada, T. Devic, C. Serre and H. Garcia, *Catal. Sci. Technol.*, 2012, **2**, 324-330.
- 29 (a) T. Loiseau, C. Serre, C. Huguenard, G. Fink, F. Taulelle, M. Henry, T. Bataille, G. Férey, *Chem. -Eur. J.*, 2004, **10**, 1373; (b) A. Dhakshinamoorthy, M. Alvaro and H. Garcia, *Adv. Synth. Catal.*, 2009, **351**, 2271-2276.
- 30 (a) J. P. S. Mowat, S. R. Miller, A. M. Z. Slawin, V. R. Seymour, S. E. Ashbrook and P. A. Weight, *Microporous Mesoporous Mater.*, 2011, **142** 322-333; (b) L. Mitchell, B. Gonzalez-Santiago, J. P. S. Mowat, M. E. Gunn, P. Williamson, N. Acerbi, M. L. Clarke and P. A. Wright, *Catal. Sci. Technol.*, 2013, **3**, 606-617.
- 31 (a) K. Barthelet, J. Marrot, D. Riou, and G. Férey, *Angew. Chem. Int. Ed.*, 2002, **41**, 281-284; (b) K. Leus, I. Muylaert, M. Vandichel, G. B. Marin, M. Waroquier, V. Van Speybroeck and P. Van der Voort, *Chem. Commun.*, 2010, **46**, 5085-5087; (c) K. Leus, M. Vandichel, Y.-Y. Liu, I. Muylaert, J. Musschoot, S. Pyl, H. Vrielinck, F. Callens, G. B. Marin, C. Detavernier, P. V. Wiper, Y. Z. Khimyak, M. Waroquier, V. Van Speybroeck and P. Van Der Voort, *J. Catal.*, 2012, **285**, 196-207.
- 32 (a) M. Dinca, A. Dailly, Y. Liu, C. M. Brown, D. A. Neumann and J. R. Long, *J. Am. Chem. Soc.*, 2006, **128**, 16876-16883; (b) S. Horike, M. Dinca, K. Tamaki and J. R. Long, *J. Am. Chem. Soc.*, 2008, **130**, 5854-5855.
- 33 M. H. Xie, X. L. Yang and C. D. Wu, *Chem. -Eur. J.*, 2011, **17**, 11424-11427.
- 34 (a) M. Tonigold, Y. Lu, B. Bredenkotter, B. Rieger, S. Bahnmueller, J. Hitzbleck, G. Langstein and D. Volkmer, *Angew. Chem. Int. Ed.*, 2009, **48**, 7546-7550; (b) M. Tonigold, Y. Lu, A. Mavrandonakis, A. Puls, R. Staudt, J. Mollmer, J. Sauer and D. Volkmer, *Chem. -Eur. J.*, 2011, **17**, 8671-8695.
- 35 (a) P. D. C. Dietzel, Y. Morita, R. Blom, H. Fjellvag, *Angew. Chem., Int. Ed.*, 2005, **44**, 6354; (b) H.-Y. Cho, D.-A. Yang, J. Kim, S.-Y. Jeong and W.-S. Ahn, *Catal. Today*, 2012, **185**, 35-40.
- 36 S. Biswas, M. Maes, A. Dhakshinamoorthy, M. Feyand, D. E. De Vos, H. Garcia and N. Stock, *J. Mater. Chem.*, 2012, **22**, 10200.
- 37 (a) S. S.-Y. Chui, S. M. F. Lo, J. P. H. Charmant, A. G. Orpen and I. D. Williams, *Science*, 1999, **283**, 1148-1150; (b) K. Schlichte, T. Kratzke and S. Kaskel, *Microporous Mesoporous Mater.*, 2004, **73**, 81-88.
- 38 L. Alaerts, E. Seguin, H. Poelman, F. Thibault-Starzyk, P. A. Jacobs and D. E. De Vos, *Chem. -Eur. J.*, 2006, **12**, 7353-7363.
- 39 A. Corma, M. Iglesias, F. X. Llabres i Xamena and F. Sanchez, *Chem. -Eur. J.*, 2010, **16**, 9789-9795.
- 40 (a) E. Pérez-Mayoral and J. Čejka, *ChemCatChem.*, 2011, **3**, 157-159; (b) E. Perez-Mayoral, Z. Musilova, B. Gil, B. Marszalek, M. Polozij, P. Nachtigall and J. Čejka, *Dalton Trans.*, 2012, **41**, 4036-4044; (c) M. Opanasenko, M. Shamzhy and J. Čejka, *ChemCatChem.*, 2013, **5**, 1024-1031.
- 41 (a) M. Wang, M. H. Xie, C. D. Wu and Y. G. Wang, *Chem. Commun.*, 2009, 2396-2398; (b) L. X. Shi and C. D. Wu, *Chem. Commun.*, 2011, **47**, 2928-2930.
- 42 (a) L. C. Tabares, J. A. R. Navarro and J. M. Salas, *J. Am. Chem. Soc.*, 2001, **123**, 383-387; (b) F. X. Llabrés i Xamena, A. Corma, *J. Catal.*, 2010, **276**, 134-140; (c) I. Luz, F. X. Llabrés i Xamena and A. Corma, *J. Catal.*, 2012, **285**, 285-291.
- 43 (a) D. Shi, Y. Ren, H. Jiang, B. Cai and J. Lu, *Inorg. Chem.*, 2012, **51**, 6498-6506; (b) N. T. S. Phan, P. H. L. Vu, T. T. Nguyen, *J. Catal.*, 2013, **306**, 38-46; (c) A. Pichon, C. M. Fierro, M. Nieuwenhuyzen, S. L. James, *CrystEngComm*, 2007, **9**, 449-451.
- 44 (a) R. Yang, L. Li, Y. Xiong, J.-R. Li, H.-C. Zhou, C.-Y. Su, *Chem. Asian J.* 2010, **5**, 2358-2368. (b) T. Yang, H. Cui, C. Zhang, L. Zhang and C. Y. Su, *Inorg. Chem.*, 2013, **52**, 9053-9059; (c) T. Yang, H. Cui, C. Zhang, L. Zhang and C.-Y. Su, *ChemCatChem.*, 2013, **5**, 3131-3138; (d) S. Wang, L. Li, J. Zhang, X. Yuan and C.-Y. Su, *J. Mater. Chem.*, 2011, **21**, 7098-7104; (e) X. Tan, L. Li, J. Zhang, X. Han, L. Jiang, F. Li and C.-Y. Su, *Chem. Mater.*, 2012, **24**, 480-485.
- 45 D. N. Dybtsev, A. L. Nuzhdin, H. Chun, K. P. Bryliakov, E. P. Talsi, V. P. Fedin and K. Kim, *Angew. Chem. Int. Ed.*, 2006, **45**, 916-920.
- 46 K. Gedrich, M. Heitbaum, A. Notzon, I. Senkowska, R. Frohlich, J. Getzschmann, U. Mueller, F. Glorius and S. Kaskel, *Chem. -Eur. J.*, 2011, **17**, 2099-2106.

- 47 (a) K. S. Park, Z. Ni, A. P. Cote, J. Y. Choi, R. Huang, F. J. UribeRomo, H. K. Chae, M. O'Keeffe, O. M. Yaghi, *Proc. Natl. Acad. Sci. U.S.A.*, 2006, **103**, 10186; (b) C. M. Miralda, E. E. Macias, M. Zhu, P. Ratnasamy and M. A. Carreon, *ACS Catal.*, 2012, **2**, 180-183.
- 48 X. Jing, C. He, D. Dong, L. Yang and C. Duan, *Angew. Chem. Int. Ed.*, 2012, **51**, 10127-10131.
- 49 (a) R. Sen, D. Saha and S. Koner, *Chem. -Eur. J.* 2012, **18**, 5979-5986; (b) D. Saha, R. Sen, T. Maity and S. Koner, *Dalton Trans.*, 2012, **41**, 7399-7408.
- 50 (a) J. H. Cavka, S. Jakobsen, U. Olsbye, N. Guillou, C. Lamberti, S. Bordiga and K. P. Lillerud, *J. Am. Chem. Soc.*, 2008, **130**, 13850-13851; (b) F. Vermoortele, R. Ameloot, A. Vimont, C. Serre and D. De Vos, *Chem. Commun.*, 2011, **47**, 1521-1523; (c) F. Vermoortele, M. Vandichel, B. Van de Voorde, R. Ameloot, M. Waroquier, V. Van Speybroeck and D. E. De Vos, *Angew. Chem. Int. Ed.*, 2012, **51**, 4887-4890; (d) F. Vermoortele, B. Bueken, G. Le Bars, Ben Van de Voorde, M. Vandichel, K. Houthoofd, A. Vimont, M. Daturi, M. Waroquier, V. Van Speybroeck, C. Kirschhock, D. E. De Vos, *J. Am. Chem. Soc.*, 2013, **135**, 11465-11468.
- 51 (a) J. A. Navarro, E. Barea, J. M. Salas, N. Masciocchi, S. Galli, A. Sironi, C. O. Ania and J. B. Parra, *Inorg. Chem.*, 2006, **45**, 2397-2399; (b) F. Llabresixamena, A. Abad, A. Corma and H. Garcia, *J. Catal.*, 2007, **250**, 294-298; (c) S. Opelt, V. Krug, J. Sonntag, M. Hunger, E. Klemm, *Microporous Mesoporous Mater.*, 2012, **147**, 327-333; (d) S. Schuster, E. Klemm, M. Bauer, *Chem.- Eur. J.*, 2012, **18**, 15831-15837.
- 52 D. Dang, P. Wu, C. He, Z. Xie and C. Duan, *J. Am. Chem. Soc.*, 2010, **132**, 14321-14323.
- 53 M. Feyand, E. Mugnaioli, F. Vermoortele, B. Bueken, J. M. Dieterich, T. Reimer, U. Kolb, D. de Vos and N. Stock, *Angew. Chem. Int. Ed.*, 2012, **51**, 10373-10376.
- 54 (a) H. Lu and X. P. Zhang, *Chem. Soc. Rev.*, 2011, **40**, 1899-1909; (b) G. Cozzi, *Chem. Soc. Rev.*, 2004, **33**, 410-421.
- 55 (a) A. M. Shultz, O. K. Farha, J. T. Hupp and S. T. Nguyen, *J. Am. Chem. Soc.*, 2009, **131**, 4204-4205; (b) O. K. Farha, A. M. Shultz, A. A. Sarjeant, S. T. Nguyen and J. T. Hupp, *J. Am. Chem. Soc.*, 2011, **133**, 5652-5655; (c) S. Takaishi, E. J. DeMarco, M. J. Pellin, O. K. Farha, J. T. Hupp, *Chem. Sci.*, 2013, **4**, 1509-1513.
- 56 (a) X. S. Wang, M. Chrzanowski, C. Kim, W. Y. Gao, L. Wojtas, Y. S. Chen, X. Peter Zhang and S. Ma, *Chem. Commun.*, 2012, **48**, 7173-7175; (b) L. Meng, Q. Cheng, C. Kim, W. Y. Gao, L. Wojtas, Y. S. Chen, M. J. Zaworotko, X. P. Zhang and S. Ma, *Angew. Chem. Int. Ed.*, 2012, **51**, 10082-10085.
- 57 (a) M. H. Xie, X. L. Yang and C. D. Wu, *Chem. Commun.*, 2011, **47**, 5521-5523; (b) C. Zou, Z. Zhang, X. Xu, Q. Gong, J. Li and C. D. Wu, *J. Am. Chem. Soc.*, 2012, **134**, 87-90. (c) C. Zou, T. Zhang, M.-H. Xie, L. Yan, G.-Q. Kong, X.-Li Yang, A. Ma, C.-D. Wu, *Inorg. Chem.*, 2013, **52**, 3620-3626; (d) M.-H. Xie, X.-L. Yang, Y. He, J. Zhang, B. Chen, C.-D. Wu, *Chem. -Eur. J.*, 2013, **19**, 14316-14321.
- 58 (a) D. Feng, Z.-Y. Gu, J.-R. Li, H.-L. Jiang, Z. Wei, H.-C. Zhou, *Angew. Chem. Int. Ed.*, 2012, **51**, 10307-10310; (b) D. Feng, W.-C. Chung, Z. Wei, Z.-Y. Gu, H.-L. Jiang, Y.-P. Chen, D. J. Darensbourg, H.-C. Zhou, *J. Am. Chem. Soc.*, 2013, **135**, 17105-17110. (c) M. H. Alkordi, Y. Liu, R. W. Larsen, J. F. Eubank, M. Eddaoudi, *J. Am. Chem. Soc.*, 2008, **130**, 12639-12641; (d) Z. Zhang, L. Zhang, L. Wojtas, M. Eddaoudi, M. J. Zaworotko, *J. Am. Chem. Soc.*, 2012, **134**, 928-933.
- 59 (a) S. H. Cho, B. Ma, S. T. Nguyen, J. T. Hupp and T. E. Albrecht-Schmitt, *Chem. Commun.*, 2006, 2563-2565; (b) A. M. Shultz, O. K. Farha, D. Adhikari, A. A. Sarjeant, J. T. Hupp and S. T. Nguyen, *Inorg. Chem.*, 2011, **50**, 3174-3176.
- 60 (a) F. Song, C. Wang, J. M. Falkowski, L. Ma and W. Lin, *J. Am. Chem. Soc.*, 2010, **132**, 15390-15398; (b) F. Song, C. Wang and W. Lin, *Chem. Commun.*, 2011, **47**, 8256-8258; (c) J. M. Falkowski, C. Wang, S. Liu and W. Lin, *Angew. Chem. Int. Ed.*, 2011, **50**, 8674-8678; (d) J. M. Falkowski, S. Liu, C. Wang, W. Lin, *Chem. Commun.*, 2012, **48**, 6508-6510.
- 61 (a) C. Zhu, G. Yuan, X. Chen, Z. Yang and Y. Cui, *J. Am. Chem. Soc.*, 2012, **134**, 8058-8061; (b) Y. Huang, T. Liu, J. Lin, J. Lü, Z. Lin, R. Cao, *Inorg. Chem.*, 2011, **50**, 2191-2198.
- 62 J. S. Seo, D. Whang, H. Lee, S. I. Jun, J. Oh, Y. J. Jeon and K. Kim, *Nature*, 2000, **404**, 982-986.
- 63 S. Hasegawa, S. Horike, R. Matsuda, S. Furukawa, K. Mochizuki, Y. Kinoshita and S. Kitagawa, *J. Am. Chem. Soc.*, 2007, **129**, 2607-2614.
- 64 (a) P. Serra-Crespo, E. V. Ramos-Fernandez, J. Gascon and F. Kapteijn, *Chem. Mater.*, 2011, **23**, 2565-2572; (b) J. Juan-Alcañiz, J. Ferrando-Soria, I. Luz, P. Serra-Crespo, E. Skupien, V. P. Santos, E. Pardo, F. X. Llabres i Xamena, F. Kapteijn, J. Gascon, *J. Catal.*, 2013, **307**, 295-304.
- 65 Y. K. Hwang, D. Y. Hong, J. S. Chang, S. H. Jhung, Y. K. Seo, J. Kim, A. Vimont, M. Daturi, C. Serre and G. Férey, *Angew. Chem. Int. Ed.*, 2008, **47**, 4144-4148.
- 66 (a) J. L. C. Roswell and O. M. Yaghi, *J. Am. Chem. Soc.*, 2006, **128**, 1304-1315; (b) M. J. Ingleson, J. P. Barrio, J. B. Guilbaud, Y. Z. Khimyak and M. J. Rosseinsky, *Chem Commun.*, 2008, 2680-2682.
- 67 X. Zhang, F. X. Llabrés i Xamena and A. Corma, *J. Catal.*, 2009, **265**, 155-160.
- 68 S. Bhattacharjee, D. A. Yang and W. S. Ahn, *Chem. Commun.*, 2011, **47**, 3637-3639.
- 69 (a) S. J. Garibay and S. M. Cohen, *Chem. Commun.* 2010, **46**, 7700-7702; (b) M. Kandiah, M. H. Nilsen, S. Usseglio, S. Jakobsen, U. Olsbye, M. Tilset, C. Larabi, E.A. Quadrelli, F. Bonino and K.P. Lillerud, *Chem. Mater.*, 2010, **22**, 6632-6640; (c) M. Pintado-Sierra, A. M. Rasero-Almansa, A. Corma, M. Iglesias and F. Sánchez, *J. Catal.*, 2013, **299**, 137-145.
- 70 (a) S. Bauer, C. Serre, T. Devic, P. Horcajada, J. r. m. Marrot, G. r. Férey and N. Stock, *Inorg. Chem.*, 2008, **47**, 7568-7576; (b) J. Canivet, S. Aguado, Y. Schuurman and D. Farrusseng, *J. Am. Chem. Soc.*, 2013, **135**, 4195-4198; (c) S. Aguado, J. Canivet, Y. Schuurman, D. Farrusseng, *J. Catal.* 2011, **284**, 207-214; (d) J. Canivet, S. Aguado, C. Daniel, D. Farrusseng, *ChemCatChem*, 2011, **3**, 675-678.
- 71 M. G. Goesten, J. Juan-Alcañiz, E. V. Ramos-Fernandez, K. B. Sai Sankar Gupta, E. Stavitski, H. van Bekkum, J. Gascon and F. Kapteijn, *J. Catal.*, 2011, **281**, 177-187.
- 72 Y. Zang, J. Shi, F. Zhang, Y. Zhong and W. Zhu, *Catal. Sci. Technol.*, 2013, **3**, 2044-2049.
- 73 M. Banerjee, S. Das, M. Yoon, H. J. Choi, M. H. Hyun, S. M. Park, G. Seo and K. Kim, *J. Am. Chem. Soc.*, 2009, **131**, 7524-7525.

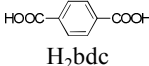
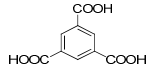
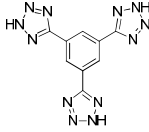
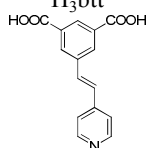
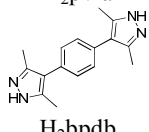
- 74 D. J. Lun, G. I. Waterhouse and S. G. Telfer, *J. Am. Chem. Soc.*, 2011, **133**, 5806-5809.
- 75 (a) D. Dang, P. Wu, C. He, Z. Xie and C. Duan, *J. Am. Chem. Soc.*, 2010, **132**, 14321-14323; (b) P. Wu, C. He, J. Wang, X. Peng, X. Li, Y. An and C. Duan, *J. Am. Chem. Soc.*, 2012, **134**, 14991-14999.
- 76 (a) K. Oisaki, Q. Li, H. Furukawa, A. U. Czaja and O. M. Yaghi, *J. Am. Chem. Soc.*, **2010**, *132*, 9262-9264; (b) J. Chun, H. S. Lee, I. G. Jung, S. W. Lee, H. J. Kim and S. U. Son, *Organometallics* **2010**, *29*, 1518-1521; (c) J. Chun, G. Jung, H. J. Kim, M. Park, M. S. Lah and S. U. Son, *Inorg. Chem.* **2009**, *48*, 6353-6355; (d) S. Wang, Q. Yang, J. Zhang, X. Zhang, C. Zhao, L. Jiang and C.-Y. Su, *Inorg. Chem.*, 2013, **52**, 4198-4204.
- 77 (a) M. B. Lalonde, O. K. Farha, K. A. Scheidt and J. T. Hupp, *ACS Catal.*, 2012, **2**, 1550-1554; (b) G. Q. Kong, X. Xu, C. Zou and C. D. Wu, *Chem. Commun.*, 2011, **47**, 11005-11007; (c) G. Q. Kong, S. Ou, C. Zou and C. D. Wu, *J. Am. Chem. Soc.*, 2012, **134**, 19851-19857.
- 78 J. M. Roberts, B. M. Fini, A. A. Sarjeant, O. K. Farha, J. T. Hupp and K. A. Scheidt, *J. Am. Chem. Soc.*, 2012, **134**, 3334-3337.
- 79 (a) C. D. Wu, A. Hu, L. Zhang and W. Lin, *J. Am. Chem. Soc.* 2005, **127**, 8940-8941; (b) C. D. Wu and W. Lin, *Angew. Chem. Int. Ed.*, 2007, **46**, 1075-1078; (c) L. Ma, C. D. Wu, M. M. Wanderley and W. Lin, *Angew. Chem. Int. Ed.*, 2010, **49**, 8244-8248; (d) L. Ma, J. M. Falkowski, C. Abney and W. Lin, *Nat. Chem.*, 2010, **2**, 838-846.
- 80 (a) E. D. Bloch, D. Britt, C. Lee, C. J. Doonan, F. J. Uribe-Romo, H. Furukawa, J. R. Long and O. M. Yaghi, *J. Am. Chem. Soc.*, 2010, **132**, 14382-14384; (b) H. Liu, B. Yin, Z. Gao, Y. Li and H. Jiang, *Chem. Commun.*, 2012, **48**, 2033-2035; (c) M. Wang, B. Yuan, T. Ma, H. Jiang and Y. Li, *RSC Adv.*, 2012, **2**, 5528-5530.
- 81 H. G. T. Nguyen, M. H. Weston, O. K. Farha, J. T. Hupp and S. T. Nguyen, *CrystEngComm*, 2012, **14**, 4115-4118.
- 82 (a) Li, H., Eddaoudi, M., O'Keeffe, M., Yaghi, O. M., *Nature*, 1999, **402**, 276; (b) S. Hermes, M. K. Schroter, R. Schmid, L. Khodeir, M. Muhler, A. Tissler, R. W. Fischer and R. A. Fischer, *Angew. Chem. Int. Ed.*, 2005, **44**, 6237-6241; (c) M. Müller, S. Hermes, K. Kähler, M. W. E. van den Berg, M. Muhler and R. A. Fischer, *Chem. Mater.*, 2008, **20**, 4576-4587; (d) Roland A. Fischer, *J. Am. Chem. Soc.*, 2008, **130**, 6119-6130.
- 83 F. Schroder, D. Esken, M. Cokoja, M. W. van den Berg, O. I. Lebedev, G. Van Tendeloo, B. Walaszek, G. Buntkowsky, H. H. Limbach, B. Chaudret and R. A. Fischer, *J. Am. Chem. Soc.*, 2008, **130**, 6119-6130.
- 84 T. Ishida, M. Nagaoka, T. Akita and M. Haruta, *Chem.-Eur. J.*, 2008, **14**, 8456-8460.
- 85 H. L. Jiang, B. Liu, T. Akita, M. Haruta, H. Sakurai and Q. Xu, *J. Am. Chem. Soc.*, 2009, **131**, 11302-11303.
- 86 D. Esken, S. Turner, O. I. Lebedev, G. Van Tendeloo and R. A. Fischer, *Chem. Mater.*, 2010, **22**, 6393-6401.
- 87 H. Liu, Y. Liu, Y. Li, Z. Tang and H. Jiang, *J. Phys. Chem. C.*, 2010, **114**, 13362-13369.
- 88 (a) A. Henschel, K. Gedrich, R. Kraehnert and S. Kaskel, *J. Mater. Chem.*, 2007, **17**, 3827-3832; (b) A. Henschel, K. Gedrich, R. Kraehnert and S. Kaskel, *Chem. Commun.*, 2008, 4192-4194; (c) T. Dang, Y. Zhu, S. C. Ghosh, A. Chen, C. L. L. Chai, A. M. Seayad, *Chem. Commun.*, 2012, **48**, 1805-1807.
- 89 (a) B. Yuan, Y. Pan, Y. Li, B. Yin and H. Jiang, *Angew. Chem. Int. Ed.*, 2010, **49**, 4054-4058; (b) Y. Pan, B. Yuan, Y. Li and D. He, *Chem. Commun.*, 2010, **46**, 2280-2282.
- 90 (a) Y. Huang, Z. Lin and R. Cao, *Chem.-Eur. J.*, 2011, **17**, 12706-12712; (b) Y. Huang, S. Liu, Z. Lin, W. Li, X. Li and R. Cao, *J. Catal.*, 2012, **292**, 111-117; (c) Y. Huang, T. Ma, P. Huang, D. Wu, Z. Lin, R. Cao; *ChemCatChem*, 2013, **5**, 1877-1833; (d) Y. Huang, S. Gao, T. Liu, J. Lü, X. Lin, H. Li, R. Cao, *ChemPlusChem*, 2012, **77**, 106-112.
- 91 H. Li, Z. Zhu, F. Zhang, S. Xie, H. Li, P. Li and X. Zhou, *ACS Catal.*, 2011, **1**, 1604-1612.
- 92 J. Hermannsdorfer and R. Kempe, *Chem.-Eur. J.*, 2011, **17**, 8071-8077.
- 93 (a) Rowsell, J. L. C.; Millward, A. R.; Park, K. S.; Yaghi, O. M. *J. Am. Chem. Soc.*, 2004, **126**, 5666; (b) S. Proch, J. Hermannsdorfer, R. Kempe, C. Kern, A. Jess, L. Seyfarth and J. Senker, *Chem.-Eur. J.*, 2008, **14**, 8204-8212.
- 94 A. Aijaz, A. Karkamkar, Y. J. Choi, N. Tsumori, E. Ronnebro, T. Autrey, H. Shioyama and Q. Xu, *J. Am. Chem. Soc.*, 2012, **134**, 13926-13929.
- 95 E. V. Ramos-Fernandez, C. Pieters, B. van der Linden, J. Juan-Alcañiz, P. Serra-Crespo, M. W. G. M. Verhoeven, H. Niemantsverdriet, J. Gascon and F. Kapteijn, *J. Catal.*, 2012, **289**, 42-52.
- 96 (a) S. Pullen, H. Fei, A. Orthaber, S. M. Cohen and S. Ott, *J. Am. Chem. Soc.*, 2013, **135**, 16997-17003; (b) K. G. M. Laurier, F. Vermoortele, R. Ameloot, D. E. De Vos, J. Hofkens, M. B. J. Roeffaers, *J. Am. Chem. Soc.*, 2013, **135**, 14488-14491.
- 97 W. Vermeiren and J. P. Gilson, *Top. Catal.*, 2009, **52**, 1131-1161.
- 98 T. Li, H. Liu, Y. Fan, P. Yuan, G. Shi, X. T. Bi and X. Bao, *Green Chem.*, 2012, **14**, 3255-3259.
- 99 D.-Y. Hong, Y. K. Hwang, C. Serre, G. Férey, and J.-S. Chang, *Adv. Funct. Mater.*, 2009, **19**, 1537-1552.

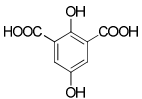
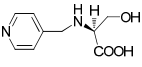
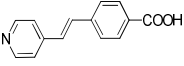
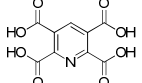
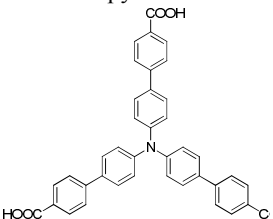
## TOC



The contributions of MOFs to the field of heterogeneous supramolecular catalysis are comprehensively reviewed with regard to active sites, selectivity, as well as host-guest chemistry.

**Table 1** List of MOFs with coordinatively unsaturated metal sites (CUMs) showing ligand, surface area, window or channel size, active metal, and catalytic reaction.

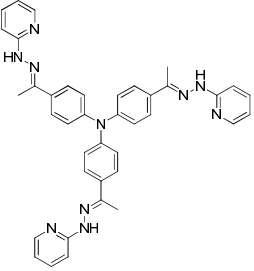
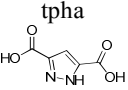
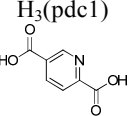
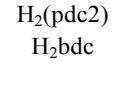
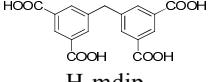
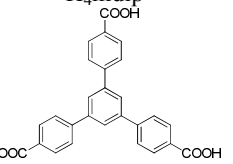
MOF formula (MOF code)	Ligand	Surface area/m <sup>2</sup> g <sup>-1</sup>		Window or channel size/Å	Active metal	Catalytic reaction	Ref.
		BET	Langmuir				
Cr <sub>3</sub> X(H <sub>2</sub> O) <sub>2</sub> O(bdc) <sub>3</sub> ; X = F, OH (MIL-101(Cr))	 H <sub>2</sub> bdc	4100 ± 200	5900 ± 300	29 & 34	Cr <sup>3+</sup>	Cyanosilylation of aldehydes; Oxidation of hydrocarbons; Oxidation of sulfides; Cycloaddition of CO <sub>2</sub> and epoxides	23b 23c,25 24 26
Fe <sub>3</sub> F(H <sub>2</sub> O) <sub>2</sub> O(btc) <sub>2</sub> (MIL-100(Fe))	 H <sub>3</sub> btc	-	3100	25 & 29	Fe <sup>3+</sup>	Friedel-Crafts benzylation; Oxidation of hydrocarbons; Ring-opening of epoxides; Claisen Schmidt condensation; Oxidation of thiophenol to diphenyldisulfide Isomerization of α-pinene oxide;	27 28a 28b 28c 28d 28e
Al <sub>2</sub> (bdc) <sub>3</sub> (MIL-53(Al))	H <sub>2</sub> bdc	1140	1590	7.3 × 7.7	Al <sup>3+</sup>	Reduction of carbon-carbon multiple bonds	29
Sc <sub>3</sub> (OH)(H <sub>2</sub> O) <sub>2</sub> O(btc) <sub>2</sub> (MIL-100(Sc))	H <sub>3</sub> btc	1000~1400	-	25 & 30	Sc <sup>3+</sup>	Intermolecular carbonyl ene reaction; Michael addition Reaction; Ketimine and aldimine formation	30b
V <sup>IV</sup> O(bdc) (MIL-47(V))	H <sub>2</sub> bdc	930±30	1225	10.5 × 11	V <sup>4+</sup>	Oxidation of hydrocarbons	31b,c
[Mn(DMF) <sub>6</sub> ] <sub>3</sub> [(Mn <sub>4</sub> Cl) <sub>3</sub> (btt) <sub>8</sub> (H <sub>2</sub> O) <sub>10</sub> ] <sub>2</sub> (Mn-btt)	 H <sub>3</sub> btt	2100	-	7 & 10	Mn <sup>2+</sup>	Cyanosilylation of aldehydes; Mukaiyama-aldol reaction	32b
Mn <sub>2</sub> (pvia) <sub>2</sub> (H <sub>2</sub> O) <sub>2</sub>	 H <sub>3</sub> btc	7.54	-	7.8 × 8.9	Mn <sup>2+</sup>	Alcohol oxidation	33
Co <sup>II</sup> <sub>4</sub> O(bdpb) <sub>3</sub> (MFU-1)	 H <sub>2</sub> bdpb	1485	-	18.1	Co <sup>2+</sup>	Oxidation of hydrocarbons	

ARTICLE					Journal Name	
Co <sup>II</sup> (bdpb) (MFU-2)	H <sub>2</sub> bpbdb	1477	-	18.6	Co <sup>2+</sup>	Oxidation of hydrocarbons 34
Co <sub>2</sub> (dhhbdc)(H <sub>2</sub> O) (Co-MOF-74)	 H <sub>2</sub> dhhbdc	1327	-	11~12	Co <sup>2+</sup>	Cycloaddition of CO <sub>2</sub> and epoxides 35
[Co(DMA) <sub>6</sub> ] <sub>3</sub> [(Co <sub>4</sub> Cl) <sub>3</sub> (btt) <sub>8</sub> (H <sub>2</sub> O) <sub>12</sub> ] <sub>2</sub> (Co-btt)	H <sub>3</sub> btt	1749	1993	10.9 & 15.6	Co <sup>2+</sup>	Ring opening of epoxides; Oxidation of hydrocarbons 36
Cu <sub>3</sub> (btc) <sub>2</sub> (HKUST-1)	H <sub>3</sub> btc	692.2	917.6	9 & 4.6	Cu <sup>2+</sup>	Cyanosilylation of aldehydes; 37 Isomerization of terpene derivatives; 38 Cyclopropanation of olefins; 40a,b Friedländer reaction 40c Pechmann condensation Biginelli reaction; 41a 1,2-Addition of $\alpha,\beta$ -unsaturated ketones
Cu <sub>2</sub> (papa) <sub>2</sub> Cl <sub>2</sub>	 Hpapa	-	-	5.1 × 2.9	Cu <sup>2+</sup>	Henry reaction 41b
[Cu <sub>3</sub> (ptdc)(pvba) <sub>2</sub> (H <sub>2</sub> O) <sub>3</sub> ] <sub>3</sub>	 Hpvba	-	-	13.8 × 23.6	Cu <sup>2+</sup>	
	 H <sub>4</sub> ptdc					
Cu(2-pymo) <sub>2</sub>	 Hpymo	200	-	8	Cu <sup>2+</sup>	Click reaction; 42b Three-component couplings of amines, aldehydes and alkynes 42c
Cu(tcba)(DMA)		588	848	9.4 × 9.8 4.7 × 5.5	Cu <sup>2+</sup>	Epoxidation of olefins 43a

Journal Name					ARTICLE	
$\text{Cu}_2(\text{bpdC})_2(\text{bpy})$		-	-	12.3 × 7.8 8.8 × 8.0	$\text{Cu}^{2+}$ cross-dehydrogenative coupling reaction	43b
$\text{Cu}_2\text{I}_2(\text{btp4})$		-	-	9 × 12	$\text{Cu}^{2+}$ Three-component coupling of azides, alkynes and amines	44
$\text{Cu-MOF-SiF}_6$ $\text{Cu-MOF-NO}_3$					$\text{Cu}^{2+}$ Oxidation of benzylic compounds	44d
$\text{CuPhos-Br}$ $\text{CuPhos-Cl}$ $\text{CuPhos-PF}_6$					$\text{Cu}^+$ Ketalization reaction	44e
$\text{Zn}_2(\text{bdc})(\text{L-lac})(\text{dmf})$		-	190	5	$\text{Zn}^{2+}$ Oxidation of thioethers	45
$\text{Zn}_3(\text{chirbtb-1})_2$		-	-	33.7	$\text{Zn}^{2+}$ Mukaiyama aldol reaction	46
$\text{Zn}_3(\text{chirbtb-2})_2$		-	-	18 × 18	$\text{Zn}^{2+}$ Mukaiyama aldol reaction	46
$\text{Zn}(\text{Meim})_2$ (ZIF-8)		1173	-	11.6	$\text{Zn}^{2+}$ Cycloaddition of $\text{CO}_2$ and epoxides	47

## ARTICLE

## Journal Name

[Ag <sub>3</sub> (tpha) <sub>2</sub> ] (Ag-tpha)		-	-	7.5 × 8.0	Ag <sup>+</sup>	1,3-Dipolar cycloaddition	48
Mg <sub>3</sub> (pdc1)(OH) <sub>3</sub> (H <sub>2</sub> O) <sub>2</sub>	tpha 	450	-	-	Mg <sup>2+</sup>	Aldol condensation reactions	49b
Mg(pdc2)(H <sub>2</sub> O)	H <sub>3</sub> (pdc1) 	211 ± 12		12.2 × (3.6 → 5.7)		Aldol condensation reactions	
Zr <sub>6</sub> O <sub>4</sub> (OH) <sub>4</sub> (bdc) <sub>6</sub> (Uio-66)	H <sub>2</sub> (pdc2) H <sub>2</sub> bdc 	891	1187	6, 8 & 10	Zr <sup>4+</sup>	Aldol condensation reactions; Cyclization of citronellal	50b 50c,d
Pd(2-pymo) <sub>2</sub>	Hpymo 	600	-	4.8 & 8.8	Pd <sup>2+</sup>	Suzuki coupling; Alcohol oxidation; Olefin hydrogenation	51b-d
Ce-mdip1		-	-	10.5 × 6.0	Ce <sup>3+</sup>	Cyanosilylation of aldehydes	52
Bi(btbt)	H <sub>4</sub> mdip COOH 	1150	-	10	Bi <sup>3+</sup>	Hydroxymethylation of 2-methylfuran	53

H<sub>2</sub>bdc = terephthalic acid; H<sub>3</sub>btc = benzene-1,3,5-tricarboxylic acid; H<sub>3</sub>btt = 1,3,5-tri(2H-tetrazol-5-yl)benzene; H<sub>2</sub>pvia = (*E*)-5-(2-(pyridin-4-yl)vinyl)isophthalic acid; H<sub>2</sub>bpdb = 1,4-bis(3,5-dimethyl-1H-pyrazol-4-yl)benzene; H<sub>2</sub>dhbdc = 2,5-dihydroxyisophthalic acid; Hpapa = (*S*)-3-hydroxy-2-((pyridin-4-ylmethyl)amino)propanoic acid; Hpvba = (*E*)-4-(2-(pyridin-4-yl)vinyl)benzoic acid; H<sub>4</sub>pdtc = pyridine-2,3,5,6-tetracarboxylic; Hpymo = pyrimidin-2(1H)-one; H<sub>3</sub>tcba = 4',4''',4''''-nitrotris((1,1'-biphenyl)-4-carboxylic acid); btpt4 = benzene-1,3,5-triyl triisonicotinate; *L*-lac = *L*-lactic acid; H<sub>3</sub>ChirBTB-1 = 5'-(4-carboxy-3-((*S*)-4-isopropyl-2-oxooxazolidin-3-yl)phenyl)-3-((*S*)-4-isopropyl-2-oxooxazolidin-3-yl)-3''-(3-isopropyl-5-oxooxazolidin-4-yl)-[1,1':3',1''-terphenyl]-4,4''-dicarboxylic acid; H<sub>3</sub>ChirBTB-2 = 3,3''-bis((*S*)-4-benzyl-2-oxooxazolidin-3-yl)-5'-(3-(3-benzyl-5-oxooxazolidin-4-yl)-4-carboxyphenyl)-[1,1':3',1''-terphenyl]-4,4''-dicarboxylic acid; Meim = 2-methyl-1H-imidazole; tpha = tris(4-((*E*)-1-(2-(pyridin-2-yl)hydrazono)ethyl)phenyl)amine; H<sub>3</sub>(pdc-1) = pyrazole-3,5-dicarboxylic acid; H<sub>2</sub>(pdc-2) = pyridine-2,5-dicarboxylic acid; H<sub>4</sub>mdip = 5,5'-methylenediisophthalic acid; H<sub>3</sub>btbt = 5'-(4-carboxyphenyl)-[1,1':3',1''-terphenyl]-4,4''-dicarboxylic acid

**Table 2** Selection of reported MOFs with metalloligands.

MOF formula	Metalloligand	Window or channel/Å	Catalytic reaction	Ref
Zn <sub>2</sub> (tcpb)(Zn-por-1)	Zn-por-1	15 × 19 11 × 9 8 × 9	Acyl-transfer reaction	55a
Zn <sub>2</sub> (Mn-por-1)(Zn-por-2)	Mn-por-1	16.6 × 22	Epoxidation of olefin and hydroxylation of cyclohexane	55b
Zn <sub>2</sub> (Al-por-1)(Zn-por-2)	Al-por-1	-	Ring opening reaction of epoxides	55c
[Co <sub>3</sub> (OH)(H <sub>2</sub> O)] <sub>4</sub> (Co(por-3)) <sub>3</sub>	Co-por-3	10 × 10	Epoxidation of olefin	56a
[Co <sub>2</sub> (μ <sub>2</sub> -H <sub>2</sub> O)(H <sub>2</sub> O)] <sub>4</sub> (Co(por-4))	Co-por-4	5.9, 7.3	Epoxidation of olefin	56b
Cd <sub>1.25</sub> (Pd-por-2)(H <sub>2</sub> O)	Pd-por-2	4.6 × 12.6 8.3 × 9.3	Styrene oxidation	57a
[Cd(DMF) <sub>2</sub> Mn <sup>III</sup> (DMF) <sub>2</sub> (por-5)](PW <sub>12</sub> O <sub>40</sub> )	Mn-por-5	5.4 × 12.4	Oxidation of alkylbenzenes	57b
Zn <sub>2</sub> (HOOC)(Mn-por-2)	Mn-por-2	7.4 × 11.8 11.8 × 11.8	Epoxidation of olefin	57c
Cd <sub>2</sub> (HOOC)(Mn-por-2)	Mn-por-2	7.4 × 11.8 11.8 × 11.8	Epoxidation of olefin	57c
Zn <sub>2</sub> (HOOC)(Fe-por-2)	Fe-por-2	8.7 × 16.7 11.8 × 11.8	Aldol reaction	57c
Zn <sub>2</sub> (MnOH-por-2)(dpni)	MnOH-por-2	6.1 × 7.8	Epoxidation of olefin	57d
Zr <sub>3</sub> (Fe-por-2)	Fe-por-2	37	Oxidation of phenols	58a
Zr <sub>4</sub> (Co-por-2)	Co-por-2	19	Cycloaddition of CO <sub>2</sub> and epoxides	58b
Zn <sub>2</sub> (bdpc)(Mn-salen-1)	Mn-salen-1	6.2 × 15.7	Epoxidation of olefin	59a
Zn <sub>2</sub> (tcpb)(Mn-salen-1)	Mn-salen-1	22.4 × 11.7	Epoxidation of olefin	59b
[Zn <sub>4</sub> (μ <sub>4</sub> -O)(Mn-salen-2) <sub>3</sub> ]·20DMF·2H <sub>2</sub> O	Mn-salen-2	8 × 6	Epoxidation of olefin	60a
[Zn <sub>4</sub> (μ <sub>4</sub> -O)(Mn-salen-3) <sub>3</sub> ]·42DMF	Mn-salen-3	15 × 7	Epoxidation of olefin	60a
[Zn <sub>4</sub> (μ <sub>4</sub> -O)(Mn-salen-2) <sub>3</sub> ]·22DEF·4H <sub>2</sub> O	Mn-salen-2	20 × 16	Epoxidation of olefin	60a
[Zn <sub>4</sub> (μ <sub>4</sub> -O)(Mn-salen-3) <sub>3</sub> ]·37DEF·23EtOH·4H <sub>2</sub> O	Mn-salen-3	25 × 23	Epoxidation of olefin	60a
[Zn <sub>4</sub> (μ <sub>4</sub> -O)(Mn-salen-4) <sub>3</sub> ]·38DMF·11EtOH	Mn-salen-4	11 × 8	Epoxidation of olefin	60a
[Zn <sub>4</sub> (μ <sub>4</sub> -O)(Mn-salen-5) <sub>3</sub> ]·40DBF·6EtOH·H <sub>2</sub> O	Mn-salen-5	29	Epoxidation of olefin	60b
Zn <sub>4</sub> (μ <sub>4</sub> -O)[(Ru <sup>II</sup> (salen-2)(py) <sub>2</sub> ) <sub>3</sub> ]	Ru-salen-2	14 × 10	Cyclopropanation	60c
Zn <sub>4</sub> (μ <sub>4</sub> -O)[(Ru <sup>II</sup> (salen-3)(py) <sub>2</sub> ) <sub>3</sub> ]	Ru-salen-3	19 × 19	Cyclopropanation	60d
Cd <sub>4</sub> (Co(salen-2)) <sub>4</sub> (DMF) <sub>4</sub> (OAc) <sub>4</sub>	Co-salen-2	12 × 8	hydrolytic kinetic resolution	61a

**Table 3** List of MOFs with functional organic sites (FOS) showing the corresponding formula, code, pore dimension and catalytic reaction.

MOF formula	MOF code	FOS	Catalytic reaction	ref
Zn <sub>3</sub> (μ <sub>3</sub> -O)(dpdc) <sub>6</sub>	D-POST-1	Pyridyl	Transesterification	62
Cd(4-btapa) <sub>2</sub> (NO <sub>3</sub> ) <sub>2</sub>	-	Amide	Knoevenagel condensation	63
Al <sub>3</sub> O(DMF)(bdc-NH <sub>2</sub> ) <sub>3</sub> (H <sub>2</sub> O) <sub>n</sub>	NH <sub>2</sub> -MIL-101(Al)	Amino	Knoevenagel condensation	64a
(ED) <sub>x</sub> (Cr <sub>3</sub> F(H <sub>2</sub> O) <sub>2</sub> O(bdc) <sub>3</sub>	ED-MIL-101(Cr)	Amino	Knoevenagel condensation	65
(SO <sub>3</sub> H) <sub>0.5</sub> Fe(OH)(bdc) <sub>3</sub>	S-MIL-53(Al)	Sulfoxy	Esterification	71
(SO <sub>3</sub> H) <sub>x</sub> (Cr <sub>3</sub> (F,OH)(H <sub>2</sub> O) <sub>2</sub> O(bdc) <sub>3</sub>	S-MIL-101(Cr)	Sulfoxy	Esterification	72
Cr <sub>3</sub> O(3-ppc) <sub>1.8</sub> (H <sub>2</sub> O) <sub>0.2</sub> F(bdc) <sub>3</sub>	CMIL-1	Pyrrolidine	Aldol reaction	73
Zn <sub>4</sub> O(Pro) <sub>3</sub>	IRMOF-pro	Pyrrolidine	Aldol reaction	74
Cd <sub>2</sub> (tbt) <sub>(L-pyi)</sub>	Cd-tbt	Pyrrolidine	Aldol reaction	75a
Zn <sub>2</sub> (H <sub>2</sub> O)(OH)(tca) <sub>(L-pyi)</sub>	Zn-pyi	Pyrrolidine	α-Alkylation of aldehyde	75b
Co <sub>3</sub> Cl <sub>3</sub> (tmtb) <sub>2</sub>	TIF-1	NHCs	Nucleophilic conjugate addition	77a
Zn <sub>2</sub> (bipy) <sub>2</sub> (cada)	NU-601	Urea	Friedel–Crafts reaction	78
Al(OH)(bpydc)	MOF-253	2,2'-Bipyridyl	Arylation	80b

Hdpdc = (4*S*,5*S*)-2,2-dimethyl-5-[(4-pyridinylamino)carbonyl]-1,3-dioxolane-4-carboxylic acid; 4-btapa = (1,3,5-benzene tricarboxylic acid tris[N-(4-pyridyl)amide]; H<sub>2</sub>bdc-NH<sub>2</sub> = 2-aminoterephthalic acid; ED = ethylenediamine; H<sub>2</sub>bdc = terephthalic acid; 3-ppc = (*S*)-*N*-(pyridin-3-yl)-pyrrolidine-2-carboxamide; Pro = (*S*)-2-(pyrrolidine-2-carboxamido)-[1,1'-biphenyl]-4,4'-dicarboxylic acid; H<sub>3</sub>tbt = 1,3,5-tris(4-carboxyphenyl)benzene; H<sub>3</sub>tca = 4,4',4''-tricarboxyltriphenylamine; L-pyi = L-pyrrolidine-2-yl-imidazole; tmtb = 1,3,5-Trimethyl imidazole-2,4,6-triethyl benzene; bipy = 4,4'-bipyridine; H<sub>4</sub>cada = 5,5'-(carbonylbis(azanediyl))diisophthalic acid; bpydc = 2,2'-bipyridine-5,5'-dicarboxylate; bdc-NH<sub>2</sub> = 2-aminoterephthalic acid

**Table 4** Selection of post-synthetically modified MOFs through complexation of the MOFs with functional organic sites (FOS).

MOF code	PSM-MOF	FOS	Metal precursor	Metal wt%	Catalytic reaction	ref
NH <sub>2</sub> -MIL-101(Cr)	MIL-100(Cr)-PMA-Cu	Amino	Cu(NO <sub>3</sub> ) <sub>2</sub> or CuEDA	9	Click reaction propargylamine formation	64b
IRMOF-3	IRMOF-3-V	Amino	VO(acac) <sub>2</sub>	2.1	oxidation of cyclohexene	66b
IRMOF-3	IRMOF-3-Au	Amino	salicylaldehyde/ NaAuCl <sub>4</sub>	2	Three-component coupling reaction	67
IRMOF-3	IRMOF-3-Mn	Amino	Mn(acac) <sub>2</sub>	1.25	Epoxidation of olefins	68
UiO-66-NH <sub>2</sub>	UiO-66-NH <sub>2</sub> (damp)Ir	Amino	Damp/ [IrCl(COD)]	3.11	nitroarenes and carbonyl compounds	69c
NH <sub>2</sub> -MIL-101(Fe)	Ni@NH <sub>2</sub> -MIL-101(Fe)	Amino	PyCHO/NiCl <sub>2</sub>	Up to 6.6	ethylene dimerization	70b
Cu_mcp	Pd/Cu_mcp	NHCs	Pd(OAc) <sub>2</sub>	11	Suzuki–Miyaura cross-coupling	77a
Zn_mcpMe	Pd/Zn_mcpMe	NHCs	Pd(OAc) <sub>2</sub>	7.8	Suzuki–Miyaura cross-coupling	77b
CdCl <sub>2</sub> -binol-1	Ti/CdCl <sub>2</sub> -binol-1	Binol	Ti-(O <i>i</i> Pr) <sub>4</sub>	-	ZnEt <sub>2</sub> addition	79a
Cd(NO <sub>3</sub> ) <sub>2</sub> -binol-1	Ti/Cd(NO <sub>3</sub> ) <sub>2</sub> -binol-1	Binol	Ti-(O <i>i</i> Pr) <sub>4</sub>	-	ZnEt <sub>2</sub> addition	79b
Zn-binol-2	Ti/Zn-binol-2	Binol	Ti-(O <i>i</i> Pr) <sub>4</sub>	-	ZnEt <sub>2</sub> addition	79c
Cu-binol-2	Ti/Cu-binol-2	Binol	Ti-(O <i>i</i> Pr) <sub>4</sub>	-	ZnEt <sub>2</sub> addition	79d
MOF-253	MOF-253-0.5CuI	2,2'-Bipyridyl	CuI	8.3	C–O Cross-coupling	80c
MIL-101(Cr)	MIL-101(Cr)-dop-V	catechol	Dopamine/ VO(acac) <sub>2</sub>	-	oxidation of thioanisole.	81

damp = 6-((diisopropylamino)methyl)picolinaldehyde; mcp = 1,1'-methylenebis-(3-(4-carboxyphenyl)-1H-imidazol-3-ium);

mcpMe = 1,1'-methylenebis-(3-(4-carboxy-2-methylphenyl)-1H-imidazol-3-ium);

binol-1 = (*R*)-6,6'-dichloro-2,2'-dihydroxy-1,1'-binaphthyl-4,4'-bipyridine;

binol-2 = (*R*)-2,2'-diethoxy-1,1'-binaphthyl-4,4',6,6'-tetrabenzoate)

**Table 5** MNPs embedded on MOFs indicating the synthesis method, some characterization data and the catalytic reactions studied.

Metal-MOF Couple	Synthesis method	Precursor	wt% metal	MNP size (nm)	Catalytic reaction	ref
Cu-MOF-5	Gas phase infiltration	CpCu(PMe <sub>3</sub> ) CpCu(CN <sup>t</sup> Bu)	10-11	1-3	Methanol synthesis	82c
Ru-MOF-5	Gas phase infiltration	Ru(cod)(cot)	30	1.5-1.7	Hydrogenation of benzene	83
Au-CPL-2	Solid grinding	Me <sub>2</sub> Au(acac)	1	2.2 ± 0.3	Alcohol oxidation	84
Au-MIL-53(Al)	Solid grinding	Me <sub>2</sub> Au(acac)	1	1.5 ± 0.7	Alcohol oxidation	84
Au-ZIF-8	Solid grinding	Me <sub>2</sub> Au(acac)	1	3.4 ± 1.4	CO oxidation	85
			5	4.2 ± 2.6		
Au-ZIF-8	Gas phase infiltration	Au(CO)Cl	up to 33	1-5	Alcohol oxidation	86
Au-MIL-101(Cr)	Colloidal deposition	HAuCl <sub>4</sub>	0.5	< 3	Alcohol oxidation	87
Pd-MOF-5	Impregnation	Pd(acac) <sub>2</sub>	1	-	Hydrogenation of olefins	88a
Pd-MOF-5	Impregnation	K <sub>2</sub> PdCl <sub>4</sub>	0.5-3	3-12	aminocarbonylation	88c
Pd-MIL-101(Cr)	Impregnation	Pd(acac) <sub>2</sub>	1	1.5	Hydrogenation of olefins	88b
Pd-MIL-101(Cr)	Impregnation	Pd(NO <sub>3</sub> ) <sub>2</sub>	1	1.9 ± 0.7	Suzuki–Miyaura coupling, Ullmann coupling, and methyl isobutyl ketone synthesis	89
Pd-MIL-101(Cr)	Impregnation	Pd(NO <sub>3</sub> ) <sub>2</sub>	0.5	2.6 ± 0.5	Heck coupling	90a
Pd-MIL-101(Cr)	Impregnation	Pd(acac) <sub>2</sub>	0.5-4	2.6 or 2.1	Indole synthesis	91
Pd-MIL-101(Cr)	Gas phase infiltration	Pd(η <sup>3</sup> - C <sub>3</sub> H <sub>5</sub> )(η <sup>5</sup> - C <sub>3</sub> H <sub>5</sub> )	Up to 44.5	2.7 (21°C) ; 1.7 (70°C)	Reduction of ketones	92
Pd-NH <sub>2</sub> -MIL-101(Cr)	Ion-exchange	[PdCl <sub>4</sub> ] <sup>2-</sup>	0.62	2.49	Dehalogenation of aryl chlorides	90b
Pt-MOF-177	Gas phase infiltration	Me <sub>3</sub> PtCp'	43	2-3	Alcohol oxidation	93
Pt-MIL-101(Cr)	Impregnation	H <sub>2</sub> PtCl <sub>6</sub>	5	1.8 ± 0.2	Ammonia borane hydrolysis, ammonia borane thermal dehydrogenation, and CO oxidation	94

MOF-systems : MOF-5=Zn<sub>4</sub>O(bdc)<sub>3</sub>; CPL-2= Cu<sub>2</sub>(pzdc)<sub>2</sub>(bipy); MIL-53 = Al(OH)(bdc); ZIF-8 = Zn(MeIM)<sub>2</sub>; MIL-101(Cr) = Cr<sub>3</sub>(bdc)<sub>3</sub>; CPL-1 = Cu<sub>2</sub>(pzdc)<sub>2</sub>(pyz); MOF-177 = Zn<sub>4</sub>O(btb)<sub>2</sub>. linker and functional groups : bdc=1,4-terephthalate; pzdc = pyrazine-2,3-dicarboxylate; bipy = 4,4'-bipyridine; MeIM=2-methylimidazole; pzdc = pyrazine-2,3-dicarboxylate; pyz = pyrazine; btb =benzene-1,3,5-teibenzoate; cod =1,5-cyclooctadiene; cot= 1,3,5-cyclooctatriene; acac = acetylacetonate; Cp' = methylcyclopentadienyl.

**Table 6** List of representative porous materials (zeolite, mesoporous silica and MOF) with pore attributes and size, surface area, stability and catalysis features.

Porous materials	Structure feature	Surface area/m <sup>2</sup> g <sup>-1</sup>	Stability	Catalytic applications	Ref.
ZSM-5	Crystalline, microporous framework with micropores of 5.6 Å.	340	<ul style="list-style-type: none"> <li>■ High thermal stability and being stable up to 800 °C;</li> <li>■ High hydrothermal stability</li> </ul>	<ul style="list-style-type: none"> <li>■ Acid catalysis;</li> <li>■ Redox catalysis;</li> <li>■ Supports for metal ions through cation exchange;</li> <li>■ Gas phase catalysis;</li> <li>■ Size-selectivity</li> </ul>	97
MCM-41	Amorphous framework containing non-intersecting hexagonal channels with controlled size in the range of 20 – 100 Å.	1040	<ul style="list-style-type: none"> <li>■ High thermal stability and being stable up to 850 °C;</li> <li>■ Lower hydrothermal stability than zeolites;</li> </ul>	<ul style="list-style-type: none"> <li>■ Acid catalysis;</li> <li>■ Redox catalysis;</li> <li>■ Incorporation of active sites in the silica walls or deposition of active species on the inner surface of the material</li> </ul>	98
MIL-101(Cr)	Crystalline framework with two kinds of quasispherical cages of 29 and 34 Å.	4100 ± 200	<ul style="list-style-type: none"> <li>■ Lower thermal stability than zeolites and being stable up to 275 °C ;</li> <li>■ Stable over months under air atmosphere.</li> </ul>	<ul style="list-style-type: none"> <li>■ Acid catalysis</li> <li>■ Redox catalysis</li> <li>■ Host for metal nanoparticles</li> <li>■ Size-selectivity</li> </ul>	99



Dr. Li Zhang was born in 1979. She received her Ph.D from The Hong Kong University of Science and Technology under the direction of Prof. Guochen Jia. After postdoctoral work with Prof. Valery V. Fokin at the Scripps Research Institute, Li began her independent career at Sun Yat-sen University, where she is now an associate Professor of Chemistry. Her current research is focused on organometallics and catalysis.



Dr. Cheng-Yong Su is the Cheung Kong Professor of Chemistry at Sun Yat-Sen University (SYSU). He obtained his Ph.D from Lanzhou University in 1996, joined Prof. Wolfgang Kaim's group at Stuttgart University in 2001 as an Alexander von Humboldt Research Fellow, continued postdoctoral work with Prof. Hans-Conrad zur Loye at the University of South Carolina in 2002, and promoted to full professor in SYSU in 2004. He is the author of over 200 peer reviewed publications and 6 book chapters. His current research interest is in the field of supramolecular coordination chemistry and materials, focusing on metal-organic materials, catalysis and nanoscience relevant to clean environment and energy.



Mr. Jiewei Liu was born in 1990. He received his B.S. degree from Wuhan University in 2012. He is currently working as a Ph.D student at Sun Yat-Sen University, and his research interest focuses on chiral porous metal-organic framework for catalysis.



Miss Lianfen Chen was born in 1990. She received her B.S. degree in Applied Chemistry from Sun Yat-Sen University in 2012. She is currently working on her Ph.D program in Sun Yat-Sen University, and her research focuses on metal-organic frameworks with functional groups for catalysis.



Mr. Hao Cui was born in 1990. He received his B.S. degree in 2011 from Northwest University, China. Now he is pursuing his Ph. D in Sun Yat-Sen University, and his research focuses on metal-organic frameworks for catalysis.



Dr. Jianyong Zhang was born in 1974. He received his Ph.D from National University of Singapore in 2003 under the supervision of Prof. T. S. Andy Hor, followed by one-year postdoctoral experience at the Institut de Recherches sur la Catalyse-CNRS with Prof. Liliane G. Hubert-Pfalzgraf. Further three-year post-doc experience was gained in the laboratory of Prof. Stuart L. James at the Queen's University of Belfast. He joined Sun Yat-Sen University in 2006, where he is currently a Professor of Chemistry. His research interests include supramolecular materials and catalysis.